ISSN 1831-9424 (PDF)
ISSN 1018-5593 (Printed)

European Commission

Bending resistance of steel tubes in combiwalls (COMBITUBE)

Research and Innovation

EUR 27829 EN

EUROPEAN COMMISSION
Directorate-General for Research and Innovation
Directorate D — Key Enabling Technologies
Unit D.4 — Coal and Steel

E-mail: rtd-steel-coal@ec.europa.eu
RTD-PUBLICATIONS@ec.europa.eu

Contact: RFCS Publications

European Commission
B-1049 Brussels

European Commission

Research Fund for Coal and Steel

Bending resistance of steel tubes in combiwalls (COMBITUBE)

Coordinator: Prof. Ir. F.S.K. Bijlaard
Delft University of Technology
Stevinweg 1, 2628 CN Delft, The Netherlands

Authors - beneficiaries:

A.M. Gresnigt and S.H.J. van Es
Delft University of Technology
Stevinweg 1, 2628 CN Delft, The Netherlands

M. Meyrer, A. Schmitt, Chr. Mohler and C. Prüm
ArcelorMittal Belval & Differdange
Rue du Luxembourg 66, LU 4221 Esch-sur-Alzette, Luxemburg

J.M. Rotter and A.J. Sadowski
University of Edinburgh
Old College South Bridge, GB EH8 9YL Edinburgh, United Kingdom

T. Ummenhofer and T. Reinke
Karlsruhe Institute of Technology
Kaiserstrasse 12, DE 76131 Karlsruhe, Germany

S.A. Karamanos and D. Vasilikis
University of Thessaly
Argonafton & Filellinon, 38221 Volos, Greece

W. Gall
BAM Infraconsult bv
H J Nederhorststraat 1, 2801 SC Gouda, The Netherlands

Grant Agreement RFSR-CT-2011-00034
1 July 2011 to 30 June 2014

Final report

Directorate-General for Research and Innovation

2014 EUR 27829 EN

LEGAL NOTICE

Neither the European Commission nor any person acting on behalf of the Commission is responsible for the use which might be made of the following information.

The views expressed in this publication are the sole responsibility of the authors and do not necessarily reflect the views of the European Commission.

Europe Direct is a service to help you find answers to your questions about the European Union

Freephone number (*)**:**

00 800 6 7 8 9 10 11

(*) Certain mobile telephone operators do not allow access to 00 800 numbers or these calls may be billed.

More information on the European Union is available on the Internet (http://europa.eu).

Cataloguing data can be found at the end of this publication.

Luxembourg: Publications Office of the European Union, 2016

Print	ISBN 978-92-79-57674-4	ISSN 1018-5593	doi:10.2777/300984	KI-NA-278-29-EN-C
PDF	ISBN 978-92-79-57673-7	ISSN 1831-9424	doi:10.2777/961346	KI-NA-278-29-EN-N

© European Union, 2014
Reproduction is authorised provided the source is acknowledged.

Printed in Luxembourg

PRINTED ON WHITE CHLORINE-FREE PAPER

Table of Contents

Summary **5**

Conclusions **11**

1 WP1: Critical evaluation of design procedures and available test data for tubular members **17**

1.1 Task 1.1: Critical evaluation of design procedures for CombiWalls 17
1.1.1 Design practice in The Netherlands 17
1.1.2 Current regulations in The Netherlands 18
1.1.3 Eurocode 3 18
1.1.4 Application of EN 1993-5 (2008) 18
1.1.5 ETIB 19
1.1.6 Comparison of design codes 20
1.1.7 References 21

1.2 Task 1.2: Selection of parameters and construction details for further study 21
1.2.1 Construction details 21

1.3 Task 1.3: Collection and evaluation of bending test results and load introduction 24
1.3.1 References 25

1.4 Task 1.4: Evaluation of existing numerical methodologies for elastic-plastic shell buckling 25
1.4.1 Evaluations at the University of Thessaly 25
1.4.2 Evaluations at the University of Edinburgh 28

2 WP2: Specimen selection, test set-up, test design and material testing **31**

2.1 Task 2.1: Selection of test specimens and design of test set-up 31
2.1.1 Selection of test specimens 31
2.1.2 Shift of larger specimens to Delft and smaller specimens to Karlsruhe 31
2.1.3 Selection of test specimens and design of test setup in Delft 32
2.1.4 Selection of test specimens and design of test setup in Karlsruhe 34

2.2 Task 2.2: Ordering and manufacturing of test specimens 36

2.3 Task 2.3: Material testing of tube material 36
2.3.1 Material testing of tube material in Delft 37
2.3.2 Material testing of tube material in Karlsruhe 41
2.3.3 Characterisation of the material testing of tube material 44

2.4 Task 2.4: Measurement of imperfections and residual stresses 45
2.4.1 Measurement of initial dimensions and imperfections in Delft (laboratory) 45
2.4.2 Measurements of imperfections on site 49
2.4.3 Measurement of geometrical imperfections in Karlsruhe 51
2.4.4 Interpretation and evaluation of measured imperfections in Edinburgh 53
2.4.5 Residual stress measurements in Karlsruhe 59

3 WP3: Experimental testing of tubes under various loading conditions **61**

3.1 Task 3.1: Pure bending in Delft 61
3.1.1 Test setup 62
3.1.2 Test procedures 63
3.1.3 Measurements during testing 63
3.1.4 Monitoring of geometrical imperfections 64
3.1.5 Test results 65

3.2 Task 3.2: Bending with normal force in Karlsruhe 73
3.2.1 Test setup 73
3.2.2 Test procedure 73
3.2.3 Summary of experimental results 74
3.2.4 References 76

4 WP4: Numerical modelling and simulation of experiments ... 77
4.1 Task 4.1: Constitutive modelling for local buckling calculations in the plastic range ... 77
4.1.1 Introduction ... 77
4.1.2 Literature review ... 77
4.1.3 Numerical results ... 78
4.1.4 References ... 79
4.2 Task 4.2: Modelling of the spirally welded tube ... 79
4.2.1 Introduction ... 79
4.2.2 Numerical simulation of cold bending process ... 79
4.2.3 Description of numerical model ... 80
4.2.4 Calculation of residual stresses ... 81
4.3 Task 4.3: Modelling of imperfections and residual stresses ... 83
4.3.1 Introduction ... 83
4.3.2 Modelling of imperfections ... 83
4.3.3 Modelling of residual stresses ... 84
4.4 Task 4.4: Simulation of experimental results ... 85
4.4.1 Simulation of experiments carried out in Delft ... 85
4.4.2 Simulation of experiments carried out in Karlsruhe ... 87
5 WP5: Numerical parametric analyses ... 91
5.1 Task 5.1: Pure bending (U-Thessaly) ... 91
5.1.1 Wrinkling imperfection sensitivity ... 91
5.1.2 Effect of residual stresses ... 92
5.1.3 Effect of material properties ... 92
5.1.4 Effect of girth welds and coil connecting welds ... 95
5.1.5 Effect of spiral weld cap and overmatching ... 96
5.2 Task 5.2: Bending with radial loads ... 96
5.3 Task 5.3: Bending and normal force with load introduction at the top ... 96
5.4 Task 5.4: Bending with large ovalisation ... 97
5.4.1 Introduction ... 97
5.4.2 Numerical modelling ... 97
5.4.3 Numerical results ... 97
5.4.4 Discussion of the numerical results ... 98
5.4.5 References ... 99
6 WP6: Development of design guidelines ... 101
6.1 Task 6.1: Safety evaluation for development of design rules ... 101
6.2 Task 6.2: Design guidelines ... 101
6.2.1 Design guidelines for EN 1993-5 Piling ... 102
6.2.2 Design guidelines for EN 1993-1-6 Shell Structures ... 111
6.3 Task 6.3: Background documents ... 114
6.3.1 Ongoing research – PhD thesis ... 114
6.4 Task 6.4: Design examples ... 115
6.4.1 According to the design guidelines for EN 1993-5 Piling ... 115
6.4.2 According to the design guidelines for EN 1993-1-6 Shell Structures ... 115
7 WP7: Project coordination ... 117
7.1 Task 7.1: Establish an efficient management process ... 117
7.2 Task 7.2: Monitoring of project activities and evaluation of progress ... 117
7.3 Task 7.3: Progress and final reports ... 117
8 Publications from the Combitube project ... 119
List of Figures ... 120
List of Tables ... 123

Summary

The present design rules of Eurocode 3 for tubes in CombiWalls lead to over-conservative and uneconomical designs, because the rules for local buckling for the diameter to wall thickness ratios as applied in CombiWalls are inadequate. Experimental and numerical investigations have been carried out to find the bending strength and deformation capacity of spirally welded tubes that are commonly used in CombiWalls, taking proper account of the influences on local buckling of the material behaviour, the structural detailing and the load introduction.

Use of spirally welded tubes

Tubular piles are widely used in combined walls as primary elements. The tubes fulfil two structural functions: as retaining elements for horizontal loads from soil and water pressures, and as bearing piles for vertical loads. In Figure 1 an example is given for a typical harbour application.

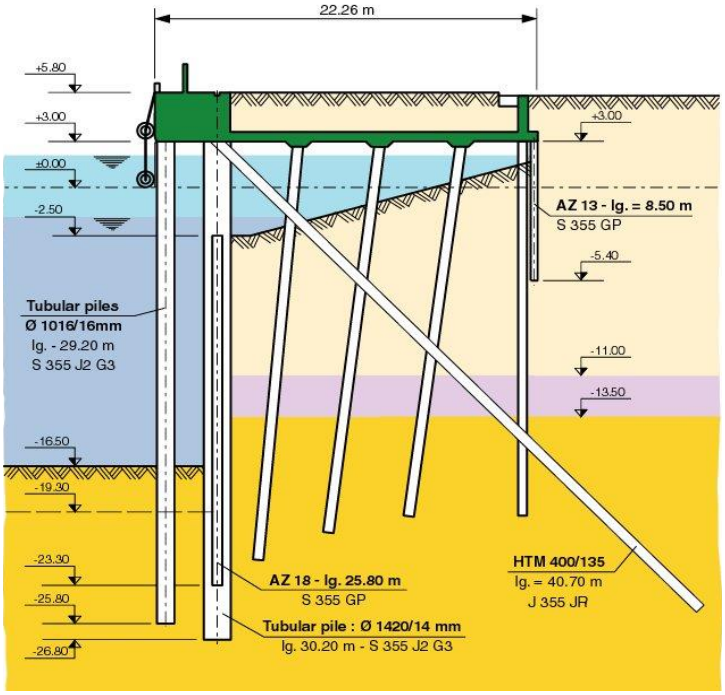

Figure 1 - Typical harbour wall or quay wall construction; for other construction types see Figure 7.

Typically the tubes for these applications are manufactured from hot rolled coils (t=10–24mm) by spirally welding in a diameter range of 900–2400mm. Steel grades with yield stresses between 350MPa and 480MPa are commonly used. The usual length of the piles ranges from 20 to 30m. In the future, tube lengths up to 40m are anticipated for deeper harbours.

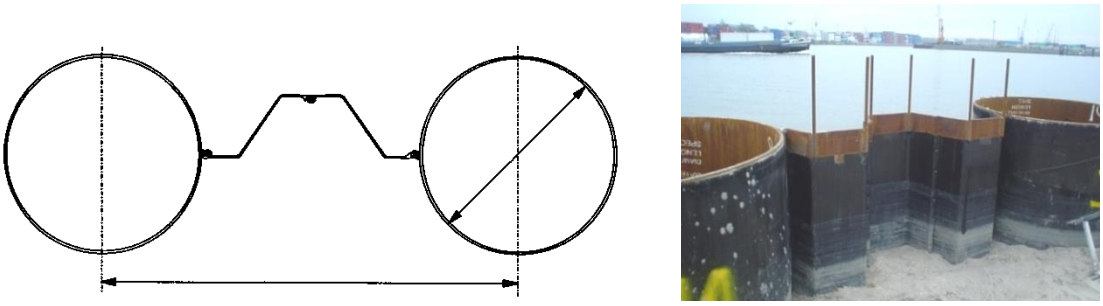

Figure 2 - Schematic and photo of a CombiWall (combined wall of tubes and infill sheeting connected with welded slots to the tube).

Figure 3 - Left: Welding of the slots for the tube-sheeting connection; Right: installation of tubular piles in the soil.

Figure 4 - Left: Installation of infill sheeting; Right: CombiWall with waling for the new central railway and metro station in Rotterdam (2008).

In CombiWalls a range of construction details and loading conditions may occur in practice. In the Combitube project a selection of most typical details is covered.

(a) Changes in the tube wall thickness. Thicker-walled tubes may be chosen for long piles in zones with high bending moments. At the connection (girth weld) the thinner-walled tube is sensitive to local buckling, mainly due to geometrical discontinuities, including misalignment.

In the Combitube project, the geometrical imperfections and misalignment at girth welds are investigated experimentally and with finite element analyses to be used for the development of design rules. Because of limitation of parameters, it was agreed not to perform specific research into the effect of stepwise changes in nominal wall thickness.

(b) Imperfections in the tube geometry. In addition to imperfections inherent to the fabrication, also imperfections are possible due to handling. In building pit work, tubes are often reused. Small local dimples may occur.

Measurements were performed on site. The effect of dimples was investigated with finite element analyses.

(c) "Unforeseen" loads. Contractors may need temporary supports for construction work. Attachments are often welded to the CombiWall, causing unanticipated loads. This effect has not been investigated. This was proposed in the project group (partners) and agreed with RFCS, TGS8.

(d) Tube form. Both spirally welded tubes and longitudinally welded tubes are used. Tubes that do not meet the high quality specifications for pipelines are sometimes used in CombiWalls.

In the test program in Delft two additional tests were performed on large scale longitudinally welded UOE tubes.

(e) Material mechanical behaviour. The shape of the stress strain curve (yield plateau, strain hardening modulus) and residual stresses have an influence on the pre- and post-buckling behaviour of the tube. In extensive numerical simulations the influence of these effects has been studied.

(f) Soil fill. The effects of soil fill in the tube and soil pressure distribution in the circumferential direction.

The results of the research in the European Research project "Enhanced Economy of Tubular Piles by Improved Buckling Design (ETIB)" have been studied. Bending tests have been carried out to study the effect of the sand fill on the bending moment capacity and deformation capacity, in particular the curvature at local buckling and the post buckling behaviour.

Actual design rules

Eurocode 3 Part 5 (EN 1993-5, Piling) covers design rules for CombiWalls.

For economic design, a high diameter to wall thickness ratio (D/t) is important. The key limitation is the possibility of local buckling. For verification of the local buckling failure mode, EN 1993-5 refers to EN 1993-1-6, Strength and Stability of Shell Structures. The present design rules lead to uneconomical designs and do not provide sufficient guidance for safe designs in the D/t application range that is relevant to CombiWalls.

To account for local buckling, design specifications used in current practice classify tubular members in terms of their cross-sectional geometry (i.e. the value of their D/t ratio, where D is the external diameter and t is the wall thickness). More specifically, the cross-sectional classification expresses the ability of a cylindrical member under axial compressive stresses (in the absence of Euler global buckling) to attain a certain load level in the inelastic range without local buckling. The limiting values of the D/t ratio for a given steel grade that define the various classes are called "slenderness limits".

In a survey among 11 standards in Europe (Eurocode, Netherlands, Germany, UK, Japan, Australia, USA and Canada, a large scatter was found in the slenderness limits (Gresnigt, 2010). For instance, for the plastic moment (Class 2) the values vary between 44·(235/fy) and 76,6·(235/fy) for the USA and Canada respectively. For EN 1993-1-1 this value is 70·(235/fy).

Scatter in test results

Comparisons of local buckling test results with design rules show a significant scatter in the data. For elastic thin-walled shells this scatter appears in the stress or strain at local buckling. In thick-walled shells local buckling occurs after the yield stress has been reached and a part of the cross-section experiences significant plasticity. A large scatter is found in the strain at which local buckling occurs. Causes for this scatter have been identified. These are in particular geometrical imperfections, variations in material behaviour (shape of stress strain diagram, strain hardening, Bauschinger effect), eccentricities in load introduction, misalignment at welds, etc.

For more economical and safe designs, the effect of the various sources of scatter on the strength and deformation capacity of tubes must be better quantified. In the Combitube project, numerous finite element calculations have been performed to quantify these effects and to come up with suitable design rules.

Strain-based design versus stress-based design

From practical design experience with the present EN 1993-5 and EN 1993-1-6 standards, it is clear that the verification calculations for local buckling lead to very uneconomical designs. The main reason is that the local stress based strength limitation used for thin shell structures in the hand

design calculations of EN 1993-1-6 are extremely restrictive, and unable to deal with conditions in which substantial parts of the shell yield before buckling, unless the stress state is completely uniform (i.e. it cannot deal with bending of a tube in a CombiWall).

In thin shells, the chief focus is on geometrical imperfections, geometric nonlinearity and load introduction, which lead to reductions in the local stress at which local buckling occurs. By contrast, the thicker shells of the CombiWalls are less sensitive to these factors, and a procedure that includes those leads to the very uneconomic designs. Tubes in CombiWalls withstand substantial zones of yielding and post-yield deformations before local buckling, and this phenomenon must be included for economic design. Thus there is a critical difference in the conceptual basis required for thin shells and for tubes as applied in CombiWalls, since the thin shell local stress criterion cannot accommodate substantial yield at either the strength or the deformation limit. This accommodation is essential for economic design of thicker cylindrical members.

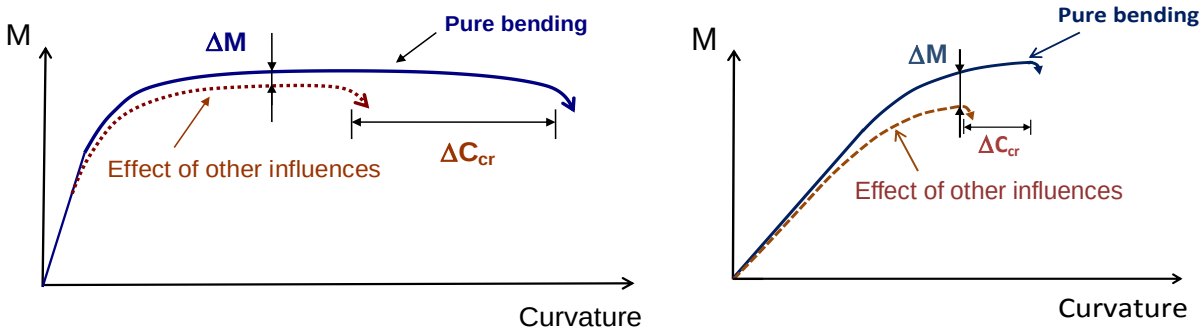

Figure 5 - Effect of other influences such as imperfections, soil loads, residual stresses, ovalisation of the cross section, etc. on the bending moment-curvature behaviour for a thick walled tube and for a thinner walled tube.

In strain-based design, the critical curvature at which local buckling occurs is determined. It offers a better insight into the effect of other influences such as imperfections, soil loads, residual stresses, ovalisation of the cross section, etc. on local buckling and thereby on the bending moment capacity, as is indicated in Figure 5. The effect of changes of the critical curvature on the bending moment capacity ΔM is often small and relatively easy to calculate. Strain based design permits the load deformation behaviour up to local buckling to be described accurately. The results are tools that can accurately predict the resistance and the deformation capacity.

In stress-based design the effect of other influences is usually translated into approximate reduction factors on the resistance (here the bending moment capacity). This approach often results in big decreases in capacity and over-conservative and uneconomical CombiWall designs.

Experimental testing and numerical simulations and parameter studies have been performed to quantify the various influences on the load deformation behaviour within the range of practical geometries and steel grades for tubes in CombiWalls.

In the project, advantage has been taken of the experience and knowledge of the partners in pipeline industry applications to introduce strain based design methods for tubes in structural applications such as CombiWalls.

Design guidelines

In the project team, intensive discussions were held on the set up of the design guidelines. It was recognized that especially the design rules for local buckling in the present EN 1993-1-6 need modification for the tubes as applied in combined walls because the present design rules do not

sufficiently take into account plasticity of the cross section of the relative small values of the Diameter/ Wall thickness ratio in tubes for CombiWalls.

Also EN 1993-5 Piling needs modification, because it insufficiently takes into account all the special features in the design of tubes in CombiWalls, such as soil loads, loads from infill sheeting and support from sand fill. There is a close interaction between these special features and the bending moment capacity and local buckling behaviour and especially also the safety aspects related to the post buckling behaviour. Therefore a dedicated set of design guidelines has been developed for tubes as primary elements, to be included in EN 1993-5 Piling.

Such dedicated set of design guidelines is helpful and is urgently requested by designers because the designer of CombiWalls then needs only one dedicated document. It will avoid confusion and possible errors due to the more complicated set-up of EN 1993-1-6, with a much broader scope than needed for tubes in CombiWalls. Such dedicated design rules are not unique. They are also in the design rules for pipelines in EN 1993-4-3. It was also recognized that the developed knowledge in the Combitube project needs to be implemented in the more general design rules of EN 1993-1-6.

In the project team both needs were discussed at length. Finally it was decided to report two sets of design guidelines:

(1) A set of dedicated guidelines for the design of combined walls valid for Diameter/ Wall thickness ratios from 50 to 140, fulfilling the needs of EN 1993-5 Piling.

and

(2) A set of general guidelines valid for Diameter/ Wall thickness ratios from 50 to 6000 that focus on determination of the bending moment capacity, fitting the needs of EN 1993-1-6 Shell Structures.

The design rules were verified by comparing with the finite element parameter studies results and in particular with the test results.

Long-time experience of safe design of tubes in CombiWalls

CombiWalls with tubular primary elements have been used in The Netherlands since the 1980's. Generally, elastic design criteria were adopted. The D/t ratios were in the range between 70 and 100. The specified minimum yield strength of the piles was between 355-415 N/mm².

With the large scale application of CombiWalls for the railway tunnel under the river Maas (Willemsspoortunnel) in Rotterdam (1987-1992), the first steps were made in methodically addressing the influence of the infill sheeting on the primary elements. The tensile forces that act on the interlocks, either caused by hydrostatic loads on the infill sheeting or by vertical misalignment of the piles, will tend to ovalise the tube.

The research for the application of the combined walls at the Willemsspoortunnel were laid down in a report by the Dutch railways (1988), which was later on the start document for the part on combined walls in ENV1993-5 Piling. Over all these years no failures are known that had to be attributed to unsafe design rules for the tubes as in the ENV 1993-5 Piling.

Cooperation with the Dutch CUR committee C183-1 in particular on the effect of sand fil

In the Centre for Civil Engineering Research and Codes (CUR) in Delft, Netherlands, work has been performed to revise and update the Dutch Handbook on Quay Walls. In 2013 CUR has merged with Stichting Bouwresearch (Institution for Building Research) in Rotterdam (SBR), forming SBRCURnet (http://www.sbrcurnet.nl/). SBRCURnet has several committees working on various aspects of civil engineering. Committee C183-1 is the one that is responsible for the Handbook, in particular the rules on local buckling of tubes in CombiWalls.

The motivation for the start of that research was the same as for Combitube. In addition there was a strong interest to study the effect of compacted sand in the tubes on the bending moment capacity and the deformation behaviour: local buckling and post critical behaviour.

The harbour of Rotterdam was a major sponsor in that project, because of the many new quay walls to be constructed in the extension of the harbour to the North Sea and other new quay walls.

- An extensive test program with 24 full scale bending tests has been designed and executed in the CUR C183-1 group. Twelve tests were performed on empty tubes and twelve on sand filled tubes.
- Tubes in CUR test program had different steel grades and different diameter to wall thickness ratios.
- In actual quay walls the tubes are mostly sand filled. It was expected by CUR and also found in the tests that the sand fill improves the local buckling behaviour, especially the post-buckling bending moment capacity.

It was in the interest of both research programs of CUR and Combitube to cooperate and exchange information on test results, on practical aspects such as design needs, construction methods, imperfections in tubes as installed in practice, load cases, etc. and on theoretical issues to develop design guidance for the Dutch Quay wall Handbook (also used in other European countries) and Eurocode 3.

While the CUR program is focusing on the Dutch design and construction practice, Combitube aimed to develop design guidelines for European application in EN1993-5 and EN1993-1-6. Furthermore, the RFCS project Combitube does not deal directly with geotechnical aspects related to the design of tubular piles used for CombiWalls, while the CUR project does.

In view of the above considerations it has been requested to RFCS to agree with cooperation and exchange of research data. The RFCS TGS8 and CUR partners agreed to do so. As a result, the CUR and the Combitube research program are perfectly complementary and cooperation was of outstanding importance for both.

Conclusions

In this paragraph the conclusions from the research are summarized per Work Package. At the end are the main conclusions summarized.

WP1: Critical evaluation of design procedures and available test data for tubular members

1. Current design of CombiWall piles, using EN 1993-5 and especially 1993-1-6 is much more complex compared to previous design methods (which have proved to be satisfactory and reliable on numerous projects).
2. Current EN-codes appear to be quite conservative compared to previous design codes and design practice, even when considering the ETIB recommendations.
3. Because of the complex and conservative nature of the EN-codes, a certain amount of reluctance can be observed with designers and clients in implementing the EN codes on their projects. There are examples where the older, proven design methods are favoured over the newer EN design methods.
4. Because of the complexity, the current EN-codes are more an (detailed) engineering tool than a design tool.
5. The shell-type verification of EN 1993-1-6 does not match well with the normal “beam style” verification (combined with various reduction factors for buckling, secondary elements) that is commonly used for earth retaining structures.
6. Although the general impression is that the ETIB design rules do not significantly improve the CombiWall economy, it is obvious that a lot of fundamental research has been done that can be used for the design of CombiWalls.
7. There is a need for simple and quick design tools, based on the starting point of utilizing the full elastic moment, relating this to allowable combinations of D/t and yield stress.
8. Diameter to wall thickness ratios are mainly between 70 and 100 with possible extensions to D/t=50 and D/t=120.
9. Steel grades are mainly between S355 and S460 according to European standards with possible extensions to S235 and higher strength steels up to specified minimum yield strength of 480 MPa. It is noted that often API steel grades are applied: X42 up to X70 with specified minimum yield strength of 290 MPa and 483 MPa. X80 tubes are produced for pipelines.
10. Loading in bending and normal force. Typical normal forces can be as high as 25% of the plastic normal force capacity
11. Relatively few bending tests have been performed on spirally welded tubes.
12. The test results as collected in the database, mainly consisting of longitudinally welded tubes show large scatter, both in critical strain (curvature) as in strength (bending moment capacity).
13. Finite element modelling and analysis tools have been tested and recommendations for application have been set up.

WP2: Specimen selection, test set-up, test design and material testing

1. Based on the results of WP1, adequate test tubes could be identified. However, because these had much greater diameter and wall thickness than anticipated in the proposal, substantial additional expenses were necessary for the purchase of steel and especially also in the extra equipment for the test rigs.
2. Because of the many variables some limitation appeared necessary in the selection of test specimens in order to perform testing with maximum output for the project.

3. Also because the Combitube project (together with another RFCS project) is basis for the PhD research of Sjors van Es, much more measuring equipment was applied and two extra tests were performed. These contributed substantially to the high quality of the Combitube project results. The input of other PhD students Daniel Vasilikis and Thomas Reinke is highly valuated as well.
4. Compressive material tests showed only in a limited number of cases Bauschinger effect.
5. Residual stress measurements with the hole-drilling method, which was selected as the most suitable for this project, showed large scatter. It was concluded that probably the large variations in treatment of the steel in the roiling mill on the coil, the uncoiling and the bending to the spirally shape, with various bend radii and various temperatures and cooling down rates caused this. It was found in later WP's that for tubes as applied in CombiWalls the residual stresses do not have a large effect on the bending moment capacity and the critical curvature.
6. Residual stresses as found by the "ring-cutting method" also showed large scatter between the different rings, ranging from a ring closing 154 mm to a ring opening 340 mm for rings of similar diameter, wall thickness and length.
7. Intensive measurements of imperfections in the laboratory and on site with advanced laser equipment revealed clear patterns of these imperfections that could be used for numerical simulation of the tests and for parameter studies.
8. An assessment and mathematical representation of laser imperfection measurements has been made of tubes tested in this project, for further analyses. The results clearly revealed several origins of the imperfections such as the forming tools (rollers) in the tube mill and spirally welds, coil connecting welds and girth welds.

WP3: Experimental testing of tubes under various loading conditions

1. A huge data base of test results could be obtained thank to the extensive measurements and careful test set ups.
2. Localisation of curvature is observed both before and after reaching the maximum resisted bending moment in the bending tests of spirally welded tubes. In longitudinally welded tubes this was virtually not observed.
3. The presence of a structural detail such as a girth weld or coil connection weld has, in most cases, a negative effect on the capacity of the tube, both in terms of maximum curvature and bending moment capacity. This effect highly depends on the imperfections (eccentricity, high-low) and differences in material properties on both sides of the welds.
4. If a local buckle forms in plain tube material, it generally forms at a geometrical imperfection away from the spiral weld. These imperfections have in some cases shown to be production related.
5. When defining the critical curvature, the measuring length is particularly important when variations in bending strength along the tube length are likely. A short measuring length may give a much larger critical curvature than a long measuring length. The reason for this is localisation of curvature at the weakest cross-section (in terms of bending moment capacity). A long measuring length averages the curvatures and tends to give smaller critical curvatures. This effect is not yet or only hardly recognized in testing programmes.

WP4: Numerical modelling and simulation of experiments

and

WP5: Numerical parametric analyses

1. Finite element simulation of spiral-welded cold-bending forming process indicates that the **residual stresses** are mainly in the hoop direction at about 80% of yield stress. Moreover, for a specific tube diameter, the values of residual stresses (in both the axial and the hoop direction) normalized by the material yield stress, are nearly independent on the forming angle and on the steel grade, while there exists a small effect of the D/t ratio.
2. Numerical simulation of the mechanical behaviour of large-diameter spirally welded tubes subjected to bending is also performed. A very good comparison is found between the numerical results and the experimental data of TU-Delft, in terms of maximum moment, critical curvature, and the deformed (buckled) shape, building confidence in the finite element models. In all cases, structural failure of the tubes is due to local buckling in the form of a short-wave localized wrinkling pattern.
3. Numerical results from the parametric studies show that the bending moment capacity is significantly affected by the D/t ratio. In thin-walled tubes with D/t ratio higher than 100, buckling occurs quite suddenly, associated with limited inelastic deformation, whereas the ultimate moment is slightly higher than the first yield moment M_y, and significantly lower than the full plastic moment M_p. The response of relatively thick-walled tubes with D/t ratio of about 67 is smoother with significant inelastic deformation, where local buckling occurs more gradually. For those tubes, the maximum moment M_{max}, for small amplitude of initial wrinkles (δ_o/t values less than 0,5%), may reach a value of 95% of the full-plastic moment M_p. It was further shown that the presence of a dimple imperfection reduces significantly the bending capacity in terms of both critical curvature and maximum moment.
4. Using a special-purpose finite element mesh, the effect of the spiral weld on buckling behaviour is also examined. It is shown that local buckling develops in areas located at some distance from spiral welds, and that the discontinuity because of the presence of a spiral weld cap and weld material overmatching may not have a decisive influence on tube response.
5. Material properties may have a considerable effect on bending response: the higher the yield stress, the larger the maximum moment and the smaller the critical curvature. Furthermore, the yield plateau and hardening modulus also affects the response; a large length of the yield plateau or a small value of the hardening modulus, results in a significant plastification of the tube and the development of higher strains, leading to lower values of critical curvature and maximum moment. Material anisotropy in axial and hoop direction may also influence the bending response.
6. In the case of a spiral-welded tube that includes a coil connection weld (CCW) or girth-weld (GW), the possible difference in the material strength between the connected parts decreases the bending deformation capacity. Moreover, possible girth-weld misalignment ("hi-lo" imperfection) may result in a substantial reduction in the bending strength. Finally, for the case of a steel sheet attachment carrying a force transverse to the pipe axis, the bending capacity is reduced due to excessive ovalisation.
7. The full plastic bending moment is hard to achieve, mainly because of ovalisation of the cross-section, bending moments in the tube wall due to the ovalisation and local buckling. The difference depends on the D/t ratio and the steel grade.

WP6: Development of design guidelines

As indicated and discussed before, two sets of design guidelines were developed:

(1) A set of dedicated guidelines for the design of combined walls valid for Diameter / Wall thickness ratios from 50 to 140, fulfilling the needs of **EN 1993-5 Piling**.

(2) A set of general guidelines valid for Diameter / Wall thickness ratios from 50 to 6000 that are focussing on determination of the bending moment capacity, fitting the needs of **EN 1993-1-6 Shell Structures**.

Conclusions on set (1) for EN 1993-5 Piling

1. The first set is basically a refinement of the long existing design method in ENV 1993-5 Piling which, as mentioned before, enabled economic and apparently safe quay walls designs (no failures are known as a result of not correct design rules). Influences that were not taken into account in the ENV version are now addressed and equations are presented to quantify the effect on the critical curvature and bending moment capacity.
2. In developing these guidelines, the input of the CUR research program as mentioned before was highly valued to include the effect of sand fill. Sand fill has a positive effect on the critical curvature and the bending moment capacity, in particular also on the post buckling behaviour. With sand fill the post buckling behaviour is much smoother (less steep drop) and therefore enables better redistribution of loads in a quay wall.
3. Comparisons with test results in the Combitube project have demonstrated good agreement for (1) stiffness (which is affected by ovalisation and residual stresses), (2) critical curvature and (3) bending moment capacity.
4. The effect of imperfections, ovalisation, residual stresses, steel grade with different strain hardening properties, soil loads, bending moments in the tube wall, normal force and shear force on the bending moment capacity is much larger for thinner walled tubes than for thicker walled tubes. Therefore safety factors should depend on the D/t ratio.
5. The most important failure mode with largest scatter in critical curvature is local buckling which is highly dependent on the D/t ratio.
6. The design guidelines in set (1) offer the possibility to quantify the critical curvature and to take care of adequate safety factors on the critical curvature to achieve the desired safety level. The necessary reduction in bending moment capacity is much less for thicker walled tubes than for thinner walled tubes.

Conclusions on set (2) for EN 1993-1-6 Shell Structures

1. The Edinburgh team has produced a comprehensive set of design guidelines in a final report (Rotter and Sadowski, 2015). It has about 80 pages with numerous graphs with results of FEA parameter studies. And it contains a proposal for amendment of EN 1993-1-6 Shell Structures. The report also claims strong conclusions as in subsequent items.
2. This research report reviews all the critical questions addressed by the Combitube project, identifying which could be regarded as of secondary importance and which were primary factor. The report then produced a synthesis of all the numerical and experimental data available to the Edinburgh team and produced carefully crafted design guidelines founded on a rigorous scientific assessment of this data. Not only are the recommendations produced in terms of the bending resistance to buckling and yielding, but recommendations that are compatible with these are deduced for those wishing to use strain based design.

3. During the course of this study of the bending resistance of large tubular members, a very significant advance has been made in resolving the conflicts and mismatches that formerly existed in this field. A new method of shell structure design, termed Reference Resistance Design has been devised. It has been implemented and adopted into EN 1993-1-6 as an approved amendment. A new Annex E.1 to EN 1993-1-6 (2007) has been drafted to define the resistance of tubular members and cylindrical shells subject to global bending. This annex was submitted and approved as an amendment, so that there is a new regulatory framework in place already before the closure of the project to address the specific needs of Combitubes.
4. This extensive report has documented the many factors that can affect the buckling resistance of tubular members for CombiWalls, and the discussion has identified which factors are critically important and which can be ignored as having only a secondary influence on resistance. These aspects have all been considered in the development of appropriate design rules.
5. A full set of design rules has been developed. Since the Eurocode on piles is required to refer to the standards EN 1993-1-1 (2005) for steel structural members in the cross-section classes 1, 2 and 3, and to EN 1993-1-6 (2007) for steel shells for those that fall into Class 4, the proposals developed here have been made compatible with both standards. The complete description given here has already been approved as an amendment to EN 1993-1-6 (2007) and the outcomes for less slender tubes are almost ready for implementation as an amendment to EN 1993-1-1 (2005). This comprehensive study permits tubular members and thin shell structures to be designed to a consistent and seamless set of rules that should be of considerable benefit to the structural engineering community.
6. There are several issues which could not be resolved within this project; most notable amongst these are the lack of standardised control of yield plateau and strain hardening characteristics of the steels from which these tubes are made. Since these properties have a strong influence on the resistance in the critically important range of design for Combitubes, this lack of standardisation is unfortunate.

In summary, the main conclusion are:

<u>EN 1993-5: Piling</u>

The safety level of the new set of dedicated design rules as intended for EN 1993-5 is about the same as for the ENV 1993-5 design rules. The main difference and advantage is that the proposed new set of design rules addresses more influences and will lead to even more accurate and economic designs.

<u>EN 1993-1-6: Strength and Stability of Shell Structures.</u>

For EN 1993-1-6 a new set of design rules has been developed based on numerous finite element parameter studies that take away the discontinuities and other objections that had been raised in recent years.

Work in progress after the Combitube project:

As is mentioned before, the Combitube project is part of the PhD research of Sjors van Es. It means more analyses and further refinement of the design guidelines with appropriate safety factors.

Also work will be carried out to simplify design guidelines as much as possible for easy and economic use by designers.

Scientific and Technical Results

1 WP1: Critical evaluation of design procedures and available test data for tubular members

The objectives of WP1 were the following:

- To conduct a critical evaluation of available design procedures for tubes based on national and international standards (Task 1.1).
- To determine two or three examples of typical CombiWall applications and construction details for further investigation (Task 1.2).
- To collect and evaluate available test results on bending, load introduction and other relevant cases. To set up a data base of experimental data (Task 1.3).
- To evaluate available numerical methods for their suitability to describe the local buckling behaviour, taking into account the highly materially and geometrically nonlinear behaviour (Task 1.4).

1.1 Task 1.1: Critical evaluation of design procedures for CombiWalls

In this task two reports were prepared:

- Willem Gall: Overview of design practice in The Netherlands.
- Michael Rotter and Adam Sadowski: Critical evaluation of design procedures for CombiWalls: Tubular Member Design Rules and Standards

The first report focusses on practical design issues. It gives an overview of the development of design practice of CombiWalls in The Netherlands. It is demonstrated that the application of the present Eurocode 3 design rules (EN1993-5 with EN1993-1-6) results in much less economic designs than in past decades applying Dutch design rules. It is noted that no failures of CombiWalls are known due to design rules being too liberal.

The report by Michael Rotter and Adam Sadowski focusses on current design rules for tubes, loaded in combinations of bending moment and normal force. Many standards have been examined, including several on pipeline design. These are relevant since pipelines have similar diameter to wall thickness ratios. The report gives a perspective on how to modify the present EN1993-1-6 such that the effects of plasticity of a part of the cross section of the tubes can be worked out in a future update of EN1993-1-6.

In the next two sections the main observations from these two reports are summarized.

1.1.1 Design practice in The Netherlands

CombiWalls with tubular primary elements have been used since the 1980's. Generally, elastic design criteria were adopted. The D/t ratios were in the range between 70 and 100. The specified minimum yield strength of the piles was between 355-415 N/mm². The value 415 N/mm² is because many tubes were delivered according to American pipeline standards. API X60 has a specified minimum yield stress of 60.000 psi = 415 N/mm².

Local buckling as in the Eurocode design rules is only considering a stand-alone pile. In a CombiWall, the pile is part of a system and will interact with loads and deformations of the other elements of the system, in this case mainly the infill sheeting.

With the large scale application of CombiWalls for the railway tunnel under the river Maas (Willemsspoortunnel) in Rotterdam (1987-1992), the first steps were made in methodically addressing the influence of the infill sheeting on the primary elements. The tensile forces that act on the interlocks, either caused by hydrostatic loads on the infill sheeting or by vertical misalignment of the piles, will tend to ovalise the tube.

The research for the application of the combined walls at the Willemsspoortunnel were laid down in a report by the Dutch railways (1988), which was later on the start document for the part on combined walls in ENV1993-5 Piling. The main conclusions were:

- Pile misalignments of 10mm/m, leading to ovalisation of the piles, can be accommodated without compromising the main bearing mechanism.
- Combination of pile-infill sheet needs to be reasonable (which for example means that very stiff infill sheet should not be combined with very thin walled piles).
- Selecting piles with D/t ratios > 100 should only be done with due care when pile misalignments need to be accommodated.

1.1.2 Current regulations in The Netherlands

In 2013 in the Netherlands the Handbook Quay Walls was updated by CUR (2013). The basis of this update were the design rules in the previous version, the ENV 1993-5 and the CUR test program on sand filled tubes. The rules lead to about the same economic designs for the tubes as before. Additional information is given on the effect of sand fill. In particular the sand fill has a positive effect on the critical curvature and the bending moment capacity. But since creep may cause decreasing the effect over time, the influence on the design is limited. Another important effect is the post critical behaviour. The drop of the bending moment is much less than without sand fill. This has an important effect on the safety of the CombiWall. Of course this effect is only substantial if the quality of the sand and its compaction complies with the requirements in the Handbook.

1.1.3 Eurocode 3

In order to be compatible with elastic CombiWall design, class 3 section requirements should be fulfilled. The EN 1993-1-1 requirements for class 3 are rather conservative. For elastic design (class 3) D/t is to be limited to $90\cdot(235/f_y)$. With regard to this, EN 1993-1-1 is much more conservative than ENV 1993-5 Piling and EN 1993-5 Piling in combination with EN 1993-1-6. The degree of conservatism depends on the $D/t\varepsilon^2$ value, where $\varepsilon^2 = 235/f_y$ and f_y = specified minimum yield stress.

Simple application of EN 1993-1-1 would mean that for the commonly used S355 piles D/t would be limited to 60, which would be much lower than the usual practice over the last decades in The Netherlands. In other European countries the situation is different. More stringent rules are used than in The Netherlands.

It is repeated that in over 30 years of application of the Dutch design practice no failures were reported as a result of local buckling of the primary element, the tube.

1.1.4 Application of EN 1993-5 (2008)

In EN 1993-5 (2008) the contents of attachment G of ENV1993-5 on local buckling verification is no longer present and instead trough attachment D2.2 (informative) reference is made to EN 1993-1-6 “Strength and stability of shell structures” section 8.5 and EN 1993-1-1.

Using table D-1 and figure D-2 from EN 1993-5 the forces from the secondary element (radial tensile force and bending moment) are translated to shell bending forces, basically in a similar way as previously with the ENV 1993-5.

The following verification step is essentially different. Whereas the ENV annex G used a “beam like” verification based on the main bending axis of the pile, but using reduction factors for local buckling and secondary element loading, the EN uses a shell-style verification where all section forces need to be converted to shell-style stresses (meridional stress, circumferential stress, in-plane shear stresses, meridional shear stresses, circumferential transverse shear stresses etc.). Next step is to determine the meridional, circumferential and shear buckling strength of the pile after which the total buckling check can be made using an interaction formula that combines all stress components.

The first applications of this code indicated that 10-20% larger wall thickness is required in order to meet the shell buckling verification compared to previous design practice where buckling was not considered to be critical under the D/t <100 mark.

This is a quite different approach for sheet piling/combined wall as these were normally designed and checked using a normal main axis bending criterion (“beam style”).

1.1.5 ETIB

Practically all codes as described above are based on piles that are not supported internally and or externally by soil. The EN 1993-5 only states that if a pile is filled with concrete or high grade compacted non-cohesive material, the full cross-sectional capacity may be used. As CombiWall piles are typically open-ended piles which are installed by vibrating or driving, a large part of the pile will be filled with natural soil layers. The requirements for these soil layers to be considered as “high grade compacted non-cohesive soils” are not clear. Also, piles installed in very stiff clay layers, which basically are cohesive soils but having high cohesion values, might have equivalent internal support compared to high grade compacted non-cohesive soils.

In order to give more specific guidelines on the effect of the soil support, the ETIB-study was done (ETIB = Enhanced economy of Tubular piles by improved Buckling design, published in 2009). Based on the shell-style verification of EN 1993-1-6 modified buckling parameters were defined that take into account the internal and/or external soil support.

The main trigger for the ETIB study was the 10-20% increase in wall thickness for designs using the EN 1993-5 compared to the previous designs based on the D/t <100 criterion.

- The ETIB study did not only address the issue of internal soil support, but also investigated the effect of imperfections and pressure distribution in- and outside the tube (section 8.3 A.1 of the ETIB report).
- From the examples in section 8.4 of the ETIB report it can be concluded that the gain for meridional buckling (buckling due to vertical compressive stresses) is relatively small (1,7% en 3,6%).
- For circumferential buckling (buckling caused by compressive ring stresses) the improvement is significant, but for normal CombiWall applications compressive ring stresses are relatively low and rarely governing for design.
- Based on the above the impression is that the ETIB-method does not significantly improve the buckling capacity. There are examples of projects where the initially prescribed EC + ETIB method has been replaced by previously used methods (CUR, EAU).
- Chapter 9 of the ETIB report states that the ETIB design rules will be included in the ECCS Red Book (European shell buckling recommendations) and that these rules from the Red Book will be included in next versions of EN 1993-1-6.

- Apart from the impression that the ETIB design rules do not significantly improve CombiWall economy, it is obvious that a lot of fundamental research has been done that can be used for the final recommendations in the Combitube-project.

1.1.6 Comparison of design codes

In the previous paragraphs a number of design methods and rules have been summarized, all of them dealing with local buckling in different ways.

The differences between the ENV1995-5 and the EN1993-5 with EN1993-1-6 can also be expressed in critical (compressive) strains, as is done in Figure 6.

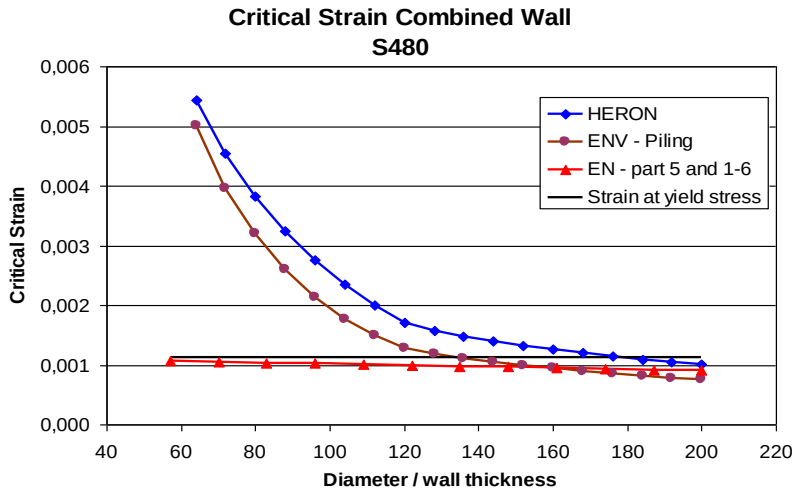

Figure 6 - Critical strains for tubes in steel S480; Heron is according to reference [4].

Although deformation capacity is not a priority in current design practice, it is an element that should be considered in the safety evaluation and in the guidelines. Apart from primary strength also robustness should play a role in the design.

General conclusions and observations are following:

- Current design of CombiWall piles, using EN 1993-5 and especially 1993-1-6 is much more complex compared to previous design methods (which have proved to be satisfactory and reliable on numerous projects).
- Current EN-codes appear to be quite conservative compared to previous design codes and design practice, even when considering the ETIB recommendations.
- Because of the complex and conservative nature of the EN-codes, a certain amount of reluctance can be observed with designers and clients in implementing the EN codes on their projects. There are examples where the older, proven design methods are favoured over the newer EN design methods.
- Because of the complexity, the current EN-codes are more an (detailed) engineering tool than a design tool.
- The shell-type verification of EN 1993-1-6 does not match well with the normal “beam style” verification (combined with various reduction factors for buckling, secondary elements) that is commonly used for earth retaining structures.
- Although the general impression is that the ETIB design rules do not significantly improve the CombiWall economy, it is obvious that a lot of fundamental research has been done that can be used for the design of CombiWalls.
- There is a need for simple and quick design tools, based on the starting point of utilizing the full elastic moment, relating this to allowable combinations of D/t and yield stress.

1.1.7 References

[1] Plantema, J.F, Collapsing stresses of Circular Cylinders and Round Tubes.

[2] De combi-wand en de invloed van hei-afwijkingen (the CombiWall and the influence of installation misalignment), F. Vahle, Dutch Railways Report, 1988.

[3] CUR (2013). “Handbook Quay Walls 2nd Edition.” Publication N. C211E, Centre for Civil Engineering Research and Codes (CUR), Gouda, The Netherlands.

[4] Gresnigt, A.M., Plastic Design of Buried Steel Pipelines in Settlement Areas, Heron, Vol. 31 (1986) No. 4.

[5] Gresnigt, A.M., C.H. Jo and S.A. Karamanos: Local buckling of tubular sections in structural applications. The 2011 World Congress on Advances in Structural Engineering and Mechanics (ASEM'11+), 18-22 September 2011 in Seoul, Korea.

[6] Chen L. (2011). "Buckling of circular cylindrical shells under different loading conditions." *PhD Thesis*, The University of Edinburgh.

[7] ECCS EDR6 (2008) European Recommendations for Steel Construction: Buckling of Shells, 5th edition, Edited by J.M. Rotter and H. Schmidt, European Convention for Constructional Steelwork, Brussels.

[8] EN 1993-1-1 (2003) Eurocode 3: Design of steel structures, Part 1.1: General rules and rules for buildings, Eurocode 3 Part 1.1, CEN, Brussels.

[9] EN 1993-1-6 (2007) Eurocode 3: Design of steel structures, Part 1.6: General rules - Strength and stability of shell structures, Eurocode 3 Part 1.6, CEN, Brussels.

[10] Gall W. (2011) "RFCS Combitube Project - Overview design practice" *Memo*, BAM Infraconsult bv, Gouda, Netherlands.

[11] Rotter, J.M. (2007) “Recent advances in the philosophy of the practical design of shell structures, implemented in Eurocode provisions”, in Recent Developments in Structural Engineering, Mechanics and Computation, ed A. Zingoni, Millpress publishers, Rotterdam.

[12] Rotter, J.M. (2011) “Shell buckling design and assessment and the LBA-MNA methodology”, Stahlbau, Vol. 80, Heft 11, Nov., pp 791-803.

[13] Schmidt, H. and Rotter J.M. (2008) “Cylindrical shells of constant wall thickness under general loading” in Stability of Steel Shells: European Design Recommendations: Fifth Edition 2008, European Convention for Constructional Steelwork, Brussels, Oct. 2008, pp 167-216.

1.2 Task 1.2: Selection of parameters and construction details for further study

In practical applications the following ranges of tubes are applied.

- Diameter to wall thickness ratios mainly between 70 and 100 with possible extensions to D/t=50 and D/t=120.
- Steel grades mainly between S355 and S460 according to European standards with possible extensions to S235 and higher strength steels up to specified minimum yield strength of 480 MPa. It is noted that often API steel grades are applied: X42 up to X70 with specified minimum yield strength of 290 MPa and 483 MPa. X80 tubes are produced for pipelines.
- Loading in bending and normal force. Typical normal forces can be as high as 25% of the plastic normal force capacity

1.2.1 Construction details

In the proposal several construction details are mentioned as candidates for further investigation. More examples of CombiWalls were collected. Some are illustrated in next Figures.

Figure 7 - New quay wall in harbour extension Rotterdam into the North Sea.

Figure 8 - Wilhelmina quay wall Groningen, The Netherlands.

Figure 9 - A4 Motorway underpass (highway between The Hague and Amsterdam).

Figure 10 - A4 Ringvaart Aquaduct (highway between The Hague and Amsterdam; the Ringvaart is the canal around the Haarlemmermeer polder, where the airport Schiphol is situated)

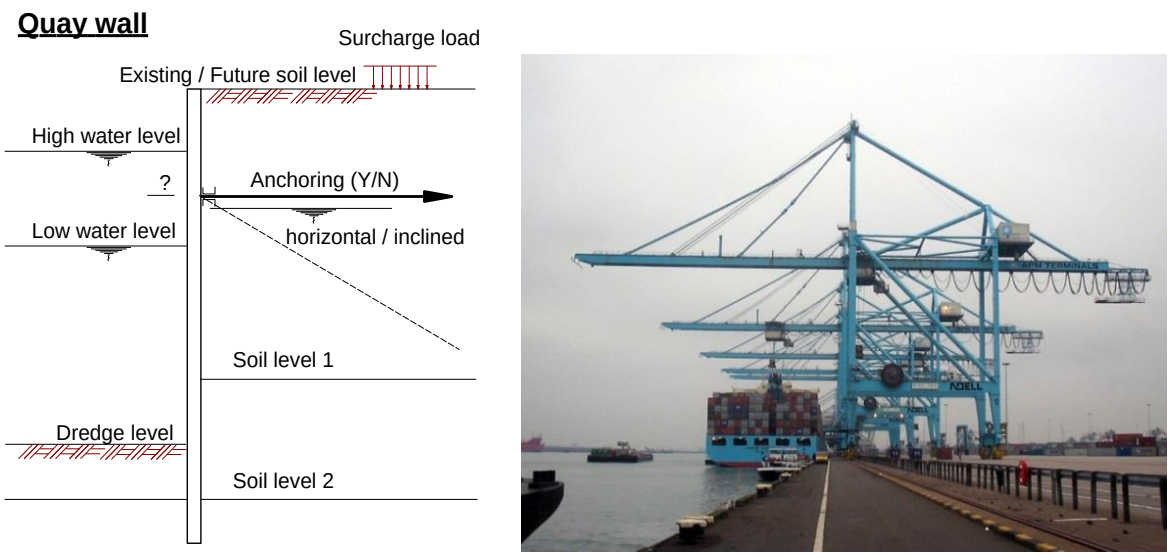

Figure 11 - An example of a CombiWall with loads.

In the meetings of the consortium many candidates for tubes with “selected details” to be tested were discussed at length. Another point of discussion was the number of pure bending tests compared to the tests with selected details.

In the original WP3 the following test programme is foreseen:

- TU-Delft: 8 tests in task 3.1: pure bending
- KIT: 6 tests in task 3.2: bending with selected construction detail
- TU-Delft: 6 tests in task 3.3: bending with selected construction detail
- Total tests: 8+6+6=20 tests

After intensive discussion it was concluded that the project should concentrate on pure bending of spirally welded tubes. An important reason is that there are only very limited test results available on those tubes. Therefore it was proposed to modify the test program accordingly. The final test set up in Karlsruhe includes a (small) normal force. More details are in chapter 3 (WP3).

1.3 Task 1.3: Collection and evaluation of bending test results and load introduction

Relatively few bending tests have been performed on spirally welded tubes. Three studies were found, of which two were sufficiently documented. Zimmerman et al. (2004) and Zimmermann et al. (2013) each performed four-point bending tests on four spirally welded tubes, all in the 48-64 D/t range, which is on the lower end of what is considered relevant for the current investigation.

These studies were focused on line-pipe applications of spiral-welded tubes, and therefore included internal pressure in half of the tests, which further reduces the relevance of these tests for combined wall applications. Both studies concluded that the performance of the spirally welded tubes was satisfactory. Preliminary results of bending tests on spirally welded tubes are presented by Fonzo et al. (2011). Also in this case, line-pipe applications were the project focus, resulting in relatively stocky tubes, and two out of three tests included internal pressure. These results are not sufficient to obtain a good insight into the bending behaviour of spirally welded tubes, since they are partly out of the scope of the current research and too few in numbers.

When the scope is broadened to local buckling of tubes in general, many reports and publications on test results are available and have been collected. The available test results are evaluated for their quality (completeness of basic information such as material properties, tube geometry, test setup, measurements of forces and deformations, reporting). A data base has been formed of local buckling results; most are on longitudinally welded tubes. Subsets are formed to investigate particular influences.

The test results in the database show large scatter, both in critical strain (curvature) as in strength (bending moment capacity).

In Figure 12 test data are presented as collected in the Combitube project and compared with the present ENV 1993-5 equation for local buckling:

$$\varepsilon_{cr} = 0,25\frac{t}{r_o} - 0,0025 \qquad \text{for} \quad \frac{r_o}{t} \leq 60 \tag{1}$$

$$\varepsilon_{cr} = 0,10\frac{t}{r_o} \qquad \text{for} \quad \frac{r_o}{t} \geq 60 \tag{2}$$

Where for pure bending:

$$r_0 = r \tag{3}$$

For pure bending the effect of ovalisation can be neglected. The reason is that the validation of these equations is done on pure bending tests, where ovalisation due to pure bending was included, so that in this case: $r_0 = r$.

The critical curvature follows from:

$$C_{cr} = \frac{\varepsilon_{cr}}{r_o} \tag{4}$$

The results that are below the design equation line are due to several influences such as large misalignment at girth welds. Also the measuring length may have a large effect on the critical compressive strain, since local buckling will occur at the cross section where the plastic moment is the smallest. In case of short measuring length it results in higher compressive critical strains than in longer measuring lengths, because the compressive critical strain is taken as the average over the measuring length.

Note that the scales in this figure as logarithmic. The red line is the equation(26).

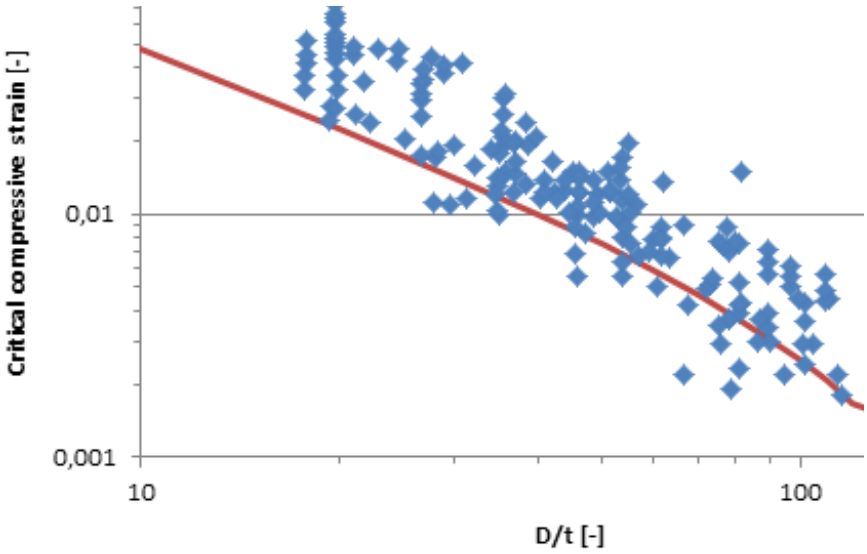

Figure 12 - Scatter in test results in pure bending as collected in the Combitube project, compared with equation (26). The red line is the equation (26). Note that the scales in this figure are logarithmic.

The results of the database are used in the development of design guidelines and evaluations of the test results in the Combitube project.

1.3.1 References

[1] Zimmerman, T., Xei, J. Timms, C., Asante, J., 2004. : Buckling resistance of large diameter spiral welded linepipe", Proceedings of the International Pipeline Conference (IPC) Calgary, Canada

[2] Zimmermann, S., Karbasian, H., Knoop, F.M., 2013. "Helical Submerged Arc Welded Line Pipe Engineered For Strain Based Design", Proceedings of the International Offshore and Polar Engineering Conference (ISOPE), Alaska, USA.

[3] Fonzo, A., Lucci, A., Ferino, J., Di Biagio, M., Spinelli, C.M., Flaxa, V., Zimmermann, S., Kalwa, C., Knoop M. (2011), "Full scale investigation on strain capacity of high grade large diameter pipes. Proceedings of the 18th JTM, San Francisco, USA

1.4 Task 1.4: Evaluation of existing numerical methodologies for elastic-plastic shell buckling

In this task available numerical methods to describe the bending behaviour of tubular members are examined in terms of their ability to predict the behaviour against experimental data. The accurate modelling of non-linear material behaviour as well as possible anisotropies is examined and discussed. The most suitable numerical methods for simulating the bending and local buckling behaviour of tubular members in the strain-hardening range will be identified in terms of constitutive models, type of finite elements and nonlinear analysis procedures.

There are two contributions:

- University Thessaly by Spyros A. Karamanos, Daniel Vasilikis, Patricia Pappa and Aglaia Pournara
- University Edinburgh by Michael Rotter and Adam Sadowski

1.4.1 Evaluations at the University of Thessaly

In task 1.4, numerical issues are examined related to modelling of the structural behaviour of steel tubes, candidates for CombiWall applications, subjected to longitudinal bending, towards selecting

the most efficient methodology for simulating experiments and conducting the numerical parametric analyses.

1.4.1.1 Description of the physical problem

The accurate prediction of buckling strength and deformation is a crucial issue towards safeguarding the structural integrity of these cylinders under bending. Elongated steel cylinders ovalise, resulting in loss of bending stiffness and limit point instability in the moment-curvature diagram, referred to as "ovalisation" or "Brazier effect" [1] have shown that the axial stress at the compression side may cause bifurcation instability (buckling) in the form of wave-type wrinkles usually before reaching an ovalisation limit moment. Due to ovalisation a multi-axial stress/strain state exists in the buckling zone. Moreover, buckling occurs in the plastic range. First yielding offers a non-reliable measure of bending strength and deformation. Towards determining the ultimate capacity of a bent tube, the curvature at which buckling would occur should be determined. Experimental and numerical works has demonstrated that for rather thick-walled cylinders, with D/t values below 50, tube wall wrinkling may not be catastrophic, allowing for significant inelastic deformations and, eventually, a limit-moment instability [2][3]. Beyond the limit point, stiffness is reduced and at a certain point the cylinder would fail because of localized deformation. On the other hand, thinner cylinders with D/t at the range of 70÷140, commonly used in CombiWalls, usually exhibit a secondary bifurcation and buckling localization, before a limit moment is reached.

1.4.1.2 Numerical simulation of tube bending

The response of steel tubes under bending can be examined semi-analytically with special purpose methodologies [3], as well as numerically using nonlinear finite element tools. One may use general-purpose finite element codes, but also in-house methodologies [4][5].

Shell or solid elements can be used in order to simulate the tube. For the purposes of the present analysis, because of the geometry of tubes used in CombiWall applications (70≤D/t≤140), shell elements should be used, whereas the use of solid (3D) elements is not recommended. Shell finite elements can be either linear or quadratic depending on the type of the in-plane interpolation functions. The linear type elements consist of two nodes in each direction, whereas the quadratic-type elements contain three nodes. In linear elements, the displacement can only vary linearly from one node to another, while in quadratic elements the shape function for the displacement field varies quadratically between the corner nodes. Naturally, a linear element is computationally more efficient than a quadratic element due to lower computational cost [7][8]. In those elements, the use of reduced integration elements is recommended, reducing the computational cost, with better accuracy for the calculation of stresses [6][9]. Linear reduced integration shell elements (S4R in ABAQUS) have shown satisfactory accuracy combining low computational cost in predicting stresses and strains in tubes under bending [7][8]. Quadratic elements can also be used.

1.4.1.3 Finite element mesh

An adequate number and size of elements has to be used in locations where stress raisers and discontinuities exist, to describe accurately abrupt variation of stress and strain. The number and size of elements to be used in the analysis within the buckling wavelength has to be also defined. The number and size of elements depends on whether one uses linear or quadratic elements [7][8]. Special attention should be given to symmetry conditions imposed by the user, because critical buckling shapes might not be symmetric [10]; in such a case, the use of a symmetric mesh may result in loss of buckling modes, leading to unrealistic results.

1.4.1.4 Constitutive modelling and detection of buckling

To examine the bifurcation of a shell deformed in the inelastic regime, the positive-definitiveness of the tangent stiffness matrix should be checked [11]. In thick-walled shells, to obtain accurate predictions, the moduli of a material model more elaborate than the J_2-flow plasticity model should

be used [11], e.g. the J_2-deformation moduli. However, for the range of interest (D/t greater than 70), the J_2-flow theory moduli can be used, without loss of accuracy.

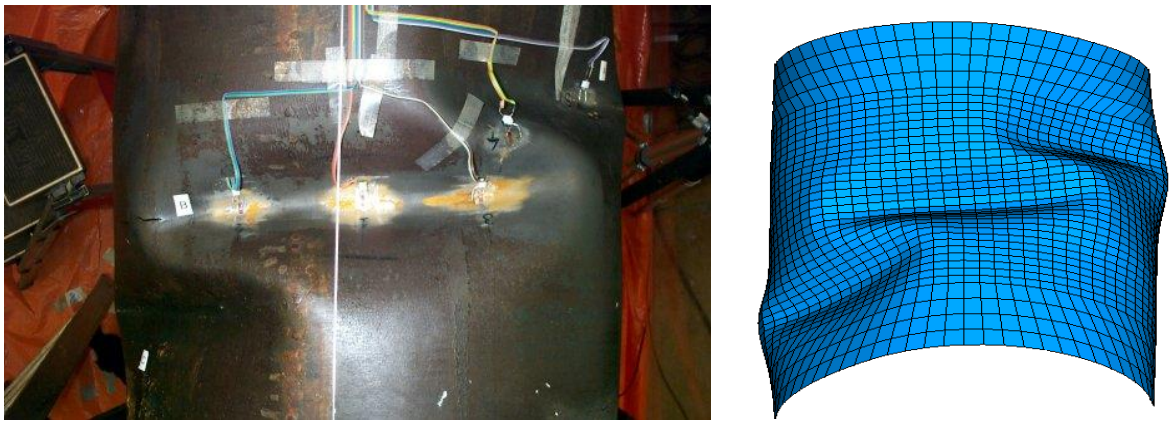

Figure 13 - Simulation of buckling formation, in a bending test of a 24-inch-diameter tube (D/t=72); from Dama et al. (2007), [8].

1.4.1.5 Type of analysis

(1) Ovalisation (2D) analysis: This is practically a two-dimensional finite element model: a small-length tube segment is assumed usually with a small number of elements longitudinally, so that no variation of loading and deformation exists in the tube axial direction. This analysis will provide the moment-curvature path or "ovalisation" path, with a limit moment instability, excluding tube wall wrinkling phenomena.

(2) Uniform wrinkling analysis: For the purposes of such an analysis, it is sufficient to analyse only a tube segment of half-wavelength with appropriate symmetry boundary conditions. Buckling wavelength is not known a priori and, therefore, a sequence of analyses should be conducted. The actual wavelength L_{hw} is the one that corresponds to the "earliest" bifurcation.

(3) Secondary bifurcation analysis: In relatively thin-walled tubes (D/t>70) after the occurrence of uniform wrinkling, a second bifurcation occurs. To simulate this, a tube segment of 1 wavelength ($2L_{hw}$) and appropriate symmetry conditions should be considered.

(4) Local buckling formation analysis: To simulate localization of buckling, it is necessary to analyse a significant length of the tube. The entire cross-section and length (or at least a significant length) of the tube may need to be simulated, because buckling shape may not be symmetric. To trigger local buckling, imperfection in the form of uniform wrinkles should be imposed.

A displacement-controlled procedure is usually used when the post-buckling path is unstable, exhibiting a ''snap-through" behaviour. In cases where post-buckling is highly unstable, exhibiting ''snap-back', the arc-length method (also referred as "Riks algorithm" [13]) should be employed.

1.4.1.6 Required tests and measurements for model calibration

To simulate tube behaviour under bending and reproduce full-scale experimental results, several tests on the steel material level and initial measurements on the specimens are necessary. For determining material yield and ultimate strength, strip specimens for tensile testing should be manufactured out of tubular members. Anisotropy can be implemented using Hill's yield function instead of von Mises using appropriate tests.

Measurements of initial imperfection are required in the following form: 1) Deviation from straightness (along tube generators), 2) Deviation from roundness (in tube sections), 3) Initial local wrinkling, 4) Tube wall distortion, 5) Wall thickness variations.

Residual stresses should be incorporated in numerical models as initial stresses. In spiral-welded tubes residual stresses come from (a) cold bending of plate and (b) welding along the spiral seam. To determine the longitudinal residual stresses on a tube, strips along the longitudinal tube axis can be extracted, whereby the deflection at each strip can be measured for the calculation of the residual stresses. However, after evaluation of the available methods for residual stress measurement, it was decided to apply the hole drilling method. In addition, ring cutting tests were performed whereby a short part of the tube (about 100 - 200 mm) was cut longitudinally. The opening after cutting gave information on the residual stresses. Also FEA modelling was performed to simulate the forming process of spirally welded tubes and to determine the residual stresses.

1.4.1.7 References

[1] Brazier, L.G., (1927). "On the flexure of thin cylindrical shells and other ''thin sections''. *Proceedings of the Royal Society*, Series A 116, 104–114.

[2] Kyriakides S. and Ju, G. T. (1992). "Bifurcation and Localization Instabilities in Cylindrical Shells under Bending I: Experiments". *Int. J. Solid & Structures*, Vol. 29, pp. 1117-1142.

[3] Ju, G. T. and S. Kyriakides (1992). "Bifurcation and Localization Instabilities in Cylindrical Shells under Bending II: Predictions". *Int. J. Solid & Structures*, Vol. 29, pp. 1143-1171.

[4] Karamanos, S.A. (2002). "Bending Instabilities of Elastic Tubes", *International Journal of Solids and Structures*, Vol. 39, No. 8, pp. 2059-2085.

[5] Houliara, S. and Karamanos, S.A. (2006). "Buckling and Post-Buckling of Pressurized Thin-Walled Elastic Tubes under In-Plane Bending". *Int. J. Nonlinear Mechanics*, Vol. 41, No. 4, pp. 491-511.

[6] Hibbit, H.D., Karlsson, B.I., and Sorensen, P. (2007). *Theory Manual*, ABAQUS, version 6.7, Providence, RI, USA.

[7] Tsouvalas, D., (2003). "Finite Element Analysis of Industrial Pipes under Pressure and Bending Loads," M.Sc. Diploma thesis (in Greek), Department of Mechanical & Industrial Engineering, University of Thessaly, Volos, Greece.

[8] Dama, E., (2005). "Fatigue of Locally Buckled Underground Steel Pipelines. Finite Element Simulation and Design". Diploma thesis (in Greek), Department of Mechanical & Industrial Engineering, University of Thessaly, Volos, Greece

[9] Zienkiewicz, O.C., (1977). *The Finite Element Method*, Third Edition, Tata McGraw-Hill, New Delhi.

[10] Dama, E., Karamanos, S.A., and Gresnigt A.M., (2007). "Failure of Locally Buckled Pipelines", Journal of Pressure Vessel Technology, ASME, Vol. 129, No. 2, pp. 272-279.

[11] Gellin, S., (1979). Effect of an axisymmetric imperfection on the plastic buckling of an axially compressed cylindrical shell, ASME J. Appl. Mech. 46, 125–131.

[12] Batterman, S.C., (1965). Plastic buckling of axially compressed cylindrical shells, AIAA Journal, 3, 316-325.

[13] Crisfield, M.A., (1983). "An arc-length method including line searches and accelerations". *International Journal for Numerical Methods in Engineering,* 19, 1269–1289.

1.4.2 Evaluations at the University of Edinburgh

The Edinburgh team performed an exhaustive set of rigorous numerical experiments to investigate the performance of the ABAQUS finite-strain reduced-integration S4R shell element in the accurate modelling of thick shell behaviour and elastic-plastic shell buckling.

Since ABAQUS is the dominant commercial program used by high level researchers in the fields of buckling and plasticity in structural engineering, it is critically important that its predictions should be

explored to identify how well they meet the needs of tubular members under global bending with plasticity, as is relevant to Combitubes.

The question of plasticity in thicker tubular members under bending cannot be divorced from the question of the relative thickness of the tube, and the issue of when such a tube can be represented as a thin shell and when solid elements are required. This aspect formed a major study at Edinburgh, leading to a peer-reviewed journal publication that clearly identifies when the shell treatment is reliable (Sadowski and Rotter, 2013, [1]). The analyses of buckling were conducted with huge attention to the details of the final buckling predictions after extensive yielding and strain hardening. The overall conclusion was that quite thick tubes can be very accurately modelled using well-chosen shell elements. The uncertainties associated with material property variations and geometrical imperfections greatly outweigh any doubts that can arise from such modelling questions.

The S4R element in ABAQUS was found to perform very well and was accepted for use in all the numerical studies at Edinburgh. The findings were presented to the partners and in the international journal (Sadowski and Rotter, 2013, [1]).

1.4.2.1 References

[1] Sadowski A.J. and Rotter J.M. (2013). “Solid or shell finite elements to model thick cylindrical tubes and shells under global bending.” International Journal of Mechanical Sciences, 74, 143-153.

2 WP2: Specimen selection, test set-up, test design and material testing

The objectives of WP2 were the following:

- To select, order and prepare the specimens for testing and to design the test set-ups.
- To conduct material testing to determine the material properties which are necessary for the interpretation of the test results in the numerical work (WP4) and for the setup of the design guidance (WP6).
- To determine the geometrical imperfections and residual stresses that must be taken into account.

2.1 Task 2.1: Selection of test specimens and design of test set-up

2.1.1 Selection of test specimens

In the RFCS proposal two steel grades e.g. S355 and S460 and diameters up to 700 mm were foreseen. The total number of tests in the program was 21 (15 in Delft and 6 in Karlsruhe).

In WP1 a survey was done on the application of spirally welded tubes in CombiWalls. Based on these results it was decided to aim at testing in the following combinations. The focus was on high strength and high D/t ratios, in particular combination 4.

1. Low yield strength Low D/t Tests: 2	2. High yield strength Low D/t Tests: 5
3. Low yield strength High D/t Tests 6	4. High yield strength High D/t Tests: 8

A selection was made of candidates for the tests on the basis of available spirally welded tubes in stock at ArcelorMittal Projects in Heijningen in The Netherlands.

It appeared that in particular for the combinations with high yield strength (2. and 4.) only larger diameter tubes are available than anticipated: 1067 mm versus 700 mm. This will give much more steel and larger and stronger test rigs than was foreseen. The plastic moment increase is about (1067/700)^3 = 3,5. On the other hand, testing larger diameters is expected to provide more convincing results.

Finally a set of tubes was selected, based on the above table and based on the available tubes. The details of the tested tubes are in the tables in par. 2.1.3 and 2.1.4.

The specified minimum yield strength (SMYS) of the steel grades in the tables is:

X52: 359 MPa
X60: 414 MPa
X70: 483 Mpa

2.1.2 Shift of larger specimens to Delft and smaller specimens to Karlsruhe

For reasons of efficient cost effective performance of the testing, it was agreed that all large diameter (1067 mm) tests would be performed in Delft and the smaller diameter (820mm and 863mm) tests in Karlsruhe. This resulted in a total of 8 tests in Karlsruhe and 13 tests in Delft. In Delft two extra tests were performed on longitudinally welded tubes (D15 and D16 in Table 1).

In Delft the set-up is on pure bending, while the set-up in Karlsruhe is on bending with a (small) normal force.

2.1.3 Selection of test specimens and design of test setup in Delft

The testing program in Delft (see Table 1) has been extended with two longitudinally welded tubes on initiative and cost of TU-Delft. The results have been included in the analyses since they are considered relevant for the Combitube project, since the addition of these tests offers a direct comparison between the behaviour of spirally welded and longitudinally welded tubes.

The main variables in the test program were:

- Diameter / wall thickness ratio
- Steel grade
- Circumferential weld
- Coil connecting weld (weld where two plates from the coil are welded to achieve a continuous tube making process)

Table 1 - Overview of testing program in Delft.

Test Nr.	D x t [mm]	Grade	Specimen layout
D1	1067x16	X70	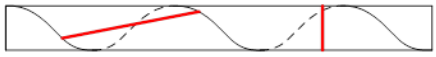
D2	1067x16	X70	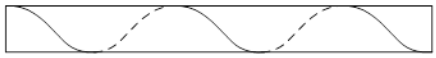
D3	1067x9	X60	
D4	1067x9	X60	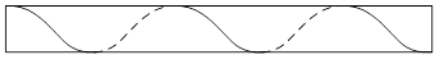
D5	1067x9	X60	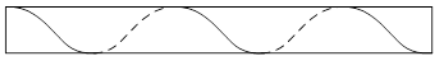
D6	1067x13.5	X60/X52	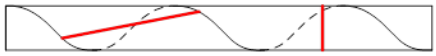
D7	1067x13.5	X60/X52	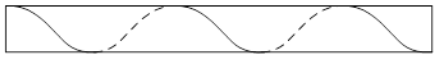
D9	1067x16	X70	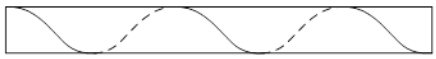
D10	1067x16	X70	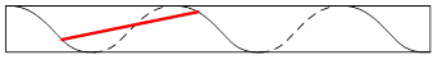
D11	1067x9	X60	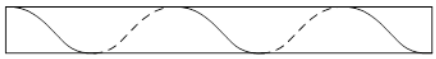
D12	1067x9	X60	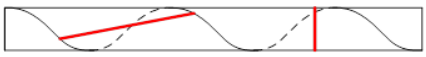
D13	1067x9	X60	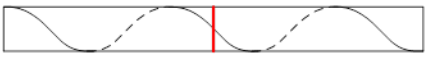
D14	1067x9	X60	
D15	1067x10	X60	Longitudinally welded (UOE) - Plain
D16	1067x15	X70	Longitudinally welded (UOE) - Plain
Note that there is no test called D8. Total number of tests is 15.			

Test D14 was open at the Mid-term report. In the discussions for test D14 a test with a concrete plug was proposed to simulate the situation near the top of the CombiWall and at the location of an anchor. After discussion in the consortium it was decided to skip the test with the plug and instead test an extra tube with a girth weld (as in D13) to obtain more information about scatter. It was considered that the concrete plug would be object of the FEA in WP5.

In this list is no test D8, because of the shift of test specimens between Delft and Karlsruhe. The resulting total number of tests on spirally welded tubes in the table is 13. This is 1 more than in the original contract.

When setting up the test plan all tests had 9 mm wall thickness or 16 mm. In the table there are also 13.5 mm wall thickness test specimens. The main reason is that it appeared hard to find suitable tubes with coil connecting welds in 16 mm wall thickness. Such coil connecting welds were found in the 13.5 mm wall thickness tubes.

All in all there are only a couple of duplications. It must be noted that some duplications are quite useful in view of the large scatter that is found in local buckling testing. As initial imperfections and actual dimensions are carefully measured, also nominally the same specimens are quite useful for the validation of the FEA models.

2.1.3.1 Design of test setup in Delft

The test setup for tubes with diameter 1067 mm in Delft is given in Figure 14. The test rig was designed for 30% higher yield strength than the specified minimum values of the strongest tube, while the stroke of the hydraulic cylinders was such that they could accommodate about two times the critical compressive strain according to the ENV1993-5 design rules.

In the test setup it is important to avoid influences of load introduction as much as possible. To that aim thin steel straps were used that minimise possible indents of the tube wall and ovalisation due to load introduction and to minimise the risk of local buckling at the load introduction points.

Furthermore, the load in the straps close to the centre is kept small in order to further minimise the risk of local buckling at the load introduction points. The measuring length is chosen quite long to study the effect of possible variations of the tube properties, e.g. on both sides of a girth weld.

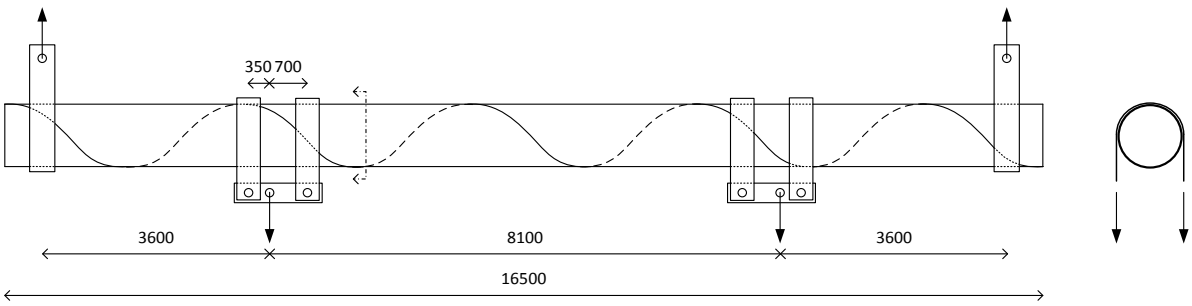

Figure 14 – Design of test set-up in Delft in 4-point bending.

The influence of localised ovalisation stretches about 3 – 4 diameters depending on the D/t ratio. However, because of the very limited size of the ovalisation at the load introduction points, the final ovalisation in the centre measuring part is minimal.

In previous testing in other research projects in Delft, using similar bending test setups, local buckling always occurred away from the load introduction points.

Figure 15 shows the actual test rig. In chapter 3 of this final report an extensive description is given of the equipment for measuring imperfections, forces and deformations.

Figure 15 – Test rig in Delft in 4-point bending.

2.1.4 Selection of test specimens and design of test setup in Karlsruhe

Object of the tests were 8 spirally welded steel tubes, named K1 to K8, with a length of 10500 - 10520 mm that were tested in bending with normal force. The outside diameter of the specimens varied from 820 – 863 mm with D/t-ratios ranging from 73,5 to 101,5.

The steel grades were X52. The actual mechanical properties were measured in own material tests. Table 2 shows a summary of the specimens. Besides the dimensions of the specimens the table contains information on weld specifications such as the positions of coil connecting welds. In the case of test K7 the specimen consisted of two different tubes that were connected with a girth weld in the centre of the specimen. The specimens were provided by the project partner ArcelorMittal.

Table 2 - Summary of specimens.

Specimen	Material	Dimensions D x t [mm]	Length [mm]	Welds
K1	X52	820 x 11	10500	Coil connecting weld at the end
K2	X52	820 x 11	10500	Coil connecting weld in the centre
K3	X52	820 x 8	10500	Coil connecting weld at the end
K4	X52	820 x 8	10500	-
K5	X52	820 x 8	10500	Coil connecting weld in the centre
K6	X52	863 x 8,4	10500	Coil connecting weld in the centre
K7	X52	863 x 8,4	10500	Girth connecting weld in the centre
K8	X52	863 x 8,6	10500	-

Most of the tubes possessed coil connection welds at different positions which have to be taken into account when evaluating the test results. The available length of tubes led to a uniform specimen length of 10500 mm. Additional material samples were available at least for one of the ends of each specimen.

Additional material samples had to be taken from the specimens after testing. Since most of the cross section of the test tubes was strained beyond the yield strain during the tests, the additional material samples were taken from a location close to the neutral axis at the specimen ends.

Figure 16 - K1: Coil weld at the end, K2: Coil weld in the centre.

2.1.4.1 Design of test setup in Karlsruhe

The test setup has been designed as a frame construction, see Figure 17. The main objectives of the frame construction were to construct a test rig where normal forces and bending moments could be introduced at the same time. Due to the overall dimensions, the test rig was installed outdoors. The frame consisted of the specimen tube, two brackets at each end of the tube and a pulling device. The pulling device was powered by up to 4 hollow piston cylinders with a maximum force of 1 MN and a maximum stroke of 800 mm.

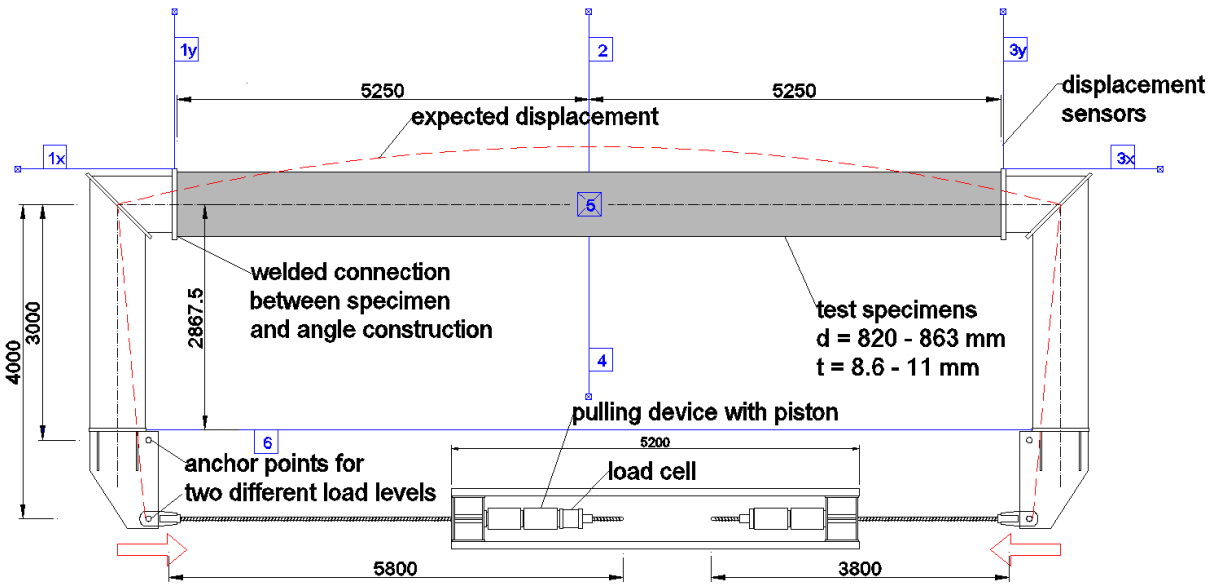

Figure 17 - Test setup, pulling device, support scheme and position of displacement transducers.

The frame was supported at four points: at the vertical plates at the ends of the longer bracket parts and at the vertical plates in the corner of the brackets. A support consisted of two Teflon layers on a heavy and plane steel plate served as a slip plane. This detail of the test setup is shown in Figure 18. The teflon supports did not restrict any movement. They provided a floating support for the frame construction. The point of rest during the execution of the tests was at the pulling device which was ballasted with a connected heavy steel beam section, which can partially be seen in Figure 18.

The tube and the angle constructions are connected by a circumferential weld to guarantee the full traceability of forces. The angle construction provides two anchorage points for the pulling device

with a distance to the centre of the tube of 3 m and 4 m to realize two different ratios of normal force and bending moment.

The overall movement of the specimen tube and the bending deformation are controlled by several displacement sensors (no. 1 to no 6.) to calculate rigid body movement, deflection and ovalisation of the tube. The resulting force in the test rig due to the cylinders stroke is taken up by a load cell applied at one of the tension rods. Furthermore, strains at different locations are monitored during testing.

Figure 18 – Overview of test rig in Karlsruhe with buckled test K1.

2.2 Task 2.2: Ordering and manufacturing of test specimens

The selection of tubes and the ordering has been done in close cooperation with partners in the project. In previous sections information is given on the development of the test matrix for Delft and for Karlsruhe.

The selected tubes for Karlsruhe (K1-K8) represent the whole range of types of spirally welded tubes concerning the possible coil connecting welds. It was expected that the tests and their evaluation reveals the influence of the coil connecting welds on the resistance in bending and normal force. The welds were in general of very uniform geometric appearance. No welds of obviously poor quality were found.

The tubes for the tests in Karlsruhe were provided by ArcelorMittal with no further construction details. The test length as delivered was 10.50 m. The original length was more. Leftovers were provided for material testing.

2.3 Task 2.3: Material testing of tube material

Both in Delft and in Karlsruhe material testing has been done. Also material testing was done in U-Thessaly.

2.3.1 Material testing of tube material in Delft

Testing of material mechanical properties has been carried out on material from the test specimens themselves from a relatively undisturbed area (see Figure 19). These test plates always include a spiral weld so that the orientation of the test specimens could be based on the weld.

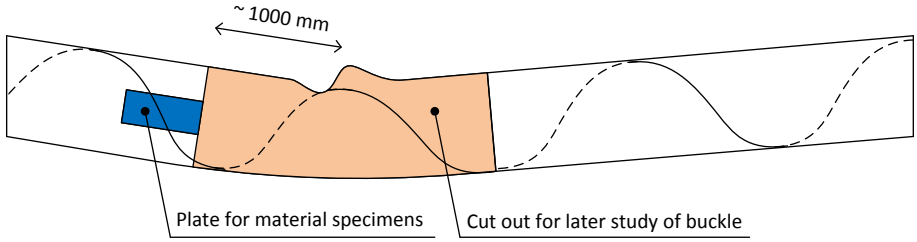

Figure 19 - Location of material specimens on four point bending test specimens.

2.3.1.1 Test specimens for material testing

Based on the preliminary testing program as reported in the Mid-term report, it was decided to proceed in Delft with tensile tests on all tubes in four configurations:

- Longitudinal direction, inside of tube wall
- Longitudinal direction, outside of tube wall
- Circumferential direction, inside of tube wall
- Circumferential direction, outside of tube wall

In addition, tensile tests on the weld material of the spiral weld have been performed for a selection of tubes.

Full thickness tensile tests that are also oriented parallel and perpendicular to the spiral weld have been performed by U-Thessaly.

The tensile specimens have been dimensioned according to NEN-EN-ISO 6892-1 (2009). The compression tests have been dimensioned based on earlier testing by Gresnigt et al.

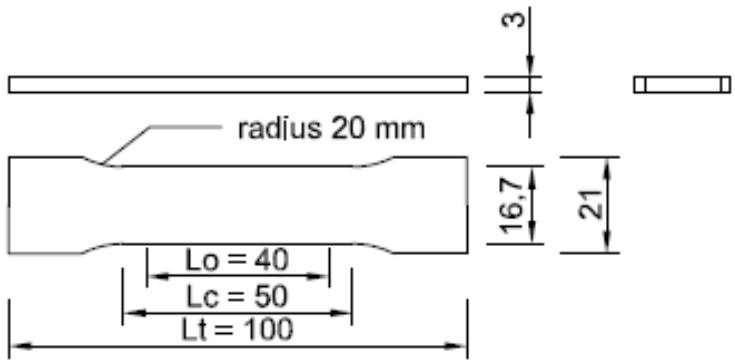

Figure 20 - Overview of material tensile testing specimens dimensions.

2.3.1.2 Tensile and compression test set-up

An overview of the test setup for tensile testing used by TU-Delft is shown in Figure 21.

Figure 21 - Overview of tensile test setup (two figures left) and compressive setup by TU-Delft.

In addition to the tensile tests, compression tests have been performed. The tests were performed in the same testing rig as the tensile specimens, but a special tool was added to sufficiently clamp the specimens to prevent premature buckling. During the tests, the force and cylinder displacements were monitored. Each specimen was equipped with three strain gauges to directly measure the strain of the steel (see Figure 22). Tensile tests have shown that tubes with similar diameter and wall thickness have very similar material behaviour. This is likely due to the tubes being from the same production batch. For this reason, compression tests have only been performed on one tube of each batch, in the same orientation and position as the tensile tests:

- Longitudinal direction, inside of tube wall
- Longitudinal direction, outside of tube wall
- Circumferential direction, inside of tube wall
- Circumferential direction, outside of tube wall

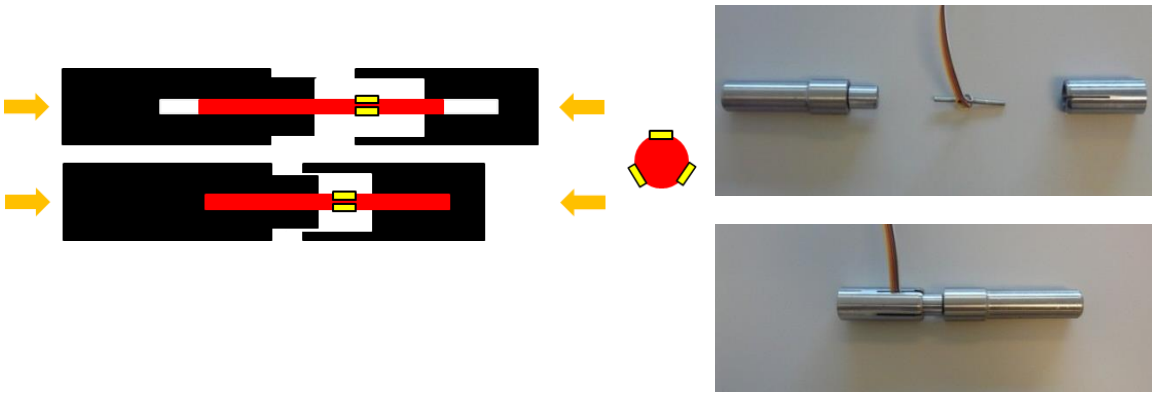

Figure 22 - Overview of restraining tool for compressive tests.

2.3.1.3 Test results

The tensile tests show very accurate stress-strain diagrams up to 2% strain. After this, the local strain measurements are out of range, and the strain can only be calculated from the cylinder displacement. This is only useful to study the overall shape of the diagram, but does not provide an exact stress strain diagram. All tensile tests that were to be performed are completed. A selection of typical test results is shown in the figures below. The actual test results of each tube were used in the simulation of bending tests as reported in WP4 and WP5.

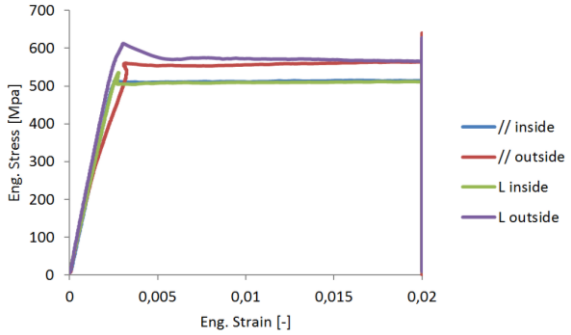

Figure 23 - Tensile test results of specimen T1D9.

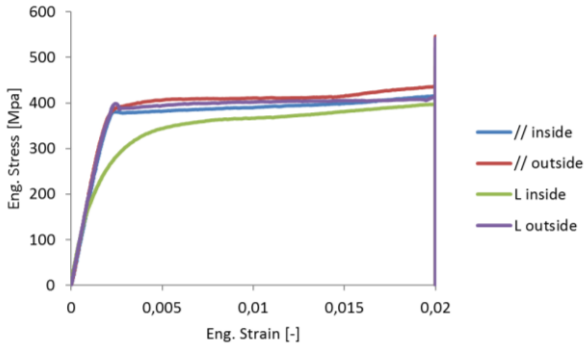

Figure 24 - Tensile test results of specimen T3D13.

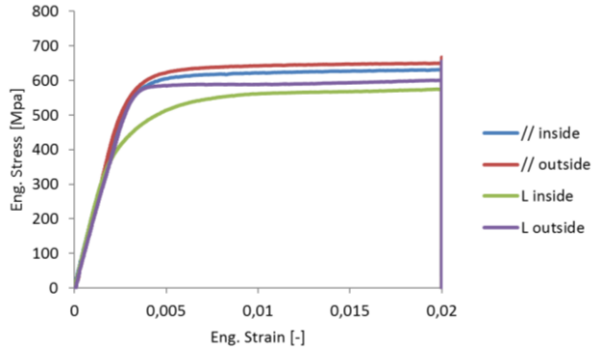

Figure 25 - Tensile test results of specimen T7D1.

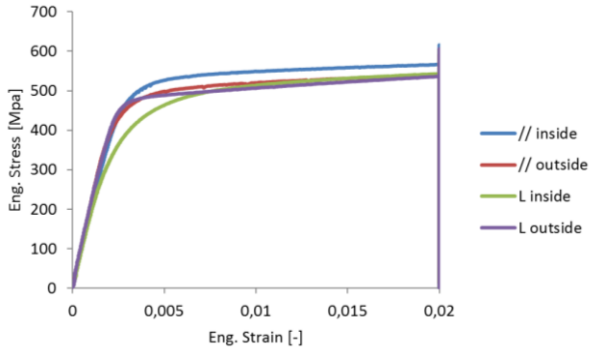

Figure 26 - Tensile test results of specimen T10D6.

For each specimen the yield strength ($f_{0.2\%}$) and tensile strength (f_t) are compared with the average value of that specimen or specimen part in the specific direction of the specimens (longitudinal or circumferential) in Figure 27 and Figure 28. The data shows that there is quite some influence of the location and orientation of the specimens with regard to yield strength ($f_{0.2\%}$) but for most specimens hardly any influence on the tensile strength.

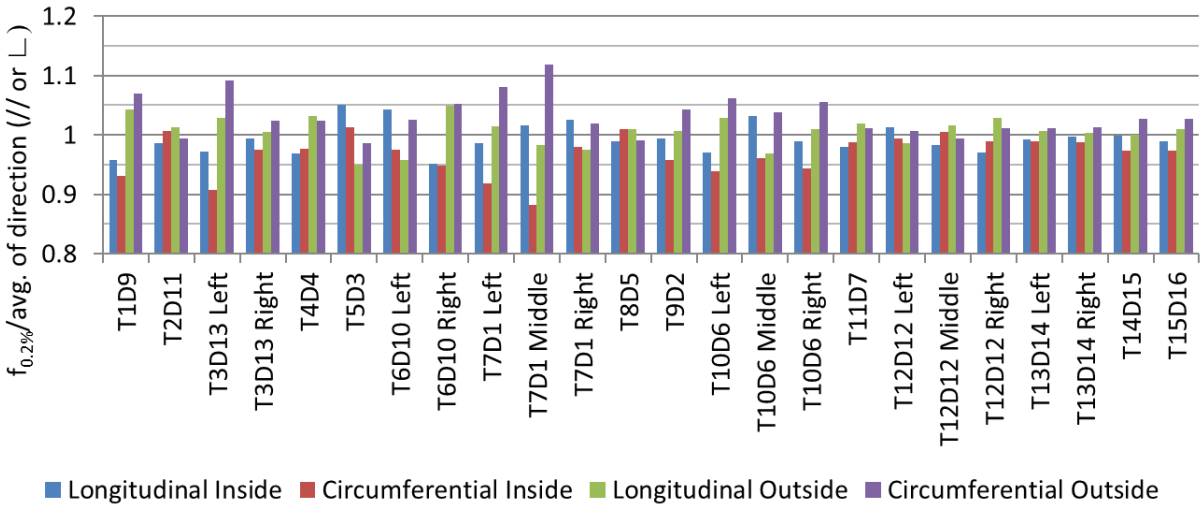

Figure 27 - Comparison of yield strength of tubes ($f_{0.2\%}$), normalized by the average value in that direction (longitudinal or circumferential) for that specimen or specimen part.

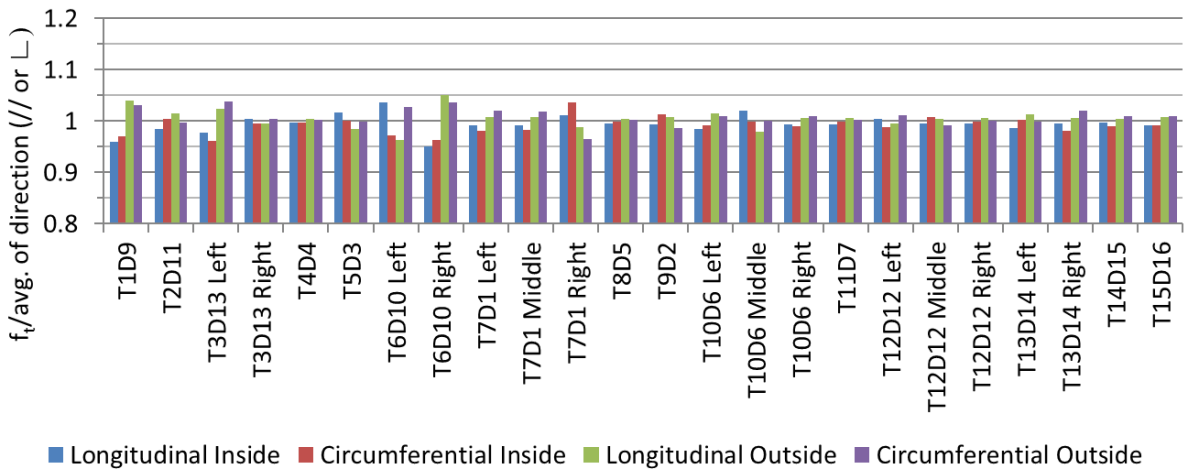

Figure 28 - Comparison of tensile strength of tubes (f_t), normalized by the average value in that direction (longitudinal or circumferential) for that specimen or specimen part.

Weld material

Tensile tests on spiral weld material have been carried out for specimens T6D10, T8D5 and T11D7. In Figure 29 and Figure 30 the results of these tests with comparing tensile tests of the base material are shown. The welds were overmatched with overmatching factors varying between 1,12 and 1,33.

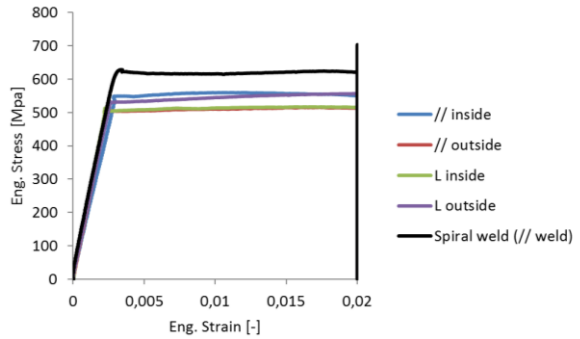

Figure 29 - Results of tensile test of specimen part T6D10 Left including a spiral weld specimen.

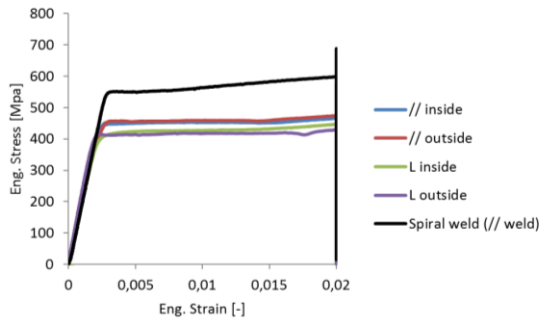

Figure 30 - Results of tensile test of specimen T8D5 including a spiral weld specimen.

Compression tests

Some examples of results of the compressive tests are presented in Figure 31 and Figure 32. The presented results show that in some cases a Bauschinger effect is noticeable (see Figure 32), while in other cases this is not the case (see Figure 31).

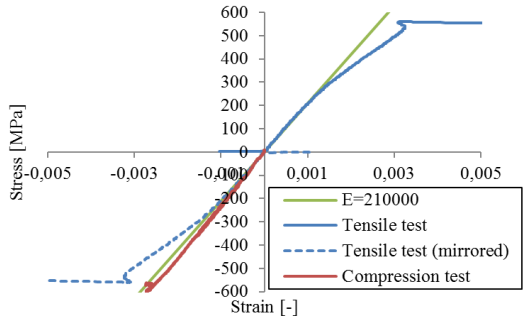

Figure 31 - Comparison of tensile test and compression test with similar orientation and location: D1D9 longitudinal outside.

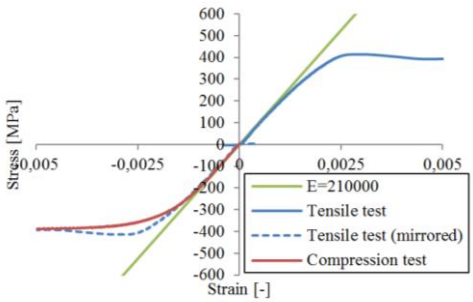

Figure 32 - Comparison of tensile test and compression test with similar orientation and location: T2D11 longitudinal outside.

Discussion and further details

All tensile specimens show a straight linear elastic behaviour up to yielding after which a yield plateau occurs. Some specimens show upper yield strength. The yield plateau in all cases extends to at least 2% strain.

There is some influence of the specimen orientation on the yield strength and tensile strength of the material. However, since this influence is rather small, it has been neglected in the numerical studies: the tube is assumed isotropic. Furthermore, there is a difference between the inside of the tube wall and the outside of the tube wall. This is probably due to the fabrication method, where plastic deformation leads to strain hardening of the material.

The compressive tests result in 3 stress strain diagrams for each specimen. Since it is impossible to produce a perfectly aligned specimen under pure compression, these individual stress-strain relationships show varying results. If the strains are averaged, and thus any bending effects are removed, more reliable stress-strain behaviour is visible.

The results show stress strain diagrams up to about 1% compressive strain. However, buckling and yielding are hard to distinguish in the early stages of buckling where the strength does not drop significantly. This means that the diagrams can be used to identify the stress level of the yield plateau, but not the exact length.

From the test results it can be concluded that mostly no Bauschinger effect is present in the tubes. If an effect is observed, it is relatively small. Furthermore, the found yield strengths are almost identical to the yield strengths found in the equivalent tensile test specimens.

Any differences between the tensile and compressive yield strength may be explained by the observed varying yield strength over the wall thickness. All specimens (compressive and tensile) were taken out as close as possible to the relevant plate surface (inside or outside). If a specimen would be taken out at a small distance from this surface, these will likely leads to different yield strength. Such small differences can be expected to occur when fabricating specimens of different dimensions. The material test results were used in the simulations of the bending tests in chapter4.

2.3.1.4 References

[1] Gresnigt, A.M., Foeken, R.J. van, “Local Buckling of UOE and Seamless Steel Pipes”, *Proceedings of Eleventh International Offshore and Polar Engineering Conference*, Stavanger, Norway.

[2] NEN-EN-ISO 6892-1 “Metallic materials – Tensile testing – Part 1: Method of test at room temperature”, *CEN*, Brussels.

2.3.2 Material testing of tube material in Karlsruhe

The material properties of the specimen tubes tested in Karlsruhe are determined by tensile tests with flat samples in accordance with DIN EN ISO 6892-1 [2].

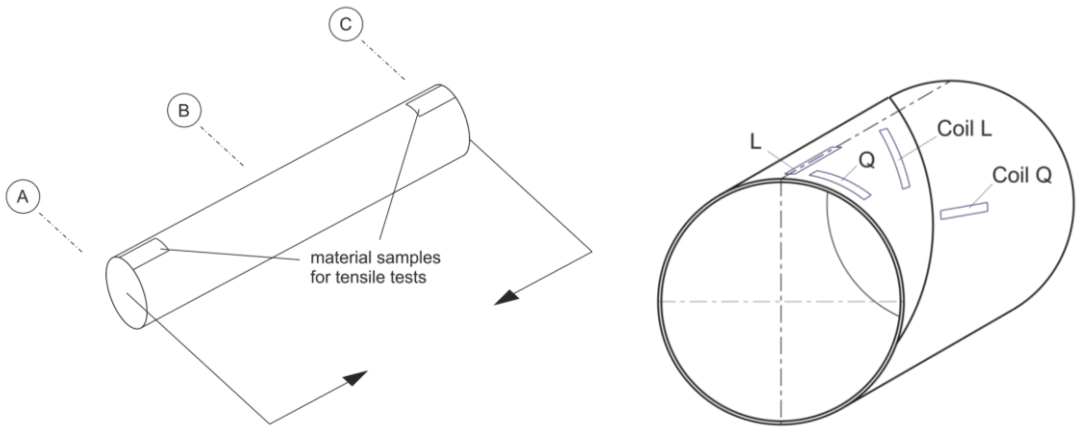

Figure 33 - Locations of material samples.

A first series of test was done with material samples taken from leftovers of the specimens. The tests are performed in four different test directions: longitudinal and transverse related to the tubes axis and the coils direction (see Figure 33). Thereby possible anisotropic properties are investigated (e.g. the material of specimen K1 and K2 shows minor yield strength in the transverse direction (Q) related to the tubes longitudinal axis).

Table 3 - K1 – K4: Comparison of yield strength $R_{p0,2}$ for different test directions.

	$R_{p0,2_L}$	$R_{p0,2_Q}$ / $R_{p0,2_L}$	$R_{p0,2_Coil_L}$	$R_{p0,2_Coil_Q}$ / $R_{p0,2_Coil_L}$	$R_{p0,2_Coil_L}$ / $R_{p0,2_L}$
	[N/mm²]	[-]	[N/mm²]	[-]	[-]
K1	419	0.91	421	1.00	1.00
K2	401	0.91	399	0.96	1.00
K3	286	1.02	298	1.01	1.04
K4	468	0.95	451	0.98	0.96

A second series of test was done after the bending tests of Task 3.2 with material samples from locations close to the ends of the tubes near the neutral axis (see Figure 33). Some specimens consisted of a mixture of different tubes (K7) or different material portions (K1, K2, K3, K5). In these cases the failure in the bending tests always occurred at the weaker part.

The provided tube materials showed a wide range of different stress strain curves, represented by material K3_C and K4_A as the most extreme ones (see Figure 34). All materials except those from specimen K3 fulfil the yield stress requirements for steel grade X52.

The material tests revealed that the specimens were of very different types of materials. To illustrate this, the stress-strain curves of the most different materials are shown in Figure 34. The properties of all materials are summed up in Table 4.

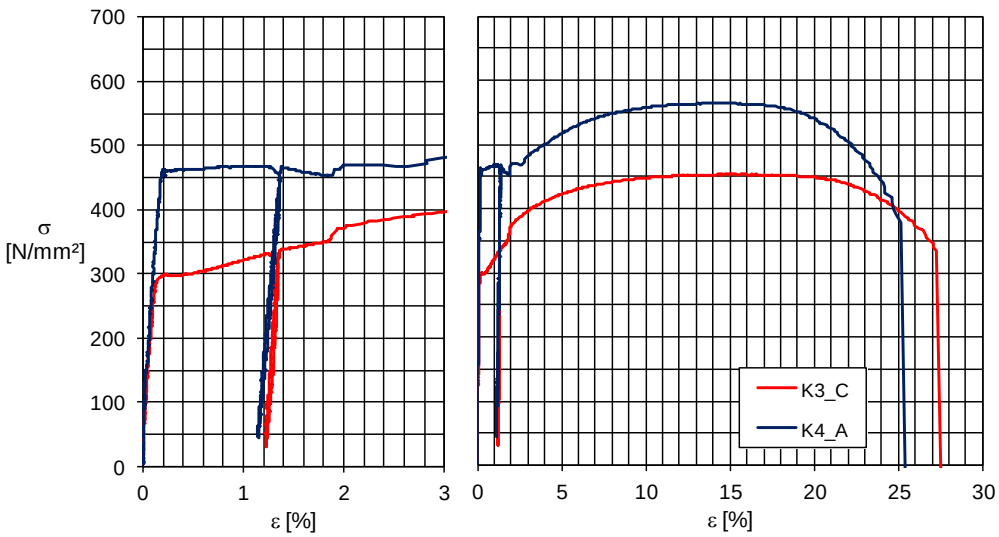

Figure 34 - Stress-strain curves of the most different materials (A: left end, C: right end)

Table 4 - Material properties.

	t	$R_{p0,2}$	R_{eH}	R_m	A_{gt}	Failure
	[mm]	[N/mm²]	[N/mm²]	[N/mm²]	[%]	
K1_A	11,3	492		573	12,8	
K1_C	11,0	443	-	543	11,8	x
K2_A	11,0	487	-	586	9,9	
K2_C	11,1	398	399	500	15,0	x
K3_A	8,8	350	-	505	14,2	
K3_C	9,1	299	300	454	15,0	x
K4_A	7,8	462	464	564	14,1	x
K4_C	8,0	462	465	568	13,9	
K5_A	8,2	425	-	572	14,0	
K5_C	7,5	418	453	563	14,0	x
K6_A	8,3	432	434	537	15,2	
K6_C	8,4	415	-	527	14,3	x
K7_A	8,4	444	465	527	11,6	x
K7_C	8,7	479	495	567	11,4	
K8_A	8,6	408	-	514	15,6	x
K8_C	8,6	401	411	515	14,9	

The range of material types is very well represented by the stress-strain curves of the materials K3_C and K4_A. K4_A is a material with a very high yield stress $R_{p,0.2}$ and ultimate stress R_m. The development of the stress-strain curve shows a pronounced plateau and a considerable strain hardening effect up to the point where the ultimate stress is reached. The ratio between R_m and $R_{p,0.2}$

is 1,22. In contrast to K4_A material K3_C shows a very early yielding and nearly no yield plateau. The yield stress of 299 N/mm² is even lower than the required value for a steel grade X52 which is 360 N/mm². The stress-strain curve of material K3_C goes on rising after the point of first yield which results in an unusual large ratio of R_m / $R_{p,0.2}$ = 1,52.

As is mentioned above, K3_C and K4_A represent the most extreme material properties in the investigated range of materials. Table 4 illustrates that all materials except those from specimen K3 fulfil the minimum requirements for the yield stress for steel grade X52. All material samples showed fracture strains larger than 23%.

More details are reported in [1].

2.3.2.1 References

[1] Ummenhofer, T; Reinke, T. (2014) WP3 TASK3.2 Test results. Background document Combitube, KIT, 2014-01-14.

[2] EN ISO 6892-1: 2009, Metallic materials – Tensile testing – Part 1: Method of test at room temperature.

2.3.3 Characterisation of the material testing of tube material

The Edinburgh team made a major contribution to the characterisation of material tensile tests for the purposes of adoption into numerical modelling predictions and the development of design rules. The data was mostly that obtained by KIT and TU-Delft. A statistical study of the outcome of tensile tests on specimens taken at different orientations from the spirally welded Combitube specimens demonstrated that these tubes may be effectively treated as isotropic in both analysis and design. The phenomena of anisotropy were found to be somewhat variable and unsystematic, as well as being relatively minor in magnitude, so that no strong conclusion could be drawn on how anisotropy should be universally adopted into computational models to predict buckling resistance. This finding was presented to partners and published in a peer-reviewed international journal (Sadowski et al., 2015a) [1].

A parallel statistical study was conducted using the huge volume of historically accumulated tensile test data at KIT. The chief focus of this study was to identify potential upper and lower bounds for the strain hardening modulus and yield plateau length of mild carbon steels found in rolled sections, plates and tubular members. This thorough statistical study appears to have been the very first of its kind and was published in a peer-reviewed international journal (Sadowski et al., 2015b) [2].

The need for reliable measures of the plateau length and hardening modulus was discovered quite early in the numerical studies of tubular member buckling performed at Edinburgh. It became a central consideration for the extensive parametric studies that the Edinburgh team later undertook. These studies covered a wide range of both of these parameters so that any later narrowing of the statistical scatter in these properties through better control during manufacture can be taken into account in further developments. Nevertheless, the findings of these extensive studies of existing data were exploited in developing the design recommendations produced by the Edinburgh team (Rotter and Sadowski, 2015c) [3], and chapter 6 of this final report.

The finding by the Edinburgh team that the shape of the stress strain diagram is very important in local buckling, confirms numerous earlier researches on local buckling of tubes and pipelines.

2.3.3.1 References

[1] Sadowski A.J., Rotter J.M., Reinke T. and Ummenhofer T. (2015a). “Statistical analysis of the material properties of selected structural carbon steels.” Structural Safety, 53, 26-35.

[2] Sadowski A.J., Rotter J.M., Reinke T. and Ummenhofer T. (2015b). “Analysis of variance of tensile tests from spiral welded carbon steel tubes.” Construction and Building Materials, 75, 208-212.

[3] Rotter J.M., Sadowski A.J. (2015c). "Final Report for Combitube WP6 Task 6.2 Design Guidelines for Tubes in CombiWalls." Research Report RR 15-01, Institute for Infrastructure and Environment, The University of Edinburgh, Edinburgh, UK and Research Report, Department of Civil and Environmental Engineering, Imperial College London, UK

2.4 Task 2.4: Measurement of imperfections and residual stresses

Diameter, wall thickness, ovalisation and geometrical imperfections have been intensively measured in the test specimens, both in Delft and in Karlsruhe. In this section the following items are reported.

- Measurements of geometry (diameter and wall thickness) and geometrical imperfections.
- Characterisation of the measurements by the University of Edinburgh.
- Residual stress measurements in Karlsruhe (hole drilling method) and Delft (ring cutting).

2.4.1 Measurement of initial dimensions and imperfections in Delft (laboratory)

Initial dimensions and geometrical imperfections were measured in the laboratory (the tubes to be tested in four point bending) and on site. As a frame of reference, a grid has been drawn on all tubes. The grid existed of eight lines in longitudinal direction and five in circumferential direction. An overview is shown in Figure 35. At this grid the wall thickness and the diameter were measured.

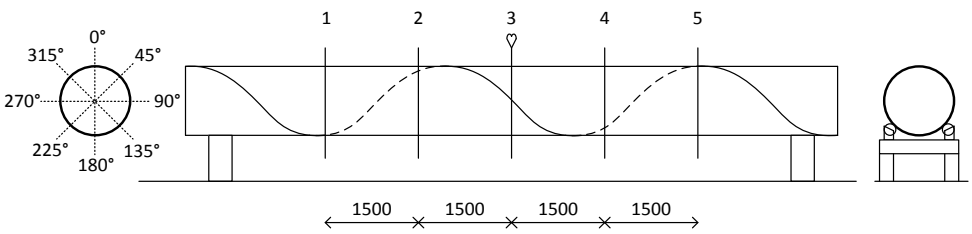

Figure 35 - Overview of measurement grid.

All tubes in the testing programme have been scanned to measure the initial geometrical imperfections. Ring cutting tests were performed to obtain an indication of the residual bending stresses in circumferential direction. In summary:

- Measurement of diameter,
- Measurement of wall thickness,
- Measurement of geometrical imperfections including dimples and bulges using advanced laser equipment,
- Indication of residual stresses in circumferential direction by ring cutting testing.

To perform the measurements, the specimens were placed on two supports which allowed a specially designed laser cart to scan the underside of the specimen. By rotating the specimen in increments of 22,5 degrees, the full tube was scanned.

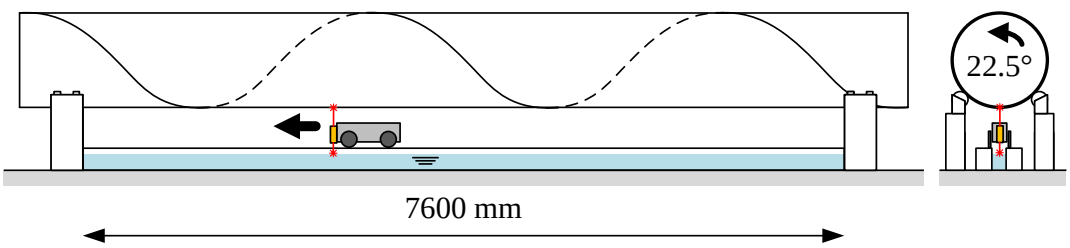

Figure 36 - Laboratory test setup to measure initial geometrical imperfections.

2.4.1.1 Diameter

The results of the diameter measurements show that the diameter is fairly constant over one specimen or specimen part (see Figure 37). Difference between the average measured diameter and the minimum and maximum outliers is limited to about 1%. The coefficient of variation within one specimen or specimen part is limited to 0.2%.

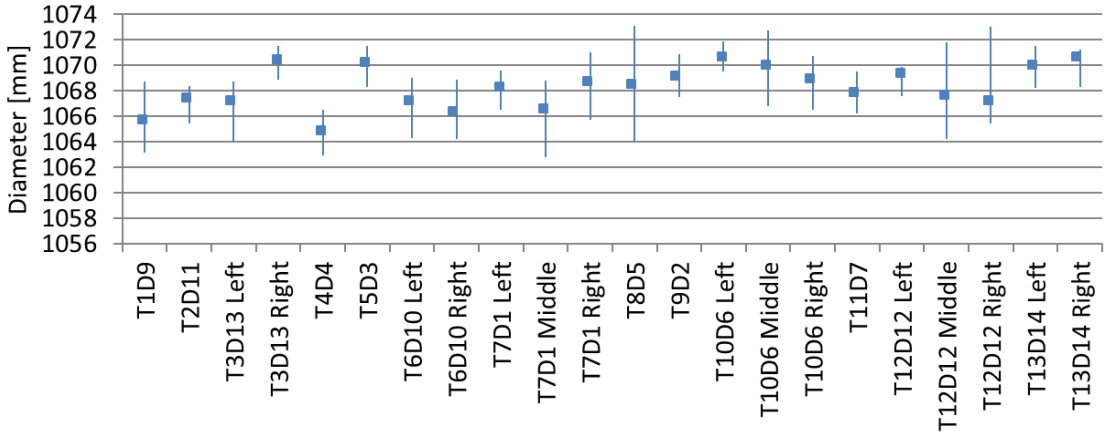

Figure 37 - Measured tube diameters and the spread of the measured data.

2.4.1.2 Wall thickness

The results of the thickness measurements show, similar to the diameter measurements, only very slight variations (see Figure 38). The maximum found coefficient of variation within one specimen or specimen part is 1.6%.

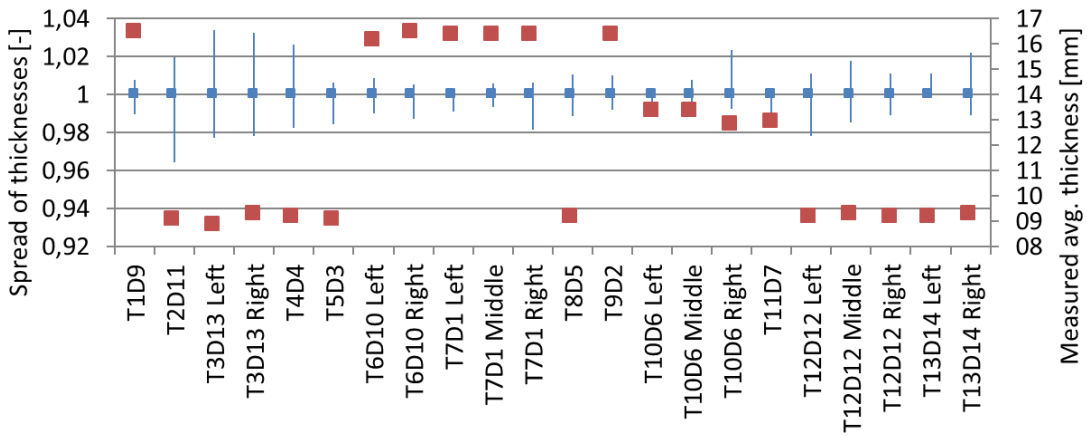

Figure 38 - Measured tube thicknesses and the spread of the measured data.

2.4.1.3 Geometrical imperfections

A typical result of this measurement is shown in Figure 39. The line represents the outer surface of the tube wall. Above the line will be air, below the line will be steel. Note the presence of the spiral welds (sharp peaks at regular distances) and more or less regular peaks and valleys in between. The geometrical imperfections have a depth or height which is an order of magnitude larger than the thickness variation. The geometrical imperfections that are measured are thus only the result of plate bending and not thickness reduction.

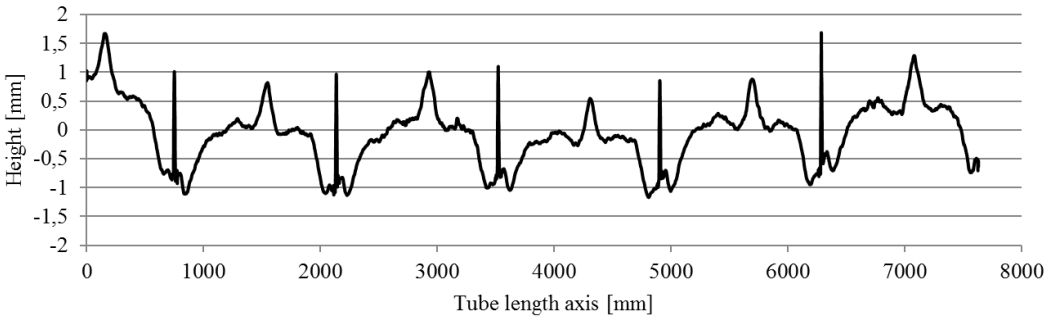

Figure 39 - Laser scan of initial imperfection in Tube T2, compression zone.

A remarkable feature of the scan shown in Figure 39 is the regularity of the initial imperfections. Some tubes, which are relatively new or have been stored indoors, show traces of rollers, presumably originating spiral forming process. In Figure 40 an overlay of initial imperfections with these roller marks is shown. It is clear that a lot of these roller marks coincide with peaks or valleys in the tube wall profile. Not every plate section shows the same amount of roller marks, but since the same number of rollers is present in every plate section, the rollers can be extrapolated, which would reinforce the earlier observation that the marks occur at dimples.

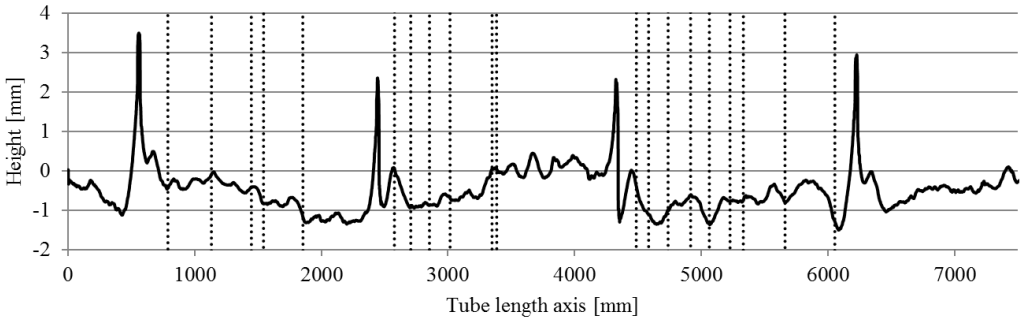

Figure 40 - Laser scan of initial imperfections with overlay of visible roller marks in tube T1, compression zone.

The regularity of the occurring dimples and the coincidence of the dimples with roller marks suggest that they find their origin in the tube manufacturing process, instead of accidents or handling damage.

2.4.1.4 Specimens in four point bending tests - placement and orientation

The orientation of the specimens in the test setup may influence the test result. Since failure by local buckling is expected, the compression zone of the tube is critical. For each tube an assessment was made of the influence of:

- Manufacturing-related geometrical imperfections
- High-low imperfections at spiral, coil connection or girth welds
- Other influences: dents, dimples, corrosion, etc.

Since the diameter and thickness have shown little variation over the tubes, these parameters are not considered in this consideration.

For each specimen a balance has been found between testing a worst case scenario in terms of initial imperfections, while keeping any present corrosion damage (as reported in the Mid-term report) away from the compression zone. The test orientation is only varied such that the outer fibre in the compression area, where buckling is expected to initiate, is always documented in one of the geometrical imperfection laser scans.

2.4.1.5 Indication of residual stresses by ring cutting

The available rings for material tensile testing have been cut to measure the ring opening or closing due to residual stresses. Cutting took place as far away as possible from the spiral weld. Since the tube was formed spirally, not only a uniform closing or opening is expected. The ring could open askew.

The opening or closing or the ring has been measured on four locations over the width of the ring to investigate the skewness of the opening. Furthermore, the warping of the ring and any difference in ring radius after opening or closing is measured. The change in radius could only be measured in case of small openings or closings.

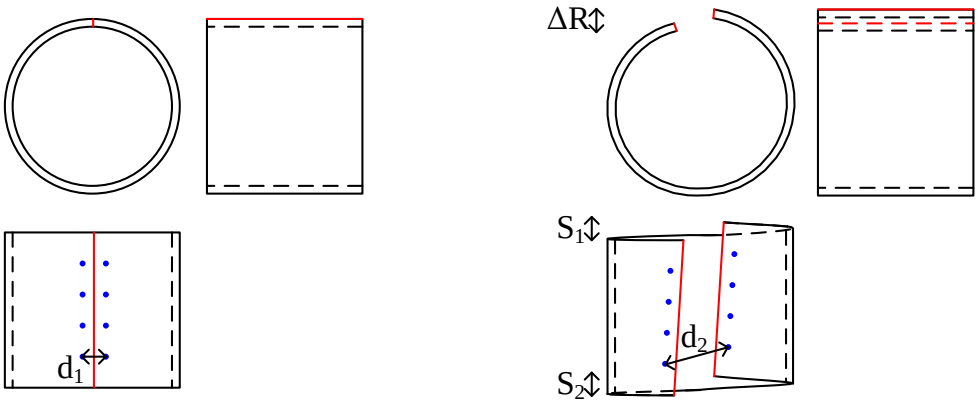

Figure 41 - Overview of ring before (left) and after cutting (right) with measurement of opening at four points (d_2-d_1), skewness (S_1 and S_2) and increase in radius (ΔR).

Some typical results are summarized in Table 5. It is clear that the results vary greatly between the different rings, ranging from a ring closing of 154 mm to an opening of 340 mm for rings of similar diameter, wall thickness and length. In case of closure of a ring, a piece of plate material was taken out so that the ring could freely deform.

Table 5 - Overview of results of ring cutting tests.

Ring I.D.	Tube part I.D.	D × t × Length [mm]	Average opening [mm]	Average skewness [mm]	Average ΔR [mm]
Ring 481	T13D14 Right	1071×9.2×492	626	48	-
D1L1	T7D1 Left	1068×16.4×400	340	77	-
D10R	T6D10 Right	1066×16.4×320	-156	0	-
D6Ring	T10D6 Right	1069×12.8×515	60	27	-
Ring D7	T11D7	1068×12.9×548	7	22	15
D11D2	T2D11	1067×9.0×395	503	30	-
Ring 480	T13D14 Left	1070×9.1×500	436	47	-
D1R	T7D1 Right	1069×16.3×473	276	30	62
D2Ring	T9D2	1069.16.3×413	214	15	50
D9D1	T1D9	1066×16.4×500	-154	< 10	-
D13F3	T3D13 Right	1070×9.2×1000	856	106	-
D13F2	T3D13 Left	1067×8.8×260	466	11	-
AK479	T4D4	1065×9.2×400	475	101	-

Figure 42 - Photos of cut rings Ring 481 (left) and D10R (right); since D10R appeared to close, more plate material was removed to let the ring freely deform.

2.4.2 Measurements of imperfections on site

In addition to the laboratory tests, measurements were performed on installed combined walls. All investigations took place on a building site of the A4 motorway between Delft and Amsterdam in The Netherlands. Near the city of Leiden, the motorway is reconstructed as a sunken motorway in a roofless tunnel (see Figure 43). Combined walls are used as soil retaining structure for the tunnel wall. Parts of the project are designed and executed by research partner BAM Infraconsult.

Figure 43 - Overview of the old motorway and new motorway under construction (image source www.beeldbank.rws.nl).

After the final stages of construction, the combined walls are hidden from sight and access. During construction the lower parts of the combined walls were accessible for measurements (Figure 44).

Figure 44 - Inside of building pit during construction with accessible combined walls.

Since the tubes in the field measurements were already in place, measurements with the laser cart, as used in the laboratory were not an option. Therefore, a hand held measuring device with similar capabilities was developed.

The field measurements are aimed at two goals:

- Verifying whether the initial imperfection due to production (spiral welding, coil connection weld) and secondary production (girth welds) are influenced by installation,
- Verifying whether the imperfections measured in laboratory conditions are representative of the imperfections present in a 'used' tube.

With these goals in mind, the tubes to be measured were selected. Some tubes were plain, similar to the plain tubes in the laboratory. In other cases, girth welds or coil connection welds were observed and scanned. Furthermore, since the tubes were handled and installed, occasionally damages were visible such as scratches and dents. Of such tubes scans were also made. In some cases several measurements were made for a tube at different circumferential locations, in other cases only one measurement was made, for example over a very noticeable dimple. An overview of the scanned tubes and their properties is shown in Table 6.

Table 6 - Overview of field measurement programme.

Scan I.D.	Tube I.D.	Orientation	D×t [mm]	D/t	Type/Remarks*)	Grade
29	L55	1	1220×12.7	96.1	GW	X56
30	L55	2	1220×12.7	96.1	GW	X56
31	L55	3	1220×12.7	96.1	GW	X56
32	L56	1	1220×12.7	96.1	2×SW	X56
33	L56	2	1220×12.7	96.1	SW (1800) +GW (2000)	X56
34	L51	1	1220×12.7	96.1	2×SW	X56
35	L37	1	1220×12.7	96.1	2×SW+GW (1100)	X56
36	L37	2	1220×12.7	96.1	2×SW+GW (1100)	X56
37	L39	1	1220×12.7	96.1	SW	X56
38	L39	2	1220×12.7	96.1	2×SW	X56
39	H22	1	1220×11.2	104.3	2×SW	X56
40	H22	2	1220×11.2	104.3	SW	X56
41	H21	1	1220×11.2	104.3	GW(1300)	X56
42	H21	2	1220×11.2	104.3	D (600); GW (1250)	X56
43	H21	3	1220×11.2	104.3	D (900); GW (1300)	X56
44	H25	1	1220×11.2	104.3	D	X56
46	G39	1	1220×11.2	104.3	CCW (800); SW	X56
47	G39	2	1220×11.2	104.3	CCW (300)	X56

*) CCW: Coil connection weld; D: dent or scratch; GW: Girth Weld; SW: Spiral weld; if necessary, between brackets the approximate X-coordinate of the feature is noted.

2.4.2.1 Measurement technique and results

The measurement unit consists of two lasers: one to measure the distance from the laser to the tube, similar to the laser on the laser cart. The second laser measured the distance from the unit to a fixed reflection panel. An overview of the test setup is shown in Figure 45. The operator smoothly and slowly moves the hand laser unit over the rails. Measurement software records the data points at regular and sufficiently small time intervals.

Figure 45 - Measuring of imperfections in building pit.

Considering the difference in measurement techniques in the building pit and the more controlled lab environment, some differences in accuracy were to be expected. Nevertheless, the measurements made in the building pit and laboratory proved to be very comparable, showing that the initial geometrical imperfections due to manufacturing that were present in the lab provide a realistic scenario for actual tubes. Of course, the laboratory tubes lacked the presence of scratches and dents.

2.4.3 Measurement of geometrical imperfections in Karlsruhe

Measurements of the geometry of different spirally welded tubes were performed to receive data of the tubes surface. The aim was to extract information on the tubes geometric character and fabrication tolerances (imperfections). The measurements and parts of the further processing of the data have been performed by Artmann Consult Karlsruhe as a contractor of KIT.

A full laser scan of the surface of the specimens has been performed to obtain a complete picture of the tubes geometric characteristics. Different to other measurement techniques the laser scanning method provides surface data with a high density of points which enables to extract geo-metric information in arbitrary directions. This is especially important in the context of the spirally welded tubes because of the major impact of this fabrication process on the geometric characteristics of the tubes.

Object of the measurements were three different spirally welded tubes (Table 7). They were chosen since they included all types of welds that occur in the set of tubes that were investigated. The first specimen K1 had beside the spiral weld an additional coil weld which was situated close to one of the ends of the tube. This tube represented the case where there was no significant influence of the coil weld on the bearing behaviour expected in the bending test. The second specimen K2 had a coil weld in the centre of the tube (Figure 46). Thereby representing the “worst case” for the tubes tested in

flexure. The third specimen, K7, possessed no coil weld but a girth weld which was situated in the centre of the tube.

The largest deviations from the nominal dimensions appeared to exist at the ends of the specimens as ovalisation. From these measurements the maximum deviation of the diameter was still smaller than 1% related to the nominal value. Individual specimens showed significant local buckles. Further details and the processing of the measurement data can be found in the KIT report on task.2.4 [1].

Table 7 - Selected tubes for measurements.

Specimen	Material	Dimensions D x t [mm]	Length [mm]	Welds
K1	X52	820 x 11	10500	Coil connection weld at the end
K2	X52	820 x 11	10500	Coil connection weld in the centre
K7	X52	863 x 8,4	10500	Girth weld in the centre

Figure 46 - Coil connection welds in specimens K1 and K2.

Figure 47 and Figure 48 show the resulting longitudinal sections for specimen K1. The sections were developed from the modelled surface data set of the “quad mesh”. The given radius of each section refers to the distance of the surface points to the axis of a best-fit cylinder calculated from the measured data points.

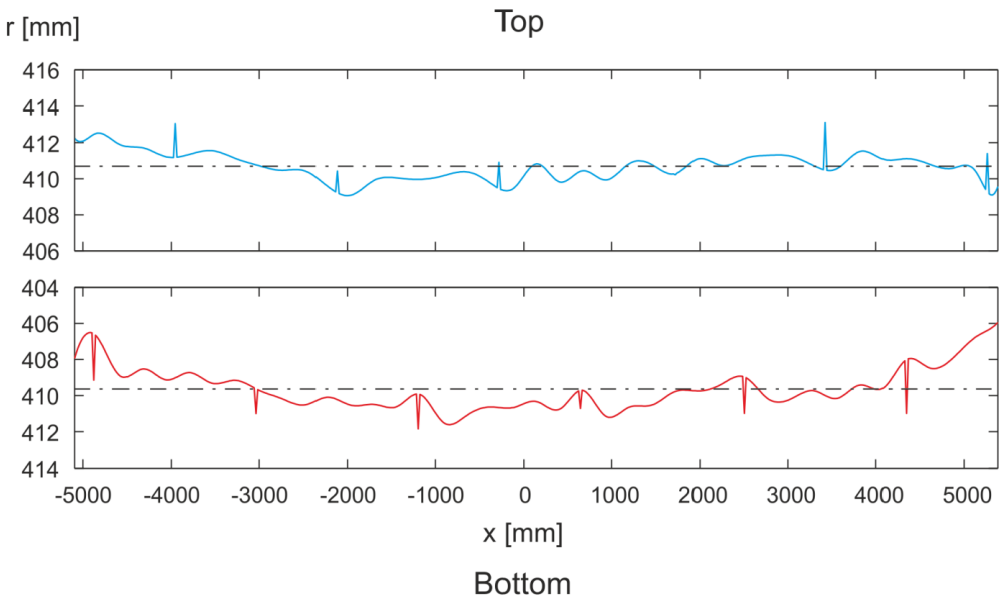

Figure 47 - Specimen K1: longitudinal section top / bottom.

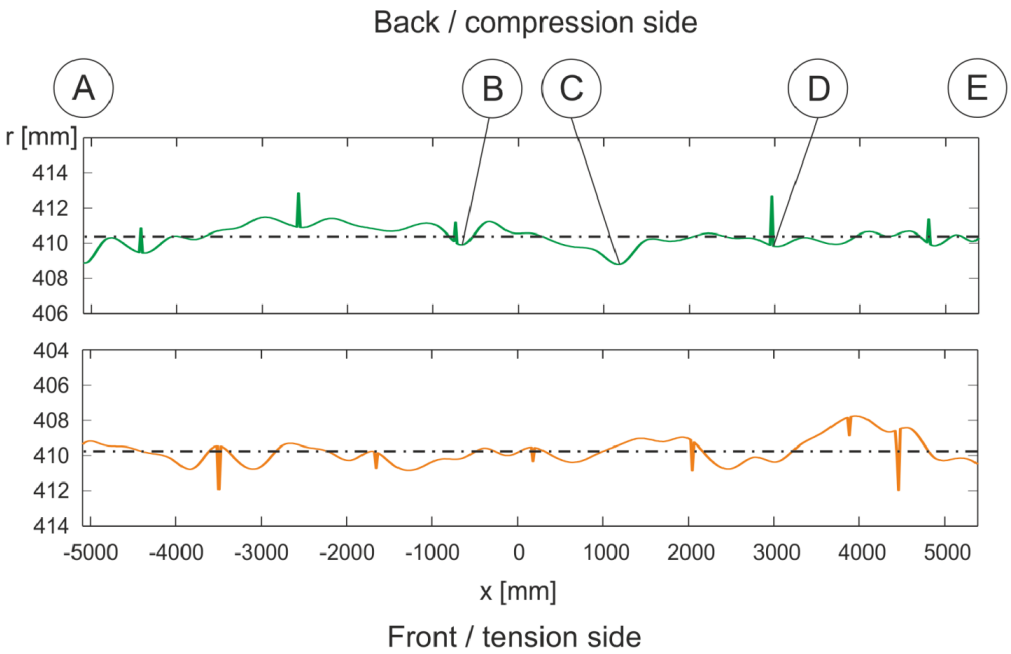

Figure 48 - Specimen K1: longitudinal section front / back.

By the longitudinal sections in Figure 47 and Figure 48 the overall deformations of the tube becomes obvious: the tube is very straight in the plane of the horizontal section (front-back) and also the vertical section (top – bottom) shows a minor overall deflection only. Clearly visible are several peaks with uniform distances which represent the positions of the spirally welding seams. Each of the diagrammed longitudinal sections is the result of approximately 525 surface data points corresponding to a point distance of 20 mm.

2.4.3.1 References

[1] Ummenhofer, T; Reinke, T.: WP2 Task 2.4 Measurement of imperfections and residual stresses. Background document Combitube, KIT, 2013-11-29.

2.4.4 Interpretation and evaluation of measured imperfections in Edinburgh

A report containing about 80 pages has been produced on this subject: Sadowski, A.J. and Rotter, J.M. (2013), [24]. Also a publication is available: Sadowski A.J., van Es S.H.J., Reinke T., Rotter J.M., Gresnigt A.M. and Ummenhofer T. (2015), [25]. A summary is presented in the paragraphs below.

2.4.4.1 Introduction

An assessment and mathematical representation of laser imperfection measurements has been made of Combitubes tested in this project, comprising of specimens D9, D11, D13 (carried out by the Technical University of Delft) and K1 (carried out by the Karlsruhe Institute of Technology, KIT).

The aim of this assessment was to explore the available data in a visual manner and identify any systematic patterns in the measured imperfections. A characterisation of these measured imperfections, with a view on identifying the critical geometrical features from a structural strength assessment perspective, has been carried out.

Imperfections of geometry have long been known to play an important role in determining the buckling resistance of shell structures. The effect is more important in thin shells than in tubular members, but it still has a significant impact on the strength of tubulars whose resistance occurs in the plastic range. The work presented in this report has been undertaken in the context of the large

literature on evaluation and interpretation of experimentally measured imperfections in shell structures.

2.4.4.2 Background to the interpretation of imperfection measurements

This study of the measured imperfections in Combitube specimens takes full advantage of the very many studies that have been undertaken over the last 40 years to measure and characterise imperfections for the purpose of accurate prediction of the buckling resistance of shell and tubular structures. A short description of the historical developments in this field is therefore given here to indicate the background to the material presented in this report.

The earliest attempts to produce a mathematical description of detailed measured imperfections was possibly that of Arbocz (1974, 1976) in which the general imperfections measured on aerospace shells were characterised using double Fourier series. The most enduring images from this period were those of Arbocz and Williams (1977) where a full survey of the geometric imperfections on a 10 foot (3.05m) diameter rocket vehicle were presented in this manner. This work led to the later proposal that an "Imperfection Data Bank" should be established to permit analysts to use realistic shapes in their buckling calculations (Arbocz, 1982). The work of Singer and his collaborators (1982, 1991, 2002) continued with this conceptual model and applied it to a wider range of structural forms.

The first attempt to measure geometric imperfections in larger structures appear to be that of Clarke and Rotter (1988), which was followed by further studies by Coleman et al (1992) and Rotter et al (1992) on a 24 metre diameter structure some 20 metres high. This considerable achievement is recorded in the papers by Ding et al. (1996a and b). These measurements finally led to another double Fourier series treatment of the measured imperfections by Teng et al. (2005). The dominant role of welds in these measurements led to further studies by Berry et al. (1997, 1999) and very well controlled laboratory tests to verify their critical role (Berry et al, 2000).

The challenge of finding ways of producing simplified characterisations of these imperfection measurements appropriate to the design of shell and tubular structures was a separate task. Many contributions to this goal have been made by different authors, as documented in the conference proceedings on the subject (Rotter, 1996). Key contributions in that conference were presented by Knödel and Ummenhofer (1996) and Ummenhofer and Knödel (1996), together with their published work (Knödel et al 1995).

These studies have all contributed to current rules for designers on the modelling of geometric imperfections in shell structures of all thicknesses and all geometries (Rotter and Schmidt, 2008).

Further studies by Rotter and Teng (1989), Holst et al. (1999, 2000) and Guggenberger (1996) have attempted to locate the causes and development of specific forms of geometric imperfections found in these structures.

The current report is based on the interpretative techniques used by Teng et al (2005).

2.4.4.3 Global overview of specimens

A global overview of the measured specimens is shown below. The measured imperfections are filtered and a 2D spline surface is fitted to gain an overview of the measured data.

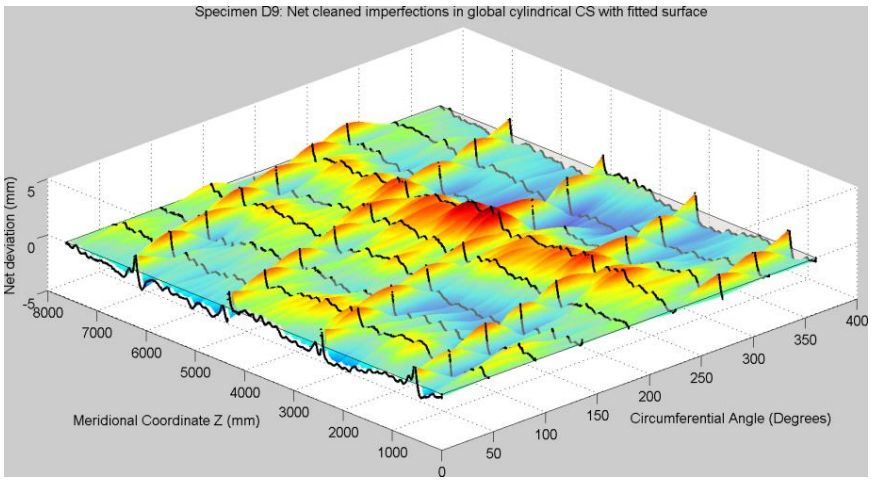

Figure 49 - Specimen D9: Fitted 2D spline surface to net 'cleaned' imperfections in the global cylindrical coordinate system.

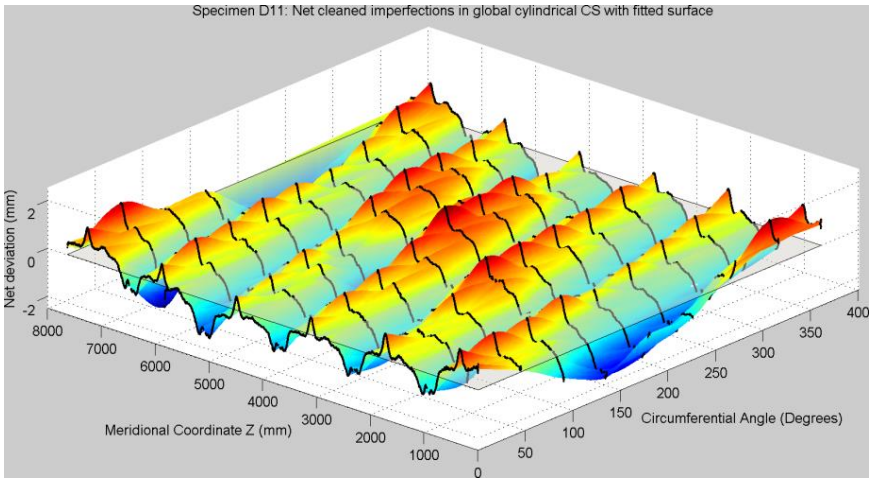

Figure 50 - Specimen D11: Fitted 2D spline surface to net 'cleaned' imperfections in the global cylindrical coordinate system.

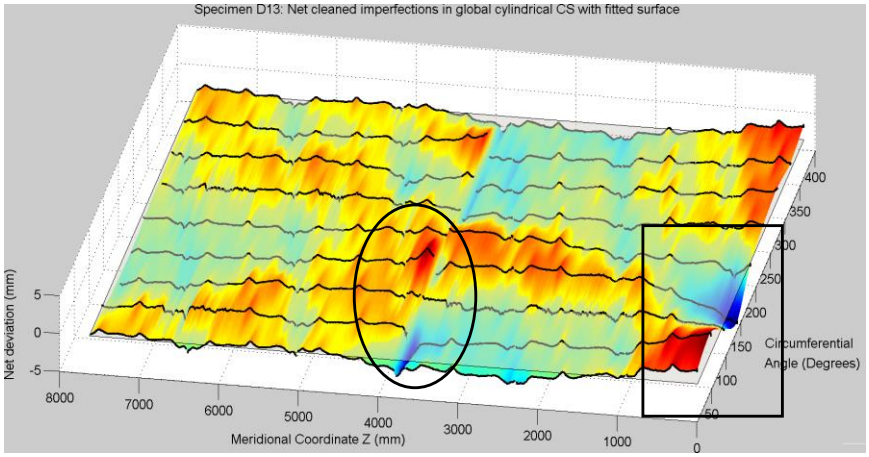

Figure 51 - Specimen D13: Fitted 2D spline surface to net 'cleaned' imperfections in the global cylindrical coordinate system. Note the occurrence of a girth weld in the middle of the specimen, leading to a sudden change in the measured surface.

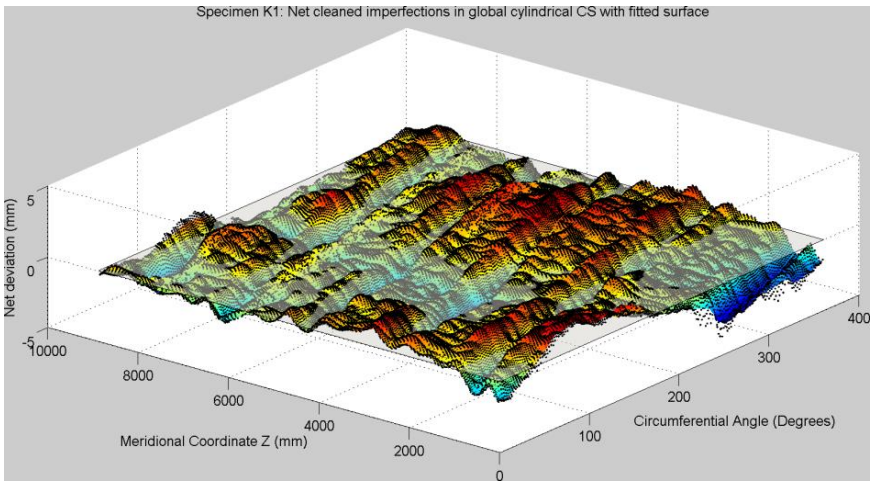

Figure 52 - Specimen K1: Fitted 2D spline surface to net 'cleaned' imperfections in the global cylindrical coordinate system.

2.4.4.4 Analysis techniques

A Fourier harmonic analysis was performed next on each circumferential cross-section of the specimens. Each cross-section measured in Delft contains only 8 data points, 9 if to include symmetry. Mathematical principles say that this is enough information for at most 4 meaningful harmonics. More harmonics can be included in the analysis of the measurements in Karlsruhe, since more circumferential data points are available. The Fourier series is defined as follows:

$$F(\theta) = \sum_{n=0}^{4} \left(a_n \cos n\theta + b_n \sin n\theta \right) \tag{1}$$

where a_n and b_n are the *n*-th coefficients of the *cos* and *sin* terms respectively.

An alternative way of expressing the same series is as follows:

$$F(\theta) = \sum_{n=0}^{4} A_n \sin\left(n\theta + \varphi_n \right) \tag{2}$$

where $A_n = \sqrt{a_n^2 + b_n^2}$ and $\varphi_n = \tan^{-1} \frac{a_n}{b_n}$ are the *n*-th modal amplitude and phase angle respectively.

Possibly the most intuitively meaningful harmonics are the lowest three:

- Harmonic 0 - axisymmetric radial expansion or contraction ('bulging')
- Harmonic 1 - rigid cross-section displacement ('column' imperfection)
- Harmonic 2 - 'ovalisation' imperfection

Where applicable, the R^2 correlation coefficient was used as a rough appraisal of the 'goodness of fit' of a Fourier series. Though strictly valid only for linear regressions, it is widely used in engineering for nonlinear regressions because of its simplicity. It is defined as:

$$R^2 = 1 - \frac{SS_{err}}{SS_{tot}} \text{ where } SS_{err} = \sum_{i=1}^{N} \left(y_i - f_i \right)^2 \text{ and } SS_{tot} = \sum_{i=1}^{N} \left(y_i - \bar{y} \right)^2 \tag{3}$$

and y_i and f_i are the *i*-th measured data point and its fitted (predicted) value respectively out of a total of *N* data points while $\bar{y}$ is the mean of all measured values.

To analyse the meridional axis, a Fourier harmonic analysis was performed next along each of the meridional generators. Each generator contains sufficient data points. A full wave Fourier series in terms of the meridional *z* coordinate is defined as follows:

$$F(z) = \sum_{m=0}^{N_m} \left(c_m \cos \frac{2\pi mz}{L} + d_m \sin \frac{2\pi mz}{L} \right) \text{ where } C_m = \sqrt{c_m^2 + d_m^2} \qquad (4)$$

Possibly the most intuitively meaningful harmonics are the lowest two:

- Harmonic 0 - axisymmetric 'offset' of the generator
- Harmonic 1 - the 'bow' imperfection of the generator

In addition to the above results, reference is made to Sadowski A.J., van Es S.H.J., Reinke T., Rotter J.M., Gresnigt A.M. and Ummenhofer T. (2015c). “Harmonic analysis of measured initial geometric imperfections in large spiral welded carbon steel tubes.” Engineering Structures, 85, 234-248, [25].

2.4.4.5 Conclusions

The main conclusions from these extensive studies are that the imperfection patterns are systematically related to the helical forming process. The critical imperfections from the point of view of local buckling were identified as related to the indents of the rollers during forming of the tubes, the coil connection welds and the girth welds.

The amplitudes in the tested specimens may be described as very modest compared to those normally assumed in shell buckling design (EN 1993-1-6, 2007) due to the high quality of factory fabrication using automated processes in these helically wound tubes.

Finally, it was concluded that the influence of imperfections on the bending capacity can be conservatively and reliably simulated using a simple girth weld imperfection whose amplitude could be reasonably chosen to produce suitable matches with the experimental buckling data.

2.4.4.6 References

[1] Arbocz, J. (1974) “The Effect of Initial Imperfections on Shell Stability”, in Thin Shell Structures, Ed. Y.C. Fung and E.E. Sechler, Prentice Hall, pp 205-246.

[2] Arbocz, J. (1982) “The Imperfection Data Bank: A Means to Obtain Realistic Buckling Loads”, in Buckling of Shells, edited by E. Ramm, Springer Verlag, Berlin 1982, pp 535-567.

[3] Arbocz, J. and Babcock, C.D. Jr (1976) “Prediction of Buckling Loads based on Experimentally Measured Initial Imperfections”, in Buckling of Structures, Ed. B. Budiansky, Proc. IUTAM Symposium, Harvard University, June 1974, Springer 1976, pp 291-311.

[4] Arbocz, J. and Williams, J.G. (1977) “Imperfection Surveys on a 10-ft-Diameter Shell Structure”, American Institute of Aeronautics and Astronautics Journal, July, Vol. 15, No. 7, pp. 949-956.

[5] Berry, PA., Bridge, R.Q. and Rotter, J.M. (1997) “Experiments on the buckling of axially compressed fabricated steel cylinders with axisymmetric imperfections”, Proc., Int. Conf. on Carrying Capacity of Steel Shell Structures, Brno, 1-3 October 1997, pp 347-353.

[6] Berry, P.A., Bridge, R.Q. and Rotter, J.M. (1999) “Characterising asymmetry of the initial imperfections in steel silos”, Mechanics of Structures and Materials, eds M.A. Bradford, R.Q. Bridge and S.J. Foster, Balkema, Rotterdam, pp. 233-238.

[7] Berry, P.A., Rotter, J.M. and Bridge, R.Q. (2000) “Compression tests on cylinders with circumferential weld depressions”, Journal of Engineering Mechanics, American Society of Civil Engineers, Vol. 126, No. 4, April, pp 405-413.

[8] Clarke, M.J. and Rotter, J.M. (1988) “A Technique for the Measurement of Imperfections in Prototype Silos and Tanks”, Research Report R565, School of Civil and Mining Engineering, University of Sydney, March.

[9] Coleman, R., Ding, X.L. and Rotter, J.M. (1992) “The Measurement of Imperfections in Full-Scale Steel Silos”, Proc., Fourth International Conference on Bulk Materials Storage Handling and Transportation, Institution of Engineers, Australia, Wollongong, June 1992, pp 467-472.

[10] Ding, X.L., Coleman, R.D. and Rotter, J.M. (1996a) “Surface profiling system for measurement of engineering structures”, Journal of Surveying Engineering, American Society of Civil Engineers, Vol. 122, No. 1, Feb. 1996, pp 3-13.

[11] Ding, X.L., Coleman, R.D. and Rotter, J.M. (1996b) “Technique for precise measurement of large-scale silos and tanks”, Journal of Surveying Engineering, American Society of Civil Engineers, Vol. 122, No. 1, Feb. 1996, pp 14-25.

[12] Holst, J.M.F.G., Rotter, J.M. and Calladine, C.R. (1999) “Imperfections in Cylindrical Shells resulting from Fabrication Misfits”, Journal of Engineering Mechanics, American Society of Civil Engineers, Vol. 125, No. 4, April, pp 410-418.

[13] Holst, J.M.F.G., Rotter, J.M. and Calladine, C.R. (2000) “Imperfections and buckling in cylindrical shells with consistent residual stresses”, Journal of Constructional Steel Research, Vol. 54, pp 265-282.

[14] Knödel, P. and Ummenhofer, T. (1996) “Substitute imperfections for the prediction of buckling loads in shell design”, Proc. Intl Workshop on Imperfections in Metal Silos: Measurement, Characterisation and Strength Analysis, CA-Silo, Lyon, France, 19 April, pp 87-102.

[15] Knödel, P., Ummenhofer, T. and Schulz, U. (1995) On the Modelling of Different Types of Imperfections in Silo Shells. Thin-Walled Structures, 23, 1995, pp. 283-293.

[16] Rotter, J.M. (Ed.) (1996) Proceedings, International Workshop on Imperfections in Metal Silos: Measurement, Characterisation and Strength Analysis, CA-Silo, Lyon, France, 240pp.

[17] Rotter J.M. and Schmidt, H. (2008) “Geometric tolerances and imperfections” in Stability of Steel Shells: European Design Recommendations: Fifth Edition 2008, European Convention for Constructional Steelwork, Brussels, Oct. 2008, pp. 69-82.

[18] Rotter, J.M., Coleman, R., Ding, X.L. and Teng, J.G. (1992) “The Measurement of Imperfections in Cylindrical Silos for Buckling Strength Assessment”, Proc., Fourth International Conference on Bulk Materials Storage Handling and Transportation, Institution of Engineers, Australia, Wollongong, June 1992, pp 473-479.

[19] Singer, J. (1982) "The Status of Buckling Investigations of Shells", Buckling of Shells, Ed. E. Ramm, Springer-Verlag.

[20] Singer, J., Arbocz, J. and Weller, T. (2002) Buckling Experiments: Experimental Methods in Buckling of Thin-Walled Structures, 2 Volumes, Wiley-VCH Verlag.

[21] Singer, J., Weller, T. and Abramovich, H. (1991) “The influence of initial imperfections on the buckling of stiffened cylindrical shells under combined loading”, Buckling of shell structures, on land, in the sea and in the air, Edited by J.F. Jullien, London: Elsevier Applied Science, 1991, pp. 1-10.

[22] Teng J.G., Lin X., Rotter J.M. & Ding X.L. (2005). "Analysis of geometric imperfection in full-scale welded silos." *Engineering Structures*, 27, 938-950.

[23] Ummenhofer, T. and Knödel, P. (1996) “Typical imperfections of steel silo shells in Civil Engineering”, Proc. Intl Workshop on Imperfections in Metal Silos: Measurement, Characterisation and Strength Analysis, CA-Silo, Lyon, France, 19 April, pp 103-118.

[24] Sadowski, A.J. and Rotter, J.M. (2013) “Measurements of imperfections in helically-wound Combitubes – Interpretation and evaluation of measured imperfection data”, *Combitube WP2 Task 2.4, Research Report RR13 04*, Institute for Infrastructure and Environment, University of Edinburgh and Imperial College London, 26 March, 80pp.

[25] Sadowski A.J., van Es S.H.J., Reinke T., Rotter J.M., Gresnigt A.M. and Ummenhofer T. (2015). “Harmonic analysis of measured initial geometric imperfections in large spiral welded carbon steel tubes.” Engineering Structures, 85, 234-248.

2.4.5 *Residual stress measurements in Karlsruhe*

Residual stresses were investigated by measurements on leftover tubes of the bending test specimens D9, D13, K1 and K2. The used hole-drilling-method (see Figure 53) provided results up to 1 mm below the surface.

The hole drilling method was chosen after intensive investigation and discussion in the consortium.

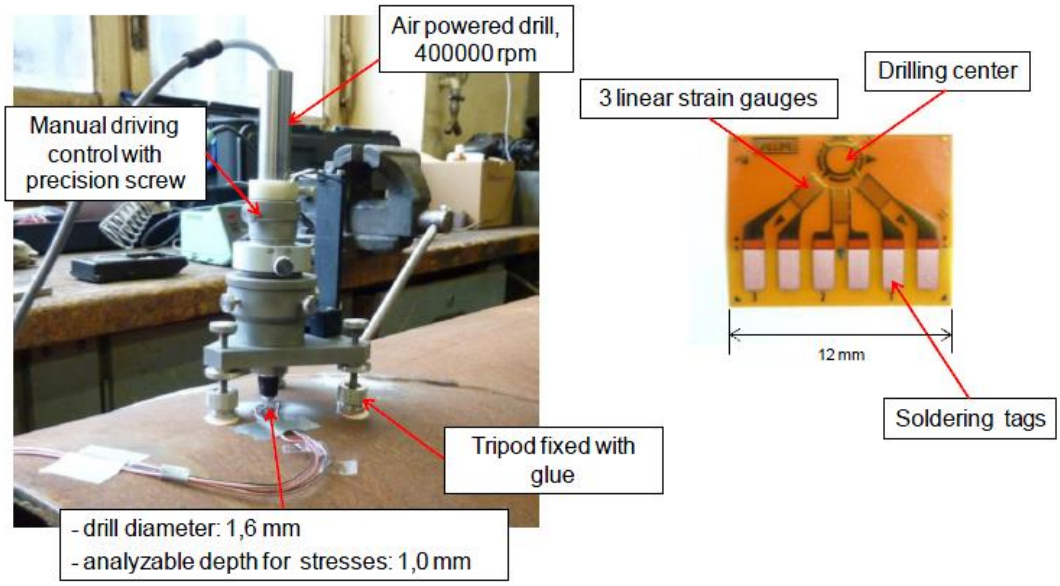

Figure 53 - Drilling mill and strain gage in the hole-drilling-method.

The measurements were performed at three different locations, close to the welds (see Figure 54), in the undisturbed base material where no weld influence is expected and at an intermediate position.

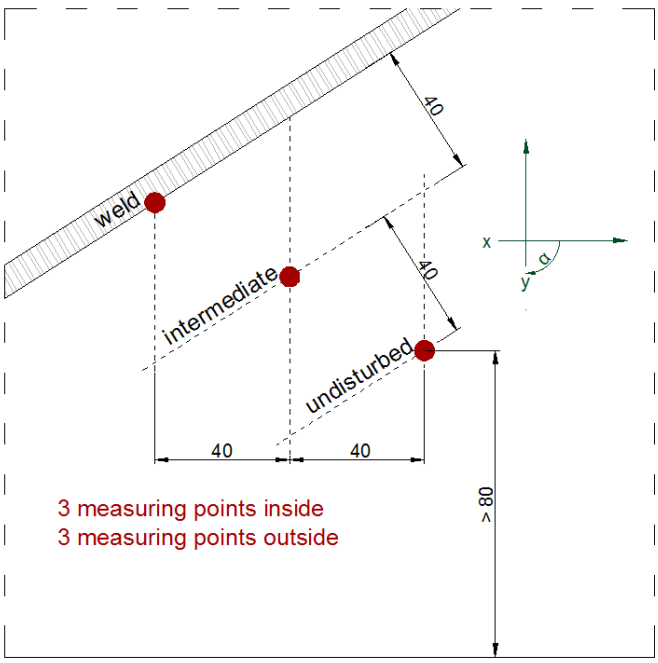

The aim of the residual stress measurements was to get the distribution of existent residual stresses in the material which are the result of the fabrication process of the base material (rolling) as well as the fabrication process of the tube itself (metal forming and welding).

From the measurements stresses were calculated in circumferential direction (x-direction), longitudinal direction (y-direction) and resulting principal stresses with indication of the angle α of the largest principal stress related to the x-direction.

Figure 54 – Measurement locations.

A selection of the results is given in Figure 55.

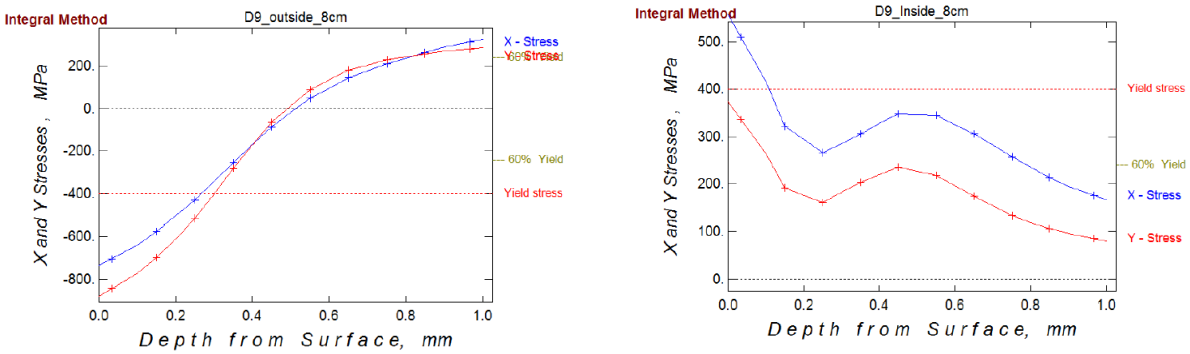

Figure 55 - Residual stresses in specimen D9, x-y stresses.

Further details on measurement technique and results can be found in the KIT report on Task 2.4 [7].

2.4.5.1 Concluding remarks residual stress measurements

The measurements reveal stresses in the circumferential direction at locations without weld influence that can be interpreted as local bending stresses (up to 220 N/mm²). In the longitudinal direction the resulting stresses are different in amount and type. The measurements reveal tensile as well as compressive stresses up to 150 N/mm².

There seems to be no generally valid stress pattern for all specimens. Next to the welds the method seems to overestimate the existing stresses.

As stated before in this report the final residual stress state depends on many factors and is hard to predict. Reference is made to the work done by U-Thessaly in WP 4. In that work the residual stresses were calculated by following (describing) the deformation history of the plate on the coil to stretching and bending again for the spirally welding.

However, results did not give a good explanation. Probably there is a lot of scatter due to the different ways of coiling and heat treatment during and after coiling. Also different tube manufacturing machines contribute to the scatter.

Finally it is noted that in relatively thick walled tubes the effect of residual stresses on bending moment curvature behaviour (max moment and critical curvature) is much smaller than in thin walled shells. This is worked out further in the FEA parameter studies (sensitivity analyses) in WP5.

2.4.5.2 References

[1] Vishay, Measurement of residual stresses by the Hole-Drilling Strain Gage Method, Tech Note TN-503, Vishay Precision Group.

[2] Marthar, J., Determination of Initial Stresses by Measuring the Deformation Around Drilled Holes. Transactions ASME, 1934. **56**(4): p. 249-254.

[3] Schajer, J., *Measurement of Non-Uniform Residual Stresses Using the Hole Drilling Method.* Journal of Engineering Materials and Technology, 1988. **110**(4): p. 338-349.

[4] Vishay, RS-200 Milling Guide for Residual Stress Measurements, Document No.: 11304 2011, Vishay Precision Group, www. micro-measurements.com.

[5] Vishay, *Special Use Sensors - Residual Stress Strain Gages, Document No.:11516*, 2010, Vishay Precision Group, www. http://www.vishaypg.com/docs/11516/resstr.pdf.

[6] Schajer, J., H-DRILL, Hole-Drilling Residual Stress Calculation Program Version 3.10, User Guide, 2007, Gary S. Schajer.

[7] Ummenhofer, T; Reinke, T.: WP2 Task 2.4 Measurement of imperfections and residual stresses. Background document Combitube. KIT, 2013-11-29.

3 WP3: Experimental testing of tubes under various loading conditions

The objectives of WP3 are the following:

- To determine the local buckling behaviour for different D/t ratios and steel grades in pure bending.
- To determine the effect of selected construction and loading details (in WP1) on the bending and local buckling behaviour.
- To determine the effect of imperfections (as selected in WP1) on the bending and local buckling behaviour.

3.1 Task 3.1: Pure bending in Delft

The testing program in Delft features the testing of thirteen spirally welded tubes with a diameter of 1067 mm and various wall thicknesses and steel grades, to cover the full range of D/t ratios and steel grades that are considered in the project. In addition, the testing programme in Delft has been extended with two longitudinally welded tubes on incentive and costs of TU-Delft. Results are included in the analyses since they are relevant for the Combitube project. The testing program, including the two additional tests, has been completed in December 2013.

An overview of the performed tests and the parameters of the test specimens is presented in Table 8. Note the presence of a selection of structural details in the specimens such as a girth weld (GW) and or coil connection weld (CCW). The latter is the weld that arises when in the continuous production process of a spirally welded tube, a coil ends and a new coil is connected.

Table 8 - Overview of test program performed at TU Delft.

Test and Tube I.D.	D × t [mm]	D/t	Grade	D/t ε^2	Fabr.	Type
T1D9	1066 × 16.4	65.1	X70	147.5	Spiral.	Plain
T2D11	1067 × 9.0	118.3	X60	204.6	Spiral.	Plain
T3D13	1069 × 9.0	118.7	X60	201.4	Spiral.	GW
T4D4	1065 × 9.2	116.2	X60	218.1	Spiral.	Plain
T5D3	1070 × 9.0	118.4	X60	200.9	Spiral.	Plain
T6D10	1066 × 16.3	65.3	X70	149.1	Spiral.	CCW
T7D1	1068 × 16.3	65.4	X70	170.6	Spiral.	GW/CCW
T8D5	1068 × 9.1	117.4	X60	226.0	Spiral.	Plain
T9D2	1069 × 16.3	65.4	X70	170.7	Spiral.	Plain
T10D6	1070 × 13.1	81.6	X52/X60	117.7	Spiral.	GW/CCW
T11D7	1068 × 12.9	83.0	X52	123.6	Spiral.	Plain
T12D12	1069 × 9.1	117.1	X60	223.8	Spiral.	GW/CCW
T13D14	1070 × 9.2	116.3	X60	220.5	Spiral.	GW
T14D15	1068 × 9.8	108.8	X60	234.5	Long.	Plain
T15D16	1070 × 14.8	72.3	X70	164.7	Long.	Plain

3.1.1 Test setup

To investigate the bending resistance and local buckling behaviour of the specimens, a four point bending test rig has been designed. The test rig has been designed to deliver 130% of the largest plastic moment capacity according to the specimen specifications and 200% of the deformation that is necessary to induce buckling according to Gresnigt (1986) and according to the ENV 1993-5 on Piling. The maximum force that could be delivered to the specimen at one of the four load application points was 3500 kN. The maximum stroke at the hydraulic actuators was 350 mm, but more deformation could be applied by relieving the load and shortening the connection bars to the floor of the laboratory at the middle supports. During the tests, this appeared not necessary.

An overview of the test setup is shown in Figure 56. At the right side one actuator could deliver the required force. At the left side in Figure 56, the test setup was equipped with two lower capacity actuators and a lever beam to enable the required force of 3500 kN. Although the test setup was asymmetric, the loading and deformation of the specimen experiences were symmetric.

At the middle supports, the specimen was anchored to the laboratory floor, which has sufficient capacity to transfer the forces to the two outer frames. A threaded rod was fitted between the specimens and the floor anchorages so that in case of insufficient stroke of the actuators, the plastic deformed specimen could be lowered as indicated before, the nuts tied and loading can continue.

Load introduction was performed by thin flexible steel straps around the specimen which were as thin as possible to only facilitate normal force in the straps, and as wide as possible to limit the contact pressure. At the mid supports an additional lever beam has been placed so that the load application at the edge of the area of constant moment was further reduced. In case that a spiral weld passes through the area of load transition, the area below the strap was filled with plywood to prevent a high local load at the spiral weld. The threaded rods were free to rotate in two directions by means of a double hinge at the floor anchorage so that the middle support does not limit tube ovalisation or induces a normal force at larger deformations.

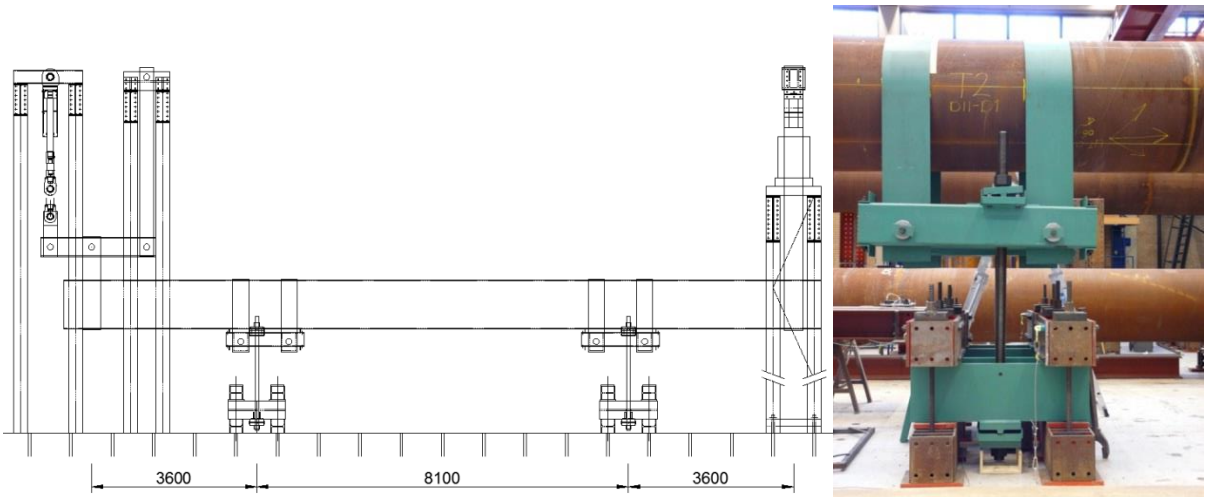

Figure 56 – Left: Overview of test setup. Right: Overview of middle support and floor anchorage. Note the fill in with triplex at the internal load application to prevent the strap from loading only the spiral weld.

Figure 57 - Overview of TU-Delft test setup.

3.1.2 Test procedures

The tests were deformation controlled. The asymmetry in the testing rig resulted in slightly different deformations at both sides of the tube as a result of different elastic rig deformations. Therefore, only during the elastic phase, after each load step, the forces working on the tube at both sides were made equal.

Although most measurements were continuously logged, some measurements could only be performed on a stationary tube. For these measurements, and to let the test be a controlled process, the deformation was applied in steps of 5 or 10 mm.

3.1.3 Measurements during testing

The loads were continuously measured at the two outer supports where the load was applied. On the right side (see Figure 56) this is a direct measurement. On the left side, the load measurement was performed with load cells on the actuators, which was multiplied with a leverage factor to calculate the load on the tube end.

The displacements of the tube with respect to the laboratory floor were measured at all four supports.

The ovalisation of the tube was measured at the four supports by means of an internal, vertical wire transducer. At regular distances the horizontal ovalisation of the tube was monitored in the area of constant moment (see Figure 58). For this, brackets were used with a flexible bottom strip which was equipped with strain gauges. By means of calibration before the test, the strain readout could be linked to a certain ovalisation (see Figure 58).

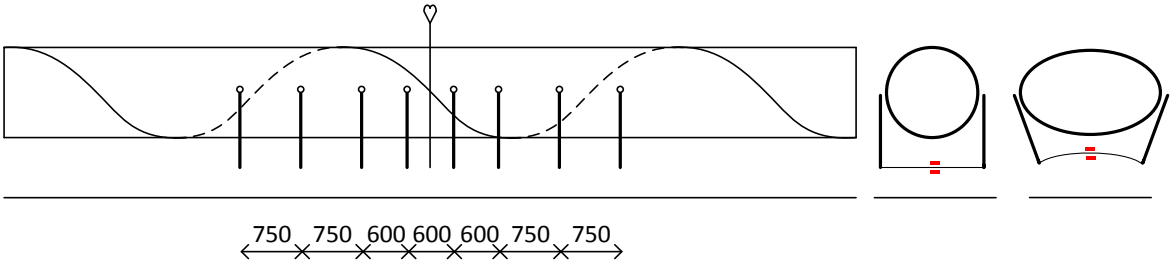

Figure 58 – Left: Overview of ovalisation measurements locations. Right: Schematics of ovalisation bracket with flexible strip and strain gauges.

To measure the curvature of the tube, four systems of three brackets were used (see Figure 59). When the tube curves, the middle bracket of the three will displace with respect to the outer two which were connected by a horizontal bar. When the distance between the horizontal bar and the middle bracket is measured, the curvature can be calculated.

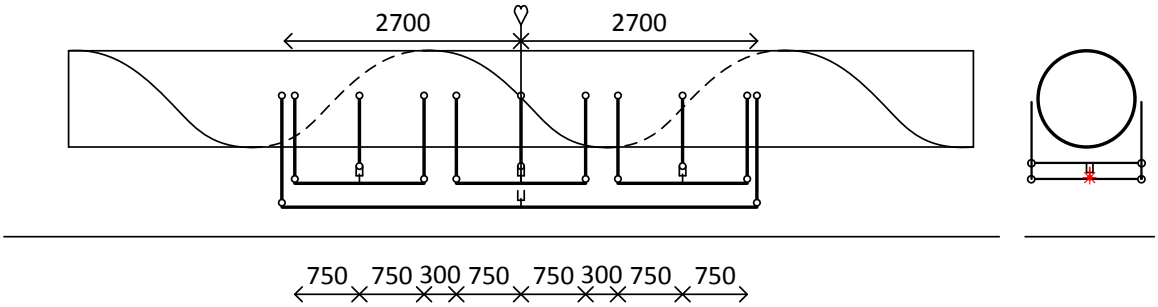

Figure 59 – Layout of curvature measurements during TU-Delft testing.

In both the tension and compression area, several strain gauges were placed. For different tests, various strain gauge layouts have been chosen due to the presence of, for example, girth welds or coil connection welds.

3.1.4 Monitoring of geometrical imperfections

Before local buckling occurred, the initial geometrical imperfections were expected to grow in amplitude. This was monitored during the test to concentrate the measurements at the correct locations during testing, and to analyse the buckling location and imperfection growth after the test.

For this measurement two devices were available. The first was a laser trolley which drives on a beam suspended above the specimen (see Figure 57). The laser trolley scans the surface of the compression zone of the tube. This measurement contains the growth of initial imperfections, curvature of the tube and ovalisation of the tube.

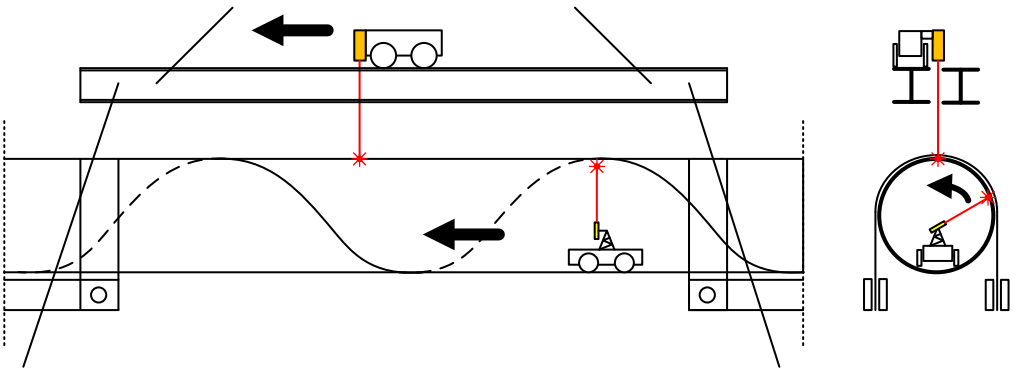

Figure 60 – Laser measurements of the tube during testing.

A second laser trolley was available for measurements inside the tube. It was used to make internal line-scans of the tube, similar to the external line scans of the external trolley, and for scanning an internal circle of the tube. This measurement can be automatically performed at determined intervals. These ring-scans contain information on the ovalisation of a cross section.

Since both laser trolleys have overlapping information output, they were not necessarily used both in each test. The use of the external laser cart was primarily due to its shorter development time.

After each load step, laser scans were made of the exterior and interior of the tube wall (see Figure 60). These measurements aided the analysis of geometrical imperfection growth during the bending test and offered ovalisation measurements both in horizontal and vertical direction in a relatively fine grid, as opposed to the only horizontal ovalisation measurements at relatively large intervals.

3.1.5 Test results

3.1.5.1 Definitions

- Moment. Resisted bending moment at the location of buckling.
- Curvature. Four measurements of curvature were used. The three local curvature measurements (see Figure 59) were denoted as K_1, K_2 and K_3. The average curvature measurement is denoted as K_{avg}.
- Local buckling. Clear (sudden) decrease in bending moment capacity.
- K_{Mmax}. Curvature at maximum moment. This value is the buckling curvature in case of a load controlled test.
- K_{crit}. Curvature at local buckling. This value is the buckling curvature in case of a load controlled test.
- Ovalisation. Change in diameter (ΔD).

3.1.5.2 Moment Curvature behaviour

The most important outputs of the tests are the moment-curvature relations of the tested specimens. A selection of these results is presented in Figure 61 and Figure 62.

The figures clearly show the behaviour of the different curvature measurements.

In principle, the four measurements behave equal in the elastic trajectory of the test. However, when parts of the tube start to deform plastically, some differences arise. In general, the local curvature measurement in which the local buckle forms is larger than other curvature measurements at the point of maximum resisted bending moment.

At the point of load drop-off, this difference is even larger. Since the plastic deformation of the tube is larger for lower D/t ratios, this effect is most clearly visible in the M-K diagrams presented in Figure 61. Notably, this behaviour was only observed for spirally welded tubes. The longitudinally welded tubes hardly showed any localisation of curvature (see e.g. Figure 62 right).

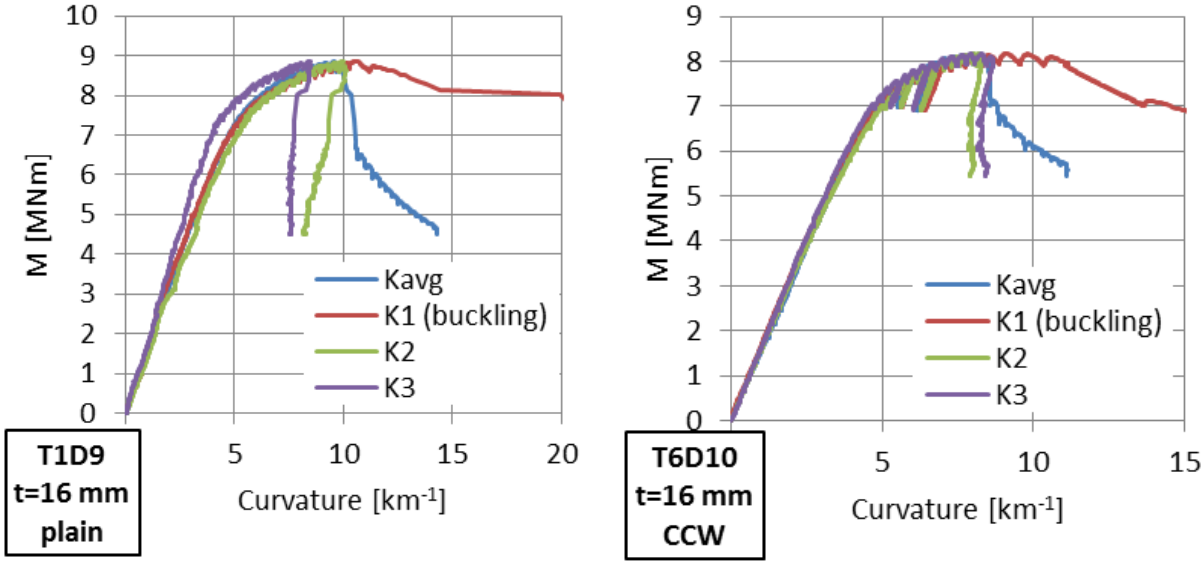

Figure 61 – Moment curvature results of test T1D9 and T6D10. Local curvature measurement in which the local buckle formed is marked as such.

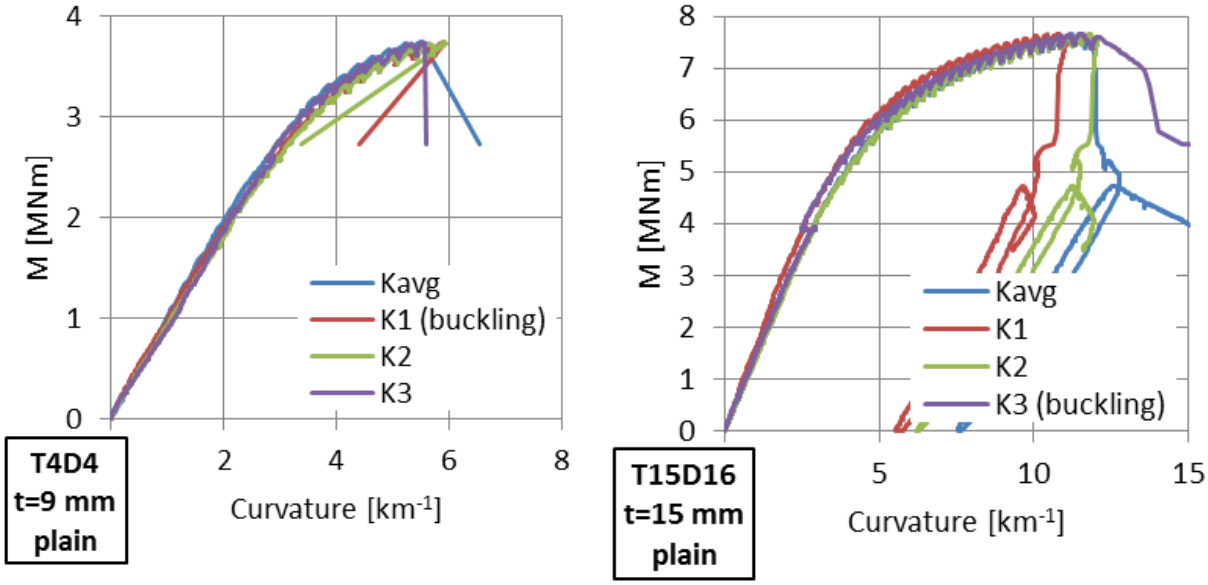

Figure 62 – Moment curvature results of test T4D4 and T15D16 (note, the latter is a longitudinally welded tube). Local curvature measurements in which the local buckle formed is marked as such.

3.1.5.3 Ovalisations

The ovalisations were measured at various locations along the tube (see Figure 58). The ovalisation measurements are numbered from left to right. In the figures the measured values are compared with the elastic theoretical value of the ovalisation (Reissner and Weinitschke, 1963). Examples of results measured during the tests are presented in Figure 63 and Figure 64. In both cases, the initial elastic part of the graphs is in good agreement with the elastic theory. When parts of the cross section start yield, agreement is less good. When a local buckle (suddenly) forms, large differences between the various measurements arise.

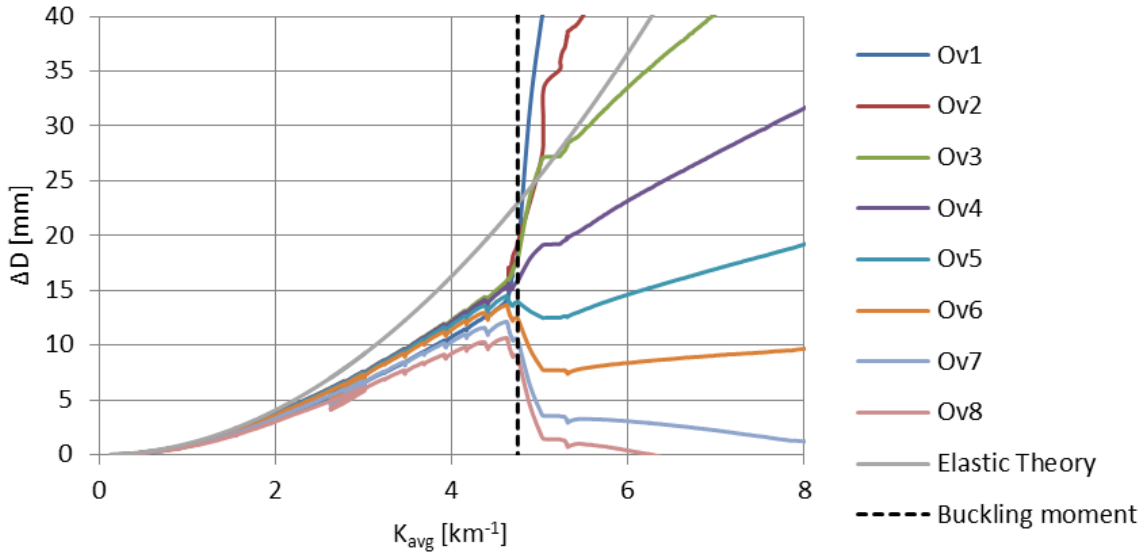

Figure 63 – Measured ovalisations during test T2D11.

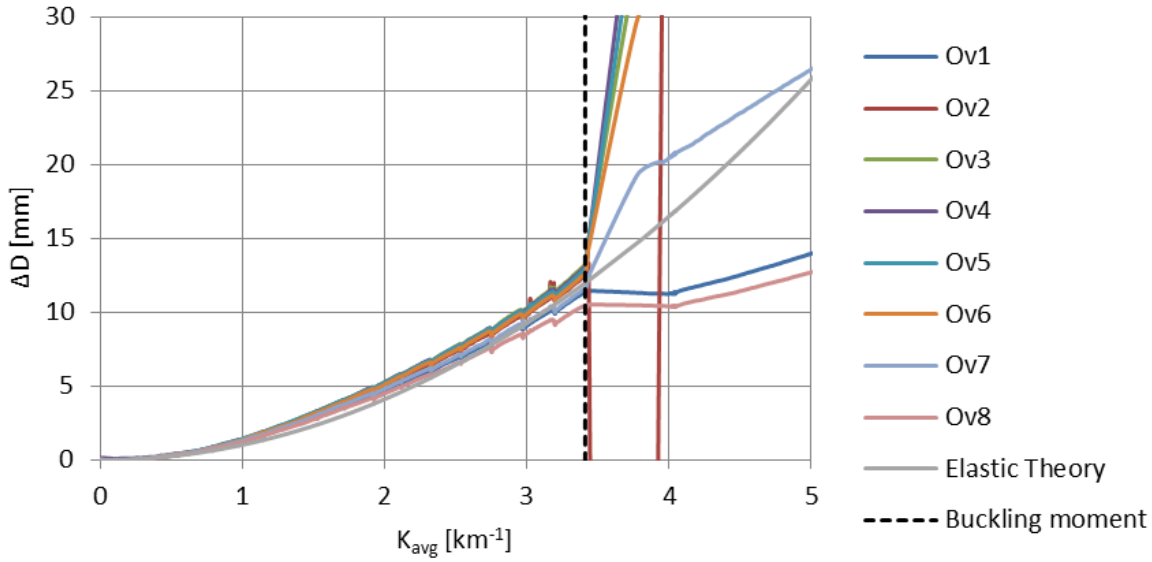

Figure 64 – Measured ovalisations during test T3D13.

3.1.5.4 Results of imperfection growth measurements

As the initial geometrical imperfections of each tube were scanned, the initial geometrical shape of the compression zone of the tubes is known. Furthermore, a laser scan is made at regular intervals, which results in a scan just before the formation of the local buckle for most specimens.

When these two scans are overlaid and compared with the location of the buckle, in many cases the origin of the local buckle is clear. The dimples that were formed during production are consistently seen as origins of the local buckle for plain specimens. For specimens that include a structural detail such as a girth weld or coil connection weld, the buckle often originates at this location. Examples of measurement results are presented in Figure 65 and Figure 66.

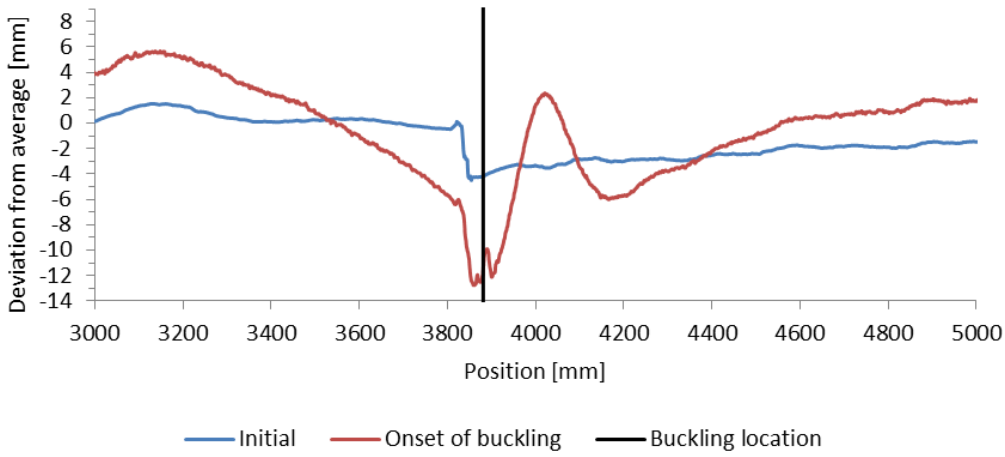

Figure 65 – Comparison of initial imperfections and measured tube wall profile at the onset of buckling for test T10DD6. The local buckle forms at the girth weld, where a misalignment of about 3 mm is present.

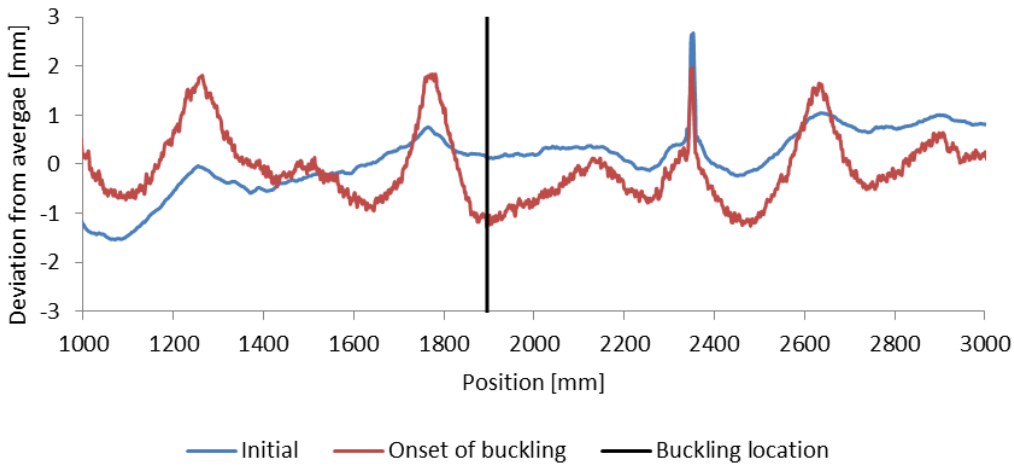

Figure 66 – Comparison of initial imperfections and measured tube wall profile at the onset of buckling for test T4D4. The local buckle formed at a regular, fabrication related, imperfection. The initial imperfection has increased 5 times in size.

The scans made with the internal laser trolley provide several interesting results. Firstly, the ovalisation measured with the ovalisation brackets (see Figure 58) can be validated. An example of this comparison is presented in Figure 67.

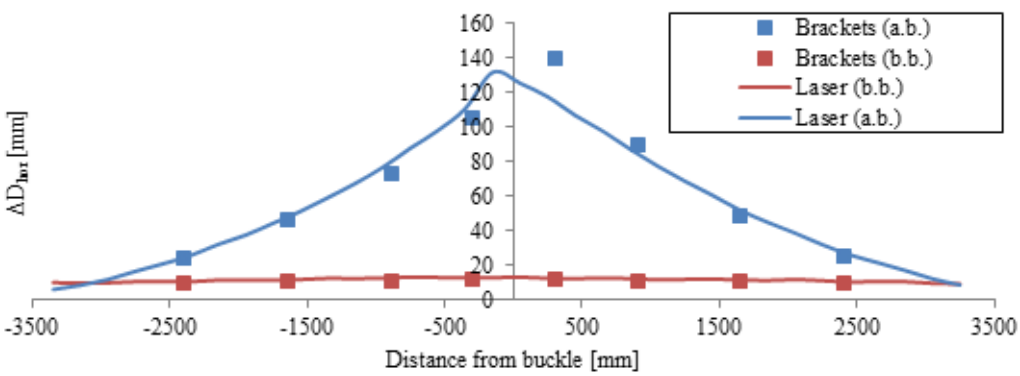

Figure 67 - Comparison of measured ovalisations with laser cart and ovalisations brackets at two different curvatures: before buckling (b.b.) and after buckling (a.b.)

Furthermore, the spacing between the ovalisation measurements can be made very small, so that the internal scan delivers a full 3D picture of the buckling mode (see Figure 68). These scans, performed directly after buckling and after final deformation, provide information on the depth and wavelength of the local buckle at these stages of deformation. This information is very valuable when validating numerical models.

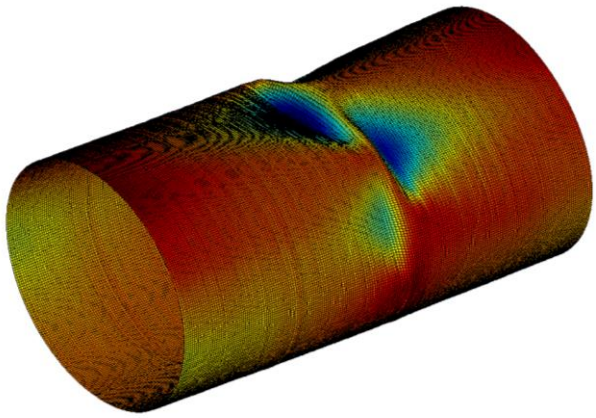

Figure 68 - 3D image of a specimen that buckled at the girth weld. Close inspection shows that both the girth weld and the spiral weld to the lower right of the girth weld are visible.

3.1.5.5 Overview and summary of test results

Two main parameters are recognized as important output of the tests. First is the deformation at which local buckling occurs. The selected parameter is the critical strain, which is calculated from the measured curvature as opposed to the readings from the strain gauges which may contain local effects. Secondly the maximum resisted moment is considered an important factor. In the graphs, this moment is normalized by the full plastic moment of the cross section where local buckling occurred.

An overview of the critical strains that were reached during the tests are presented in Figure 69. The figure shows the expected trend of lower critical strains for more slender tubes. Noteworthy is the tendency of specimens that feature a structural detail to buckle at a lower critical strain. Furthermore, longitudinally welded specimen T15D16 stands out with a very high critical strain

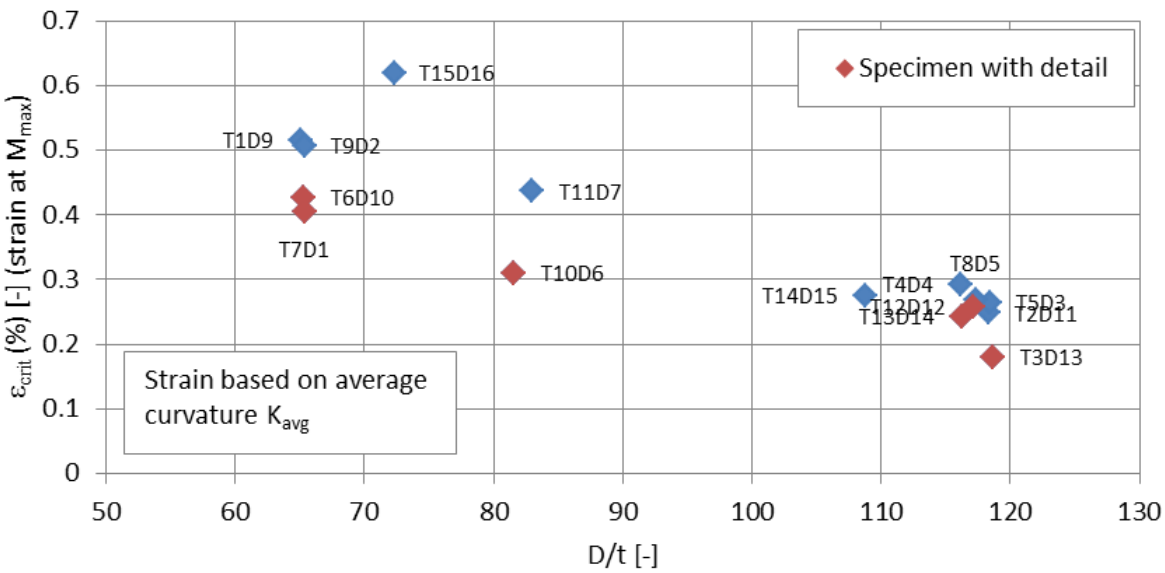

Figure 69 – Critical strains of all test specimens. Strains based on average curvatures.

A mentioned before, localisation of curvature is an important feature that was observed during the bending tests of the spirally welded tubes. Figure 70 presents the ratio between the maximum local curvature and average curvature for all specimens. The local curvature is on average about 12% higher than the average curvature at the maximum bending moment for spirally welded tubes. The two longitudinally welded specimens (T15D16 and T14D16) show no curvature localisation.

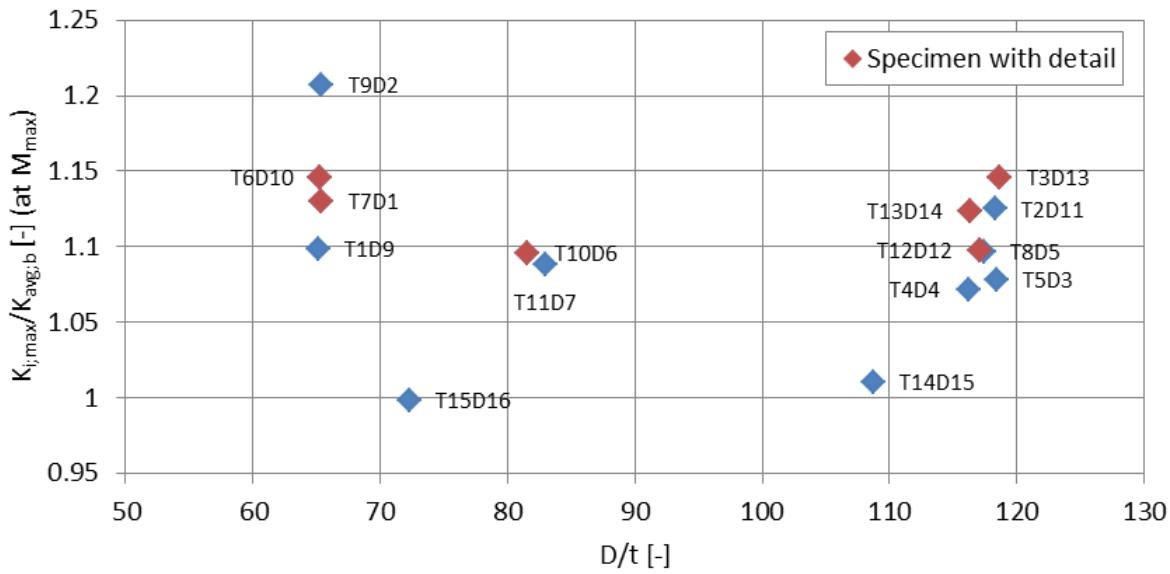

Figure 70 –Ratio between maximum measured local curvature and average curvature for all specimens.

An overview of the measured maximum resisted normalized bending moment is presented in Figure 71. Tabulated values are presented in Table 9 - Overview of test results of tests performed at TU Delft.

Similarly as for the critical curvatures, the figure shows some detrimental effect of the presence of a structural detail such as a girth weld or coil connection weld. Exception is specimen T10D6 which buckled on the weak side of a girth weld over which a large difference in yield strength existed. This allowed the weaker side to be supported by the stronger side; resulting in a high bending moment resistance.

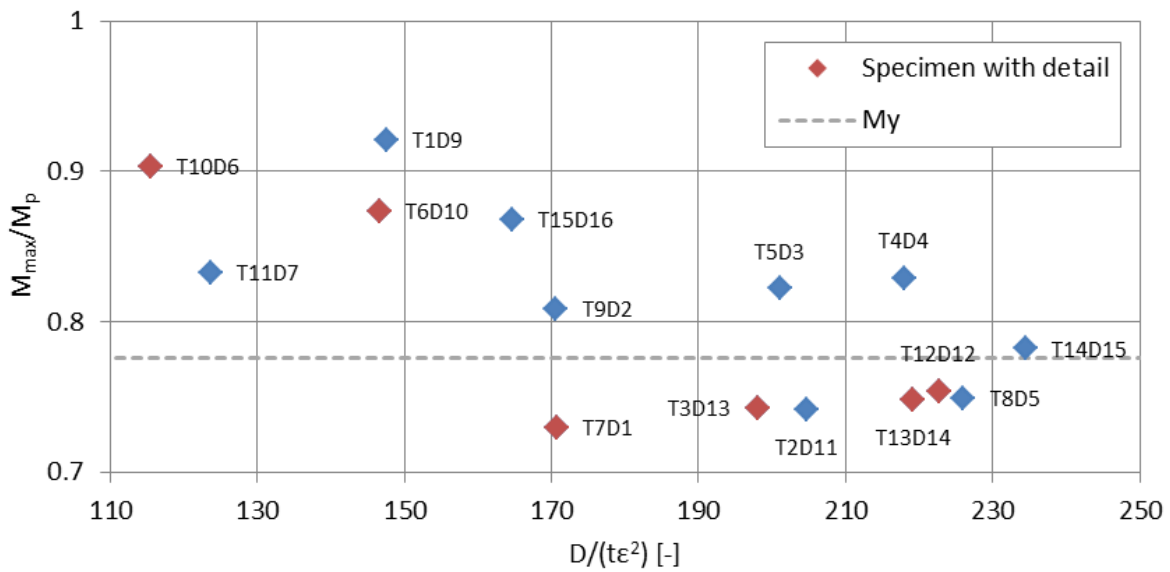

Figure 71 - Maximum resisted bending normalized moment for all specimens.

Table 9 - Overview of test results of tests performed at TU Delft.

Test and Tube I.D.	D × t [mm]	D/t	$D/(t\varepsilon^2)$	M_{max} [kNm]	M_{max}/M_{pl}
T1D9	1066 × 16.4	65.1	147.5	8840	0.921
T2D11	1067 × 9.0	118.3	204.6	3047	0.742
T3D13	1069 × 9.0	118.7	201.4	2869	0.742
T4D4	1065 × 9.2	116.2	218.1	3731	0.829
T5D3	1070 × 9.0	118.4	200.9	3338	0.822
T6D10	1066 × 16.3	65.3	149.1	8174	0.873
T7D1	1068 × 16.3	65.4	170.6	8096	0.730
T8D5	1068 × 9.1	117.4	226.0	3469	0.749
T9D2	1069 × 16.3	65.4	170.7	8979	0.809
T10D6	1070 × 13.1	81.6	117.7	4286	0.903
T11D7	1068 x 12.9	83.0	123.6	4221	0.832
T12D12	1069 × 9.1	117.1	223.8	3446	0.754
T13D14	1070 × 9.2	116.3	220.5	3393	0.748
T14D15	1068 × 9.8	108.8	234.5	4360	0.782
T15D16	1070 × 14.8	72.3	164.7	7666	0.868

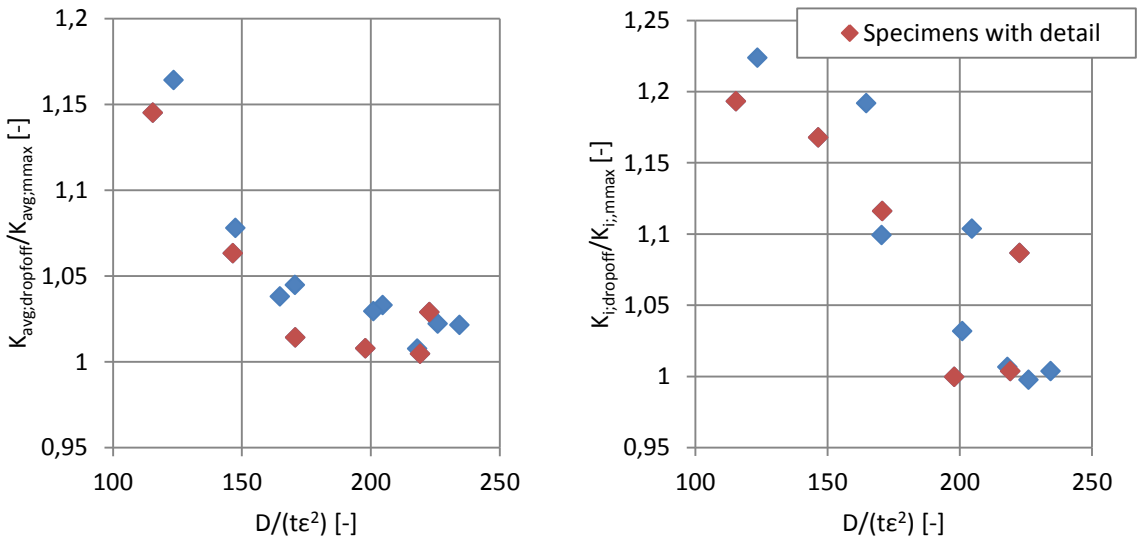

Figure 72 – Ratio between curvature at maximum bending moment and load drop-off. Left: average curvatures. Right: local curvatures at buckling location.

In a load controlled environment, the critical values of the element are indeed to be determined at the top of the M-K diagram. However, in a deformation controlled situation, the actual drop-off of the M-K curve may be of similar interest. An overview of the ductility ratio, defined as the ratio between the curvature of maximum moment and load drop-off, is presented in Figure 72. The figure shows a strong correlation between tube slenderness and the ductility ratio.

Once more, the presence of a structural detail may negatively influence the result. The extent of that influence of course strongly depends on the size of the imperfection such as misalignment. In good quality welding the effect is minimal or absent.

3.1.5.6 Buckling location and influence of structural details and spiral welds

The testing program included several specimens with a structural detail (girth weld, coil connection weld). In the two specimens with only a girth weld, both buckled at the girth weld. In the specimen with only a coil connection weld, buckling occurred at (close to) the coil connection weld. For the three specimens that included both a girth weld and a coil connection weld, one specimen showed buckling at (close to) the girth weld, and two specimens showed buckling away from the details in plain material. In case of the first of these two (D7T1), these seem to be no clear cause as to why local buckling moved away from the structural detail. In case of the second (T12D12), it appears that the middle part of the specimen was stronger, both in wall thickness and yield strength. It is possible that this stronger middle part supported the outer parts at the detail, forcing a buckling in the weaker parts plain area.

In all cases where local buckling occurred at (close to) a structural detail, the buckle initiated in the weaker side in terms of wall thickness and/or yield strength.

In the cases where buckling occurred in plain material, buckling usually occurred away from the spiral welds and initiated a production related dimple. In the one case where buckling occurred close to a spiral weld, the post buckling state clearly showed that the spiral weld acts as a stiffening rib in the buckle (see Figure 73), explaining why other tubes buckled away from the welds.

Figure 73 - Photo of the only observed buckle close to a spiral weld.

3.1.5.7 Summary of qualitative findings of TU-Delft tests

- Localisation of curvature is observed both before and after reaching the maximum resisted bending moment in the bending tests of spirally welded tubes. In longitudinally welded tubes this is not observed.
- The presence of a structural detail such as a girth weld or coil connection weld has, in most cases, a negative effect on the capacity of the structure, both in terms of maximum curvature and bending moment capacity. This effect highly depends on the imperfections (eccentricity, high-low) and differences in material properties on both sides of the welds.
- If a local buckle forms in plain tube material, it generally forms at a geometrical imperfection away from the spiral weld. These imperfections have in some cases shown to be production related. In the other cases there are strong indications that they are production related.

3.2 Task 3.2: Bending with normal force in Karlsruhe

The tests were conducted at the Research Centre for Steel, Timber and Masonry in Karlsruhe (KIT).

Object of the tests were 8 spiral-welded steel tubes, named K1 to K8, with a length of 10500 - 10520 mm that were tested in bending with normal force. The outside diameter of the specimens varied from 820 – 863 mm with D/t-ratios ranging from 73,5 to 101,5 all in grade X52 (specified minimum yield strength 52000 psi ~ 358 N/mm^2). The material properties were verified in own material tests. Table 10 shows a summary of the specimens. Besides the dimensions of the specimens the table contains information on weld specifications such as the positions of coil connection welds (CCW). In the case of K7 the specimen consists of two different tubes that are connected with a girth weld (GW) in the centre of the specimen.

Table 10 - Specimen specifications.

I.D.	D × t [mm]	D/t	type	Type	Grade
K1	820 x 11	74.5	Spiral	CCW at end	X52
K2	820 x 11	74.5	Spiral	CCW in middle	X52
K3	820 x 8	102.5	Spiral	CCW at end	X52
K4	820 x 8	102.5	Spiral	-	X52
K5	820 x 8	102.5	Spiral	CCW in middle	X52
K6	863 x 8 .4	102.7	Spiral	-	X52
K7	863 x 8 .4	102.7	Spiral	GW in middle	X52
K8	863 x 8 .6	100.3	Spiral	-	X52

The specimens were provided by the project partner ArcelorMittal Luxemburg. The selection of sections represents tubes as they are used as structural parts in combined quay walls.

3.2.1 Test setup

The test setup has been described in section 2.1.4.1.

3.2.2 Test procedure

During the tests a tensile force was created by the hydraulic cylinders that pulled the ends of the brackets together (see Figure 17 and Figure 18). The applied force was controlled by the elongation of the cylinders. The stroke and the speed of loading depended on the amount of oil that was pumped into the cylinders by a mobile aggregate.

As a result the tubes were loaded with a normal force and a bending moment. The bending moment resulted from the applied force and the lever of the brackets. The bending moment was slightly changing in size from the ends to the centre of the tube due to the deflection that led to an increase of the lever and thereby of the acting bending moment in the tube.

The relation of the normal force to the acting bending moment could be controlled by the length of the lever of the acting force. There were two anchorage points at the ends of the brackets with different distances to the tubes axis where the pulling device could be connected to (see Figure 17).

All specimens buckled at load levels between 446 kN and 661 kN. The required stroke varied approximately between 170 mm and 570 mm. The data from the load cell, the displacement transducers and in some cases further strain sensors where recorded constantly with a frequency of 2 Hz or higher during the execution of the tests.

3.2.3 Summary of experimental results

The results are shown in Table 11. The slenderness (D/t-ratio) of the sections is calculated with the measured thickness after failure. The sixth column gives the maximum applied normal force (test load). The maximum bending moment M_{max} is calculated with F_{max} multiplied by the largest distance of the axis of force to the deflected centreline of the section (which is the sum of the lever arm L and u_y. In the last column M_{max} is normalized to the elastic bending moment capacity M_{el}.

Table 11 - Test results.

I.D.	$t_{failure}$ ($t_{nominal}$) [mm]	D_{out} [mm]	Slenderness $(D_{out}-t)/t$	Slenderness $D_{out}/(t\varepsilon^2)$	Maximum force F_{max} [kN]	Deflection u_y [mm]	Lever arm L [mm]	M_{max}/M_{el} [-]
K1	11 (11)	820	73.5	140.5	649.0	183.2	4000	1.084
K2	11.1 (11)	820	72.9	125.1	595.7	126.7	4000	1.083
K3	9.1 (8)	820	89.1	114.7	445.7	116.8	4000	1.306
K4	7.8 (8)	820	104.1	206.7	465.2	86.9	4000	1.018
K5	7.5 (8)	820	108.3	194.5	531.8	37.5	3000	0.994
K6	8.4 (8.4)	863	101.7	181.4	661.2	81.9	3000	1.019
K7	8.4 (8.4)	863	101.7	194.1	526.6	76.9	4000	1.004
K8	8.6(8.6)	863	99.3	174.2	530.1	68.4	3000	0.808

The ratio between applied bending moment M and the elastic resistance M_{el} is unusual large for specimen K3. This is the result of the low yield stress of the material K3_C which is used for the calculation of M_{el}. The test showed that the section is still able to take up considerable loads above this load level.

Another peculiarity in the results is specimen K8 which failed at a very low load level. This specimen reached 80,8 % of the elastic bending moment capacity M_{el} only. The reason for this is the influence of the particular severe local pre-deformation.

From the values in Table 11, two groups with a similar outcome can be identified. The first group consists of the specimens K1 and K2 with a slenderness of D/t ≈ 73. These specimens resisted a bending moment which is approximately 8% higher than the elastic bending moment capacity M_{el}. The other group consists of the specimens K4 to K7 with a larger slenderness of D/t ≈ 105. According to this these specimens showed a lower bending moment resistance which is close to the elastic bending moment capacity M_{el}. In Figure 74 the recorded force versus the stroke of the pistons is plotted for K1 and K7 exemplary for these two groups.

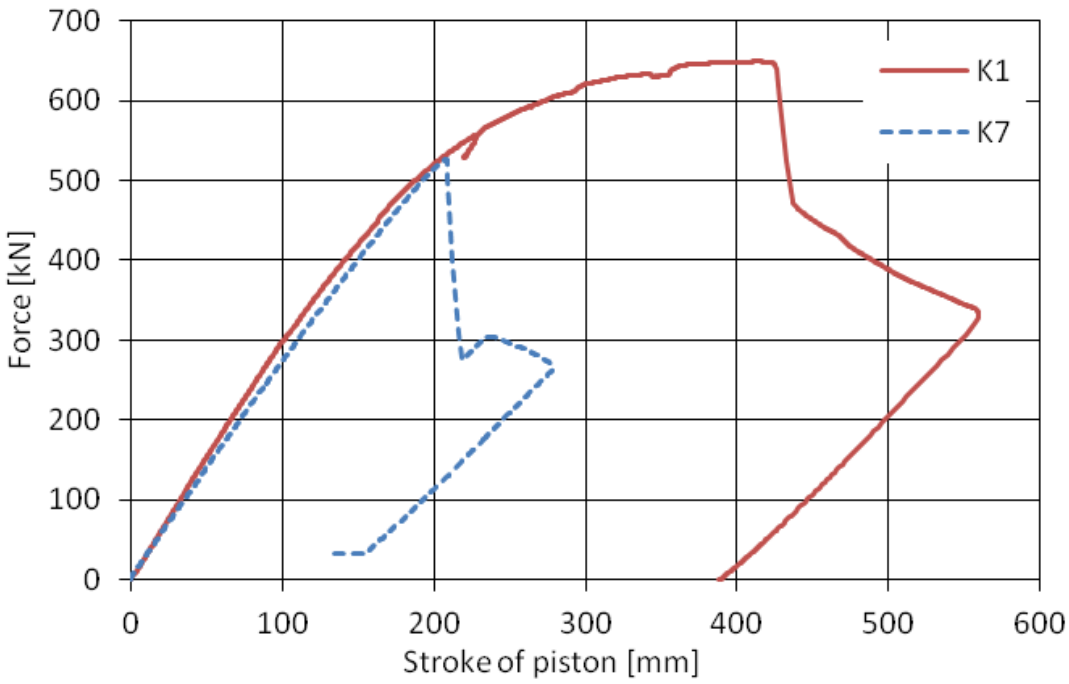

Figure 74 – Force-displacement diagram for K1 and K7.

For specimen K3 the ratio between the maximum applied bending moment M_{max} and the elastic resistance M_{el} is unusual large. It should be noted that M_{el} was calculated with the very low yield stress of the material K3_C from which only part of the tube consisted. The test showed that the section is still able to take up considerable loads above this load level.

Another peculiarity in the results is specimen K8 which failed at a very low load level. This specimen reached 81 % of the elastic bending moment capacity M_{el} only. The reason for this is the influence of a severe local initial deformation which was recorded in detail.

In

Figure 75,

Figure 76 and Figure 77, the description of the situation before the test (A), the pattern of buckles (B) and the interpretation (C) are summarized.

K1	
A. Coil connection weld close to an end. B. Buckling 2.55 m from centre. Pattern symmetric to axis. C. No influence by nearby weld.	

K2	
A. Coil connection weld near compression zone 552 mm from centre. B. Buckling pattern oriented along the spiral weld. C. Influenced by nearby weld.	

Figure 75 – Failure mechanism of specimens with D/t ≈ 73.

K4	
A. - B. Buckling pattern symmetric to axis. C. No influence by nearby weld.	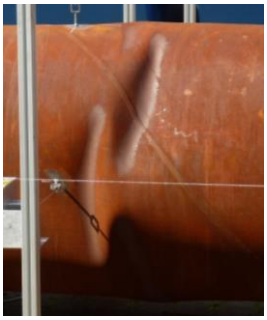

K5	
A. Intersection point of coil connection weld with spiral weld in centreline compression side, 885 mm from middle. B. Buckles eccentrically along spiral weld. C. Influenced by nearby weld.	

K6	
A. Spiral weld crossing the centreline at the compression side app 180 mm from middle. B. Buckle 1,1 m outside the middle. C. No influence of weld.	

K7	
A. Girth weld in the middle. B. Pre-deformation close to the centreline at compression zone. C. Buckles influenced by pre-dimple.	

Figure 76 – Failure mechanism of specimens with D/t ≈ 105.

K3	
A. Coil weld in tension zone and neutral zone. B. Buckles along spiral weld close to restrained ends at change of materials. C. Influenced by material properties.	

K8	
A. Scratch and dimple close to the centre at compression zone. B. Centre of buckle at pre-deformation. C. Buckles influenced by pre-dimple.	

Figure 77 - Failure mechanisms of specimens K3 and K8.

More details on this test program are given in the reference [1] below.

3.2.4 References

[1] Reinke, T., Sadowski, A. J., Ummenhofer, T., Rotter, M. J. (2014). “Large scale bending tests of spiral welded steel tubes.” Eurosteel 2014, 7th European conference on Steel and Composite Structures, Naples, Italy, 10-12 September 2014.

4 WP4: Numerical modelling and simulation of experiments

The objectives of WP4 are the following:

- To develop and incorporate a steel material plasticity model in ABAQUS appropriate for large-scale shell buckling simulations.
- To develop and establish numerical techniques to simulating the manufacturing process of spirally welded tubular members and determine the residual stresses of such tubes.
- To establish a systematic methodology to account for initial imperfection measurements and residual stresses in the numerical simulation of large-diameter tubular members, directly from measurements.
- To simulate the experimental procedure of WP3 and verify the test results.

4.1 Task 4.1: Constitutive modelling for local buckling calculations in the plastic range

4.1.1 Introduction

To predict the occurrence of local buckling of cylindrical shell subjected to bending loading well into the plastic range, the use of an appropriate constitutive plasticity model is necessary. This model should be able to account for the highly non-linear behaviour of steel material during buckling, where an abrupt change of the stress path occurs. The main question is whether classical plasticity models (e.g. “built-in” models in standard FE programs), or an enhanced plasticity model is required.

4.1.2 Literature review

Extensive testing of steel plates and shells was carried out in the 50’s and 60’s, and analytical solutions were attempted to predict the lowest bifurcation load (buckling load). In particular, buckling of thin-walled shells was a hot topic in those days, due to its important applications in aeronautical structures, as well as because of the significant discrepancy between test data and analytical predictions. More specifically, analytical predictions appear to substantially overestimate the buckling load. This discrepancy was attributed to the strong imperfection sensitivity that characterizes the shell response [1],[2] because of the infinite number of buckling modes associated with the buckling load. This problem has been more apparent in steel thin-walled cylindrical shells under uniform axial compression. The case of bending has been less imperfection sensitive but, again imperfections govern the response of a bent thin-walled cylinder. At the same time, attempts to predict the buckling load of thicker shells were conducted. Relevant experiments indicated that the response was less sensitive to initial imperfections. These analytical attempts were aimed at implementing theories of multi-axial plasticity into the shell governing equations and compute the lowest bifurcation load [3],[4].

The bifurcation of a solid deformed in the inelastic regime is examined through the so-called “comparison solid” concept [4]. In numerical simulations, this “comparison solid” concept reduces to the examination of loss of positive definiteness of an appropriate stiffness matrix of the structural member. It has been recognized that in order to obtain accurate predictions of bifurcation in the inelastic range, a material model more elaborate than the J_2-flow plasticity model should be used. This observation was denoted in early works, where analytical works based on J_2-flow plasticity provided buckling load predictions, which were quite high compared with available experimental data [3]. However, bifurcation predictions based on the J_2-deformation moduli may provide a much more reliable prediction of buckling load. The good predictions of the deformation theory as opposed to the poor predictions of the flow theory can be attributed to the normality of plastic strain increment with respect to the yield surface. More specifically, the J_2-flow theory is an associated flow with plastic strain increment always normal to the von Mises yield surface. On the other hand, one can easily demonstrate that using the rate form of the J_2-deformation theory, the plastic strain increment is non-associative, composed by two additive components, one normal to the yield surface and one tangent to the yield surface. This makes the elastic-plastic moduli of the J_2-flow

theory to be significantly stiffer than the corresponding moduli of the J_2-deformation theory, thus explaining the unreasonably high predictions of the J_2-flow theory in comparison with experimental data [5]. The question is whether such a refined non-associative plasticity model is required for the purposes of the present study.

4.1.3 Numerical results

For this purpose, a numerical model was developed to investigate the effect of the plasticity model on the buckling stress (σ_c) and critical strain (ε_c). A large range of D/t ratios was examined. The numerical results presented in Figure 78 and Figure 79 depict the predictions of the two plasticity models for axially compressed tubes, and indicate that tubes with D/t values at the order of 100 are described by the classical (J_2) flow theory with very good accuracy. In particular, it is observed that the difference in buckling stress (σ_c) of the two predictions is less than 3.4 %. Given the fact that those differences will be further reduced in the presence of initial imperfections, one may conclude that the Von Mises (J_2) flow theory of plasticity (classical plasticity theory) with isotropic hardening can be used, as incorporated in ABAQUS as a "built-in" model. In these figures, experimental data from the literature review are also included.

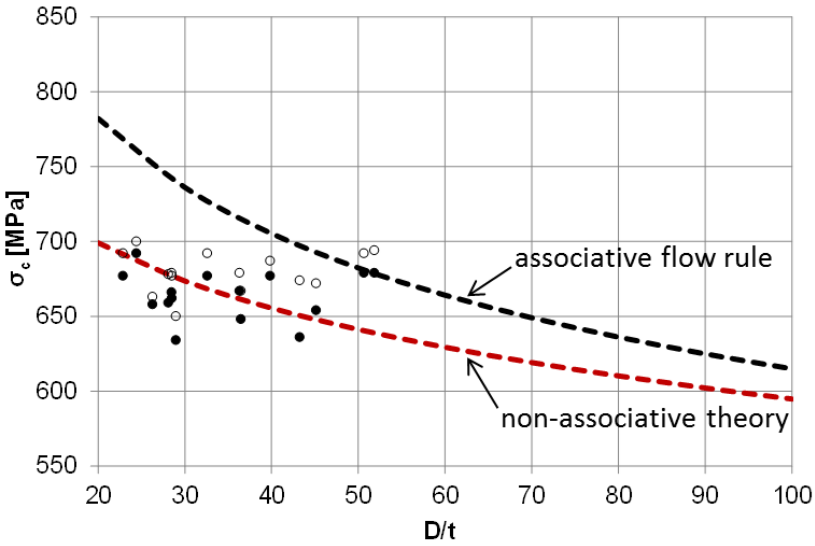

Figure 78 - Experimental values of critical stress for different values of D/t and comparison with the predictions from the 2 constitutive models.

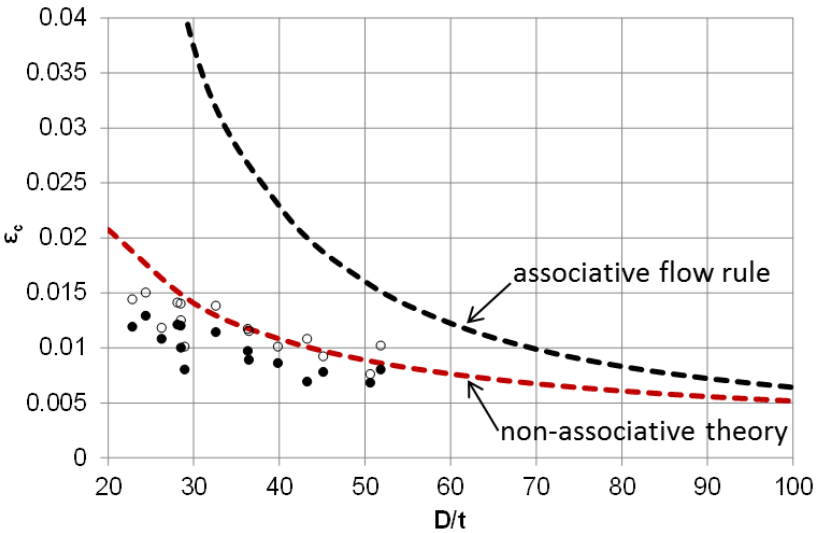

Figure 79 - Experimental values of critical strain for different values of D/t and comparison with the predictions from the 2 constitutive models.

4.1.4 References

[1] Koiter, W.T., (1945). On the stability of elastic equilibrium (in Dutch), Thesis, Delft, H.J. Paris, Amsterdam.

[2] Budiansky, B., (1974). Theory of buckling and postbuckling behavior of elastic structures, Adv. Appl. Mech. 14, 1–65.

[3] Batterman, S.C., (1965). Plastic buckling of axially compressed cylindrical shells, AIAA Journal, 3, 316-325.

[4] Gellin, S., (1979). Effect of an axisymmetric imperfection on the plastic buckling of an axially compressed cylindrical shell, ASME J. Appl. Mech. 46, 125–131.

[5] Bardi, F.C., Kyriakides, S., (2006). "Plastic buckling of circular tubes under axial compression-part II: Analysis", International Journal of Mechanical Sciences, 48, 830-841.

4.2 Task 4.2: Modelling of the spirally welded tube

4.2.1 Introduction

Spirally welded tubes offer cost benefits over UOE tubes and are used successfully in structural applications. In the production of spirally welded tube, hot rolled coiled steel plate is continuously shaped into a tube by a spiral forming facility, applying a constant bending radius. Figure 80 shows a schematic representation of the manufacturing process of a spiral-welded tube. In contrast to longitudinally welded tube production, in which each tube diameter requires a certain plate width, spirally welded tube production is characterized by the fact that various tube diameters can be manufactured from a single plate width. This is because the approach angle of the plate as it is fed into the forming unit can be modified. After bevelling the edges, the tube is formed and the inside and outside welding are completed. Finally, the tube is cut to the desired length.

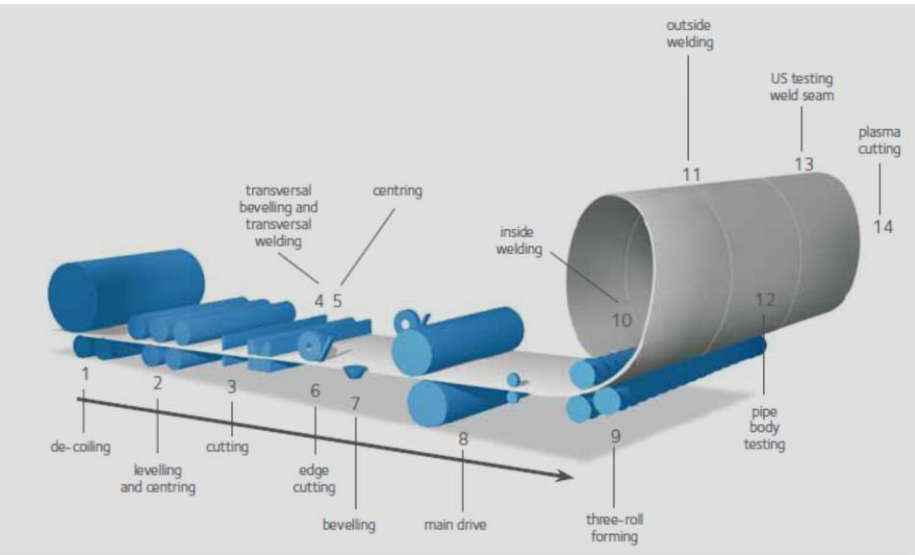

Figure 80 - Schematic representation of the manufacturing process of spirally welded tubes.

4.2.2 Numerical simulation of cold bending process

The numerical simulation presented in this section is aimed at predicting the stresses developed during the cold bending manufacturing process of the steel plate during spirally welded tube manufacturing. For this purpose, numerical modelling of bending of a steel plate is conducted. The resulting (residual) stresses are employed as initial conditions in the numerical model for the simulation of the bending response. A short parametric study is also conducted to investigate the effect of geometric and material parameters on the residual stresses.

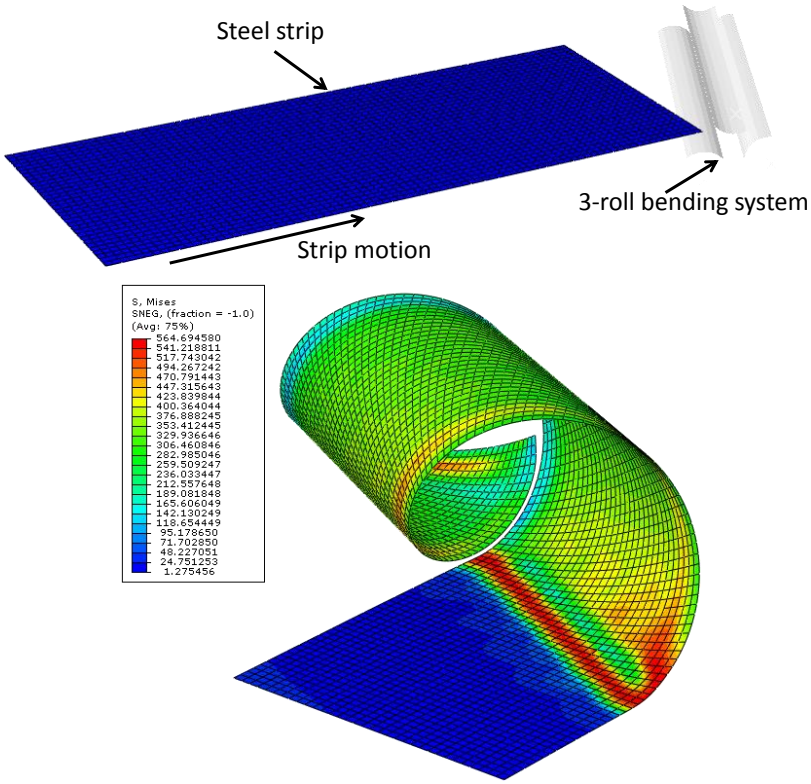

Figure 81 - (a) Finite element numerical model of spiral cold bending simulation; (b) Longitudinal motion of the plate through the rollers results in the formation of the spirally welded tube.

4.2.3 Description of numerical model

The numerical model is developed in finite element program ABAQUS/Standard. In Figure 81a, the main parts of the model are shown, i.e. the steel plate and the three-roll bending system. In the analysis, the steel plate moves continuously in the longitudinal direction, until its corner reaches the three-roller bending device, also referred to as "pyramid" roller set-up. The three rollers, placed at appropriate locations, bend the plate into a spiral cylindrical shape, and with continuous motion of the plate, a spiral tube is formed.

The deformable steel plate is simulated with four-node reduced integration shell elements (S4R), while the rollers are simulated as analytical rigid parts. The element size for the plate finite element mesh is selected equal to 5% of the tube diameter. The plate material is simulated as elastic-plastic with isotropic material. A variety of integration schemes are employed, considering 5 to 41 integration points through the thickness for the plate shell section. Furthermore, in the present analyses, the rollers-plate interaction is considered frictionless.

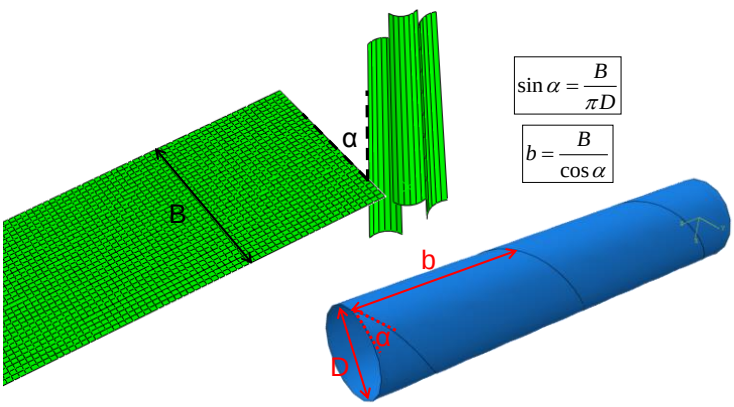

Figure 82 - Basic geometric characteristics of the numerical model for spiral-weld forming.

The basic geometric characteristics of the numerical model are depicted in Figure 82. Specifying the tube diameter D and the spiral "pitch" (sometimes referred to as "lead") b, it is possible to calculate the corresponding forming (spiral) angle α and the width of the plate B using simple geometric equations, also shown in Figure 82.

4.2.4 Calculation of residual stresses

The resulting stresses in the tube wall are obtained from the above finite element analysis. The numerical results showed that there is a quasi-uniform distribution of stresses along the tube, except for the plate edges, where edge effects occur. Based on experimental observations, buckling occurs at a certain distance from the spiral weld. Therefore, these edge effects may not be important, and in the following, the quasi-uniform values of residual stresses (away from the edges) are reported.

The distribution of residual stresses over tube thickness is depicted in Figure 83 for a 42-inch-diameter spiral tube, with thickness equal to 16.4 mm and yield stress of the plate equal to 541 MPa. The horizontal axis of Figure 83 represents a non-dimensional coordinate across the tube thickness, where the values of 0 and 1 correspond to the internal and the external surface of the tube respectively. Stresses are presented in the global coordinate system (x, θ) and normalized by the yield stress σ_y. In the results of Figure 83, nine integration points through the wall thickness have been employed. Following a short special-purpose parametric study on the number of integration points through the thickness, it has been concluded that the use of nine integration point through the tube wall thickness is optimal; the use of more integration points does not significantly affect the distribution of the calculated residual stresses.

During the spiral forming process, the steel plate undergoes significant plastic deformation due to cold bending. Figure 84 depicts the evolution of stresses at the local coordinate system of the inner surface during the passage of the plate through the rolling system. Initially, a rapid increase of stresses is observed until yielding. The maximum stress on a specific point of the plate occurs when the point is inside the rollers. Subsequently, stresses are stabilized at a lower level because of a small rebound. It is also observed that stresses change sign during the last stage of the spiral forming process.

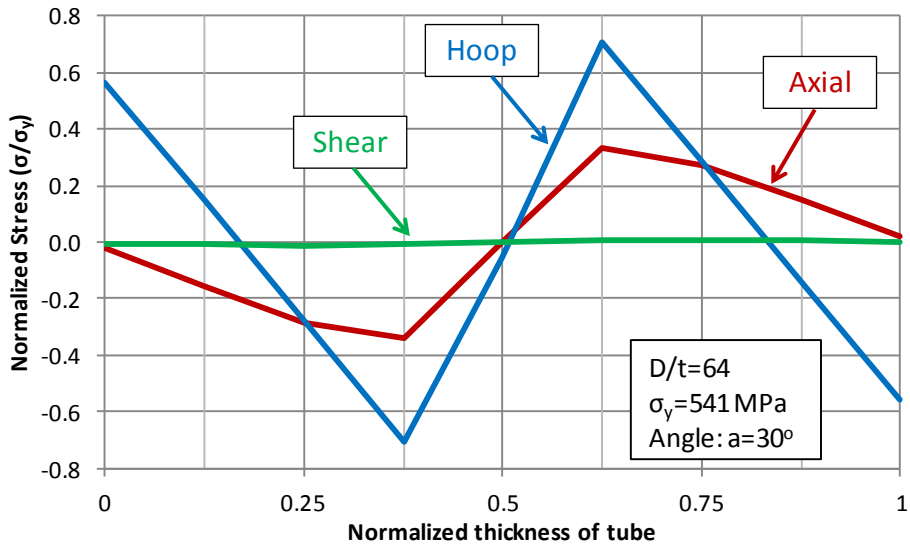

Figure 83 - Distribution of axial, hoop and shear normalized residual stresses across tube thickness.

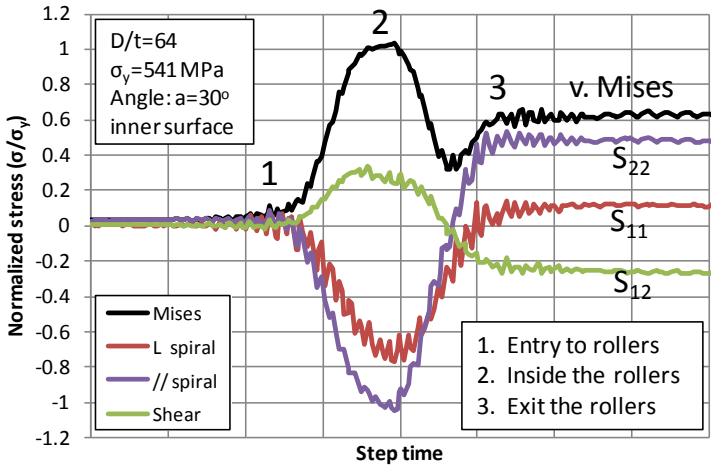

Figure 84: Evolution of normalized residual stresses during the forming process.

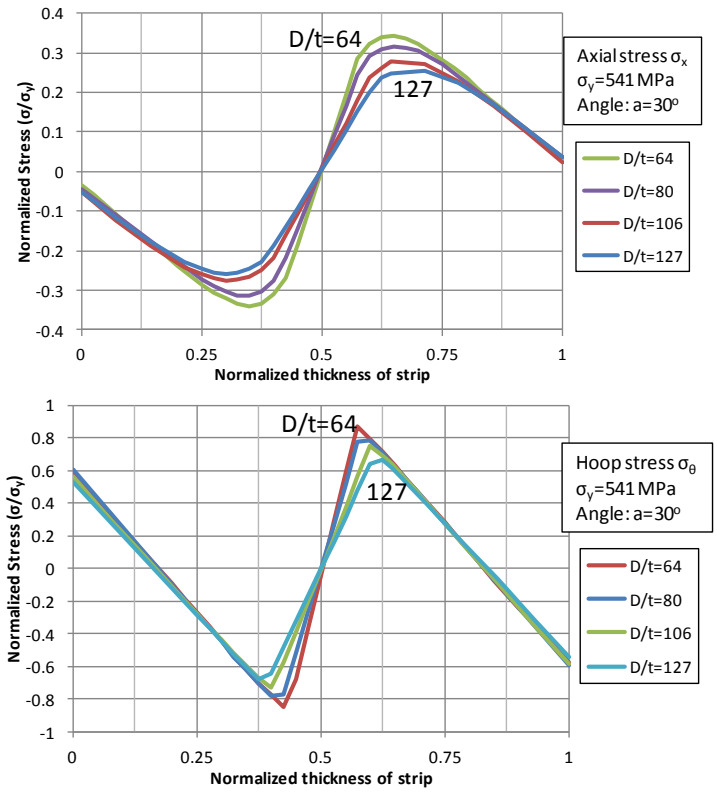

Figure 85 - Distribution of residual stresses over thickness for different values of D/t ratio; (a) axial stresses and (b) hoop stresses.

The influence of the D/t ratio is examined, repeating the cold-forming simulation for different values of tube thickness t for the forming of a 42-inch-diameter tube. The numerical results in Figure 85 indicate a small difference in the distribution of residual stresses over thickness, as shown for the variation of axial stresses σ_x and hoop stress σ_θ in the global coordinate system. The results show that thicker tubes result in somewhat higher values of residual stresses.

Numerical results were also obtained for different steel grades. The numerical results indicated that, for the same hardening characteristics of the steel material, the steel grade does not affect the maximum value of residual stresses, normalized by the value of the material yield stress. Moreover, the effect of the spiral forming angle on the residual stresses has been investigated and the numerical results indicated that, although stresses in the local CS are different, the transformed stresses in the global CS are practically unaffected by different forming angles.

4.3 Task 4.3: Modelling of imperfections and residual stresses

4.3.1 Introduction

In this section, it is discussed the numerical modelling of the imperfections and residual stresses as evaluated and characterized in the previous WPs. The actual measurements are characterized to provide generic forms of the critical components of the total imperfections, so that these can later be used in parametric studies. This task involves determining which aspects of the measured forms are the critical ones for further modelling of tubes under this loading condition.

4.3.2 Modelling of imperfections

For the simulation of tubes that do not contain a coil connection weld, a rectangular mesh of shell finite elements is employed, as shown in Figure 86. A relatively dense mesh of shell elements is used, with size of each element equal to 50 mm, i.e. less than 5% of the tube diameter. The tube is considered initially imperfect, with a wavy-type (wrinkling) geometric imperfection, in the form of the first buckling mode, obtained through a standard eigenvalue analysis of the tube under consideration subjected to pure bending conditions. This is a short-wave wrinkling pattern on the compression side of the bent tube, as shown in Figure 86b. The maximum wrinkle depth is denoted as w_0, with $w_0 = 2\delta_0$ and δ_0 is the imperfection amplitude, i.e. the maximum deviation of the wrinkled shell surface from the perfect cylinder. Based on measurements of the initial tube geometry, the imperfection amplitude is a fraction of tube thickness, with typical values of δ_0/t ranging between 2% and 10%. Seven finite elements are considered per half-wavelength, to describe accurately the wrinkling pattern. For the particular case of a tube with girth weld, different material properties are taken into account for the two parts of the tube on either side of the girth weld, as shown in Figure 87a. In addition to the rectangular mesh, a “spiral mesh” is also employed, as shown in Figure 87b. This mesh has a density similar to the rectangular finite element mesh. In that mesh, the spiral weld is modelled as a separate part, with different material properties, so that weld over-matching conditions are considered. The “spiral mesh” is also employed for the simulation of the bending response of spirally welded tubes containing a coil weld.

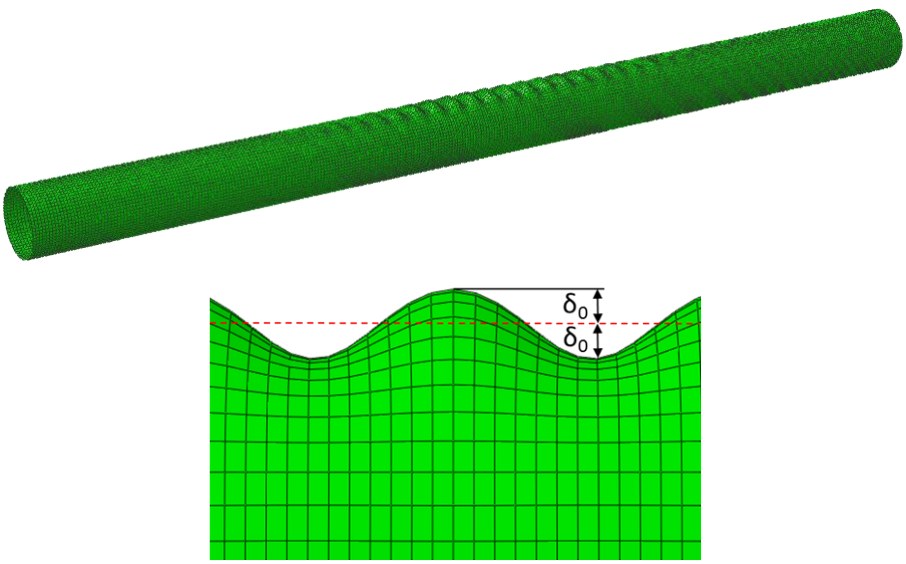

Figure 86 - (a) Rectangular finite element mesh; (b) Wrinkled pattern in the compression side - shape of the first eigenmode imperfection.

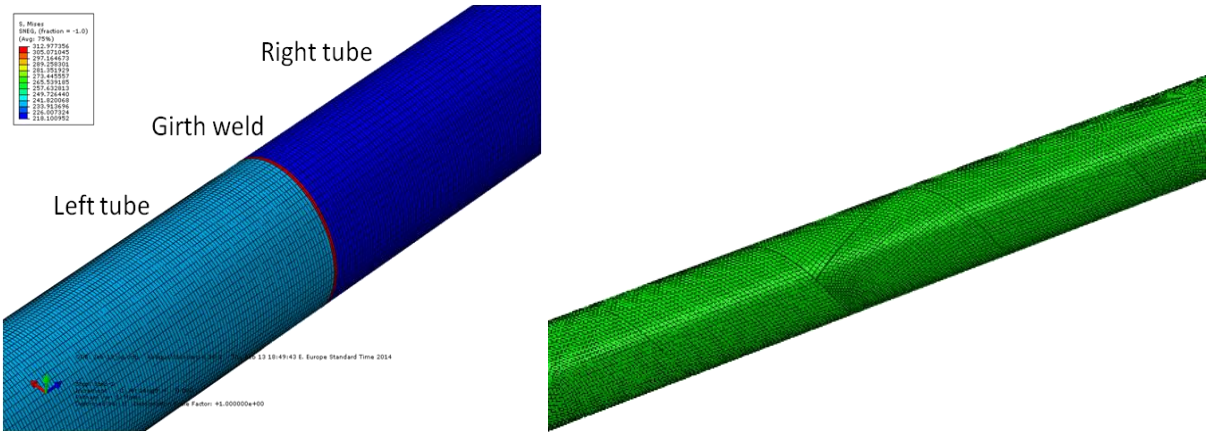

Figure 87 - a) Partitioning of tube which contains girth weld; b) Spiral mesh for the analysis of tubes containing coil weld.

4.3.3 Modelling of residual stresses

Residual stresses have been inserted in the numerical model as initial conditions before the application of bending loading. The distribution and magnitude of axial, hoop and shear residual stresses, which have been calculated by the corresponding Task 4.2, have been considered in the numerical model. Nine integration points through the wall thickness for the shell section are considered for the analysis. The distribution of normalized residual stresses over tube thickness is depicted in Figure 88.

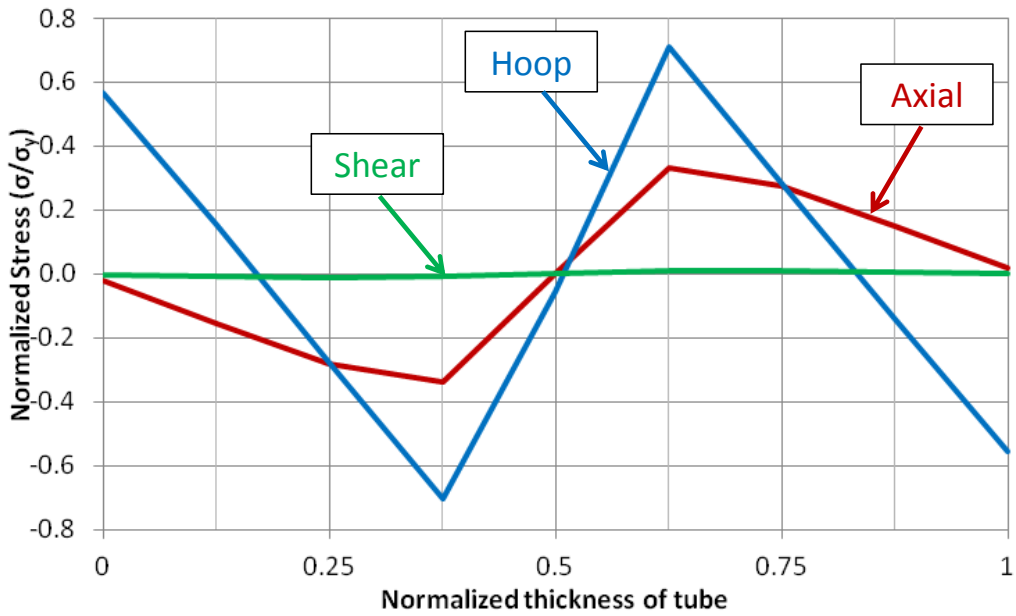

Figure 88 - Distribution of axial, hoop and shear normalized residual stresses over tube thickness.

The residual stresses in the tube wall are obtained from the above mentioned finite element analysis in the local axes of each shell element, which coincide with the directions perpendicular and parallel to spiral. Subsequently, the values of stresses are transformed from the local coordinate system, which follows the direction of the spiral, to the global coordinate system of the tube, defined by the axial x direction and the circumferential (hoop) θ direction, using appropriate tensor rotation equations.

4.4 Task 4.4: Simulation of experimental results

4.4.1 Simulation of experiments carried out in Delft

These experiments were simulated by U-Thessaly.

4.4.1.1 Finite Element Modelling of Tube Bending

A numerical model has been developed in ABAQUS/Standard for simulating the bending experiments. The tubes are modelled with four-node reduced integration shell finite elements (S4R), where the shell surface corresponds to the external tube diameter. In the finite element model, inelastic material behaviour is considered through a von Mises plasticity model with isotropic hardening.

Residual stresses are inserted in the model as initial stresses before the application of the bending moment. The residual stresses were taken from the manufacturing process simulation (numerical simulation of task 4.2). Wrinkling imperfections with amplitude as measured in each specimen at the area of buckling formation were inserted as well.

Four reference nodes have been introduced to represent the characteristic locations of the four-point bending test set-up. In particular, the first two reference points refer to the supports and the other two refer to the locations where forces are applied, accurately simulating the test conditions.

Each reference point has been associated with the corresponding cross-section nodes through the application of appropriate kinematic conditions. The general geometry of the tube and the support/loading conditions are shown in Figure 89. Bending loading is applied through two vertical upward forces at the outer reference points, leading to a four-point bending loading pattern. An arc-length continuation algorithm (Riks) is used to trace the load-displacement path, accounting for buckling and post-buckling, capable at describing accurately both “snap-through” and “snap-back” instabilities.

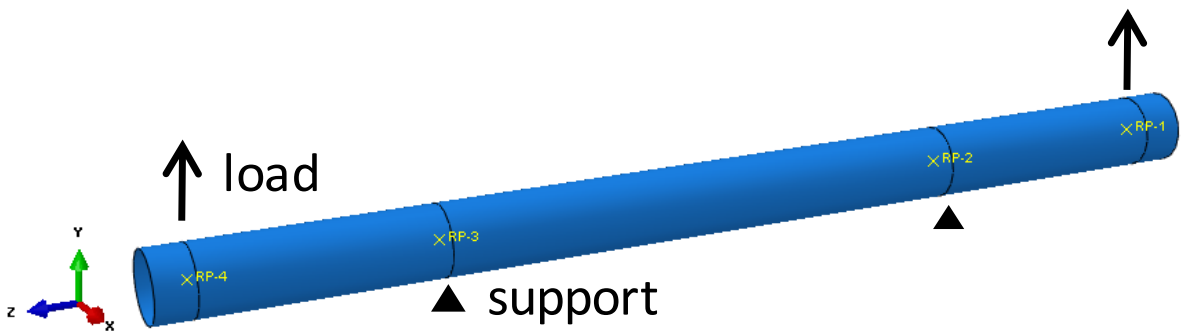

Figure 89 - Numerical model of four-point bending in ABAQUS.

4.4.1.2 Simulation of Experiments

Using the above described numerical model, the bending tests are simulated and the numerical results are compared with the experimental data. The tested tubes are classified in three categories: (a) the 7 tubes (i.e. T1, T2, T4, T5, T8, T9, T11) that do not contain any girth or coil weld connection, characterized as “plain tubes”; (b) the two tubes (i.e. T3, T13) with a girth weld at their central part (maximum moment area) but not a coil weld; and (c) four tubes (i.e. T6, T7, T10, T12) contain a coil welded connection. A list of these tubes is given in the first seven columns of Table 12.

Table 12 - Summary of bending tests; comparison between numerical and experimental results.

Test	Type	Geometric data			Yield stress	Initial wrinkle	Moment (M_{max}/M_{pl})		Curvature (k_{cr}/k_I)	
		D	t	D/t	σ_Y	δ_0/t	Test	FEM	Test	FEM
T1	Plain	1066	16.40	65.1	541	1.8	0.907	0.940	0.646	0.694
T2	Plain	1067	9.02	118	392	4.5	0.769	0.842	0.559	0.669
T4	Plain	1065	9.16	116	420	3.0	0.871	0.845	0.761	0.713
T5	Plain	1070	9.04	118	403	3.6	0.814	0.852	0.681	0.762
T8	Plain	1068	9.10	117	435	5.8	0.781	0.807	0.697	0.691
T9	Plain	1069	16.30	65.4	571	4.6	0.869	0.935	0.696	0.819
T11	Plain	1068	12.90	83	341	3.1	0.865	0.945	0.726	0.728
T3	Girth	1069	9.03	118	395	10.0	0.769	0.771	0.432	0.510
T13	Girth	1070	9.18	116	436	12.8	0.776	0.772	0.633	0.612
T6	Coil	1066	16.30	65.3	535	9.3	0.918	0.941	0.586	0.631
T7	G+C	1068	16.30	65.4	570	5.5	0.807	0.903	0.533	0.705
T10	G+C	1070	13.10	81.6	446	13.7	0.907	0.916	0.480	0.498
T12	G+C	1069	9.13	117	452	6.3	0.783	0.815	0.690	0.706

4.4.1.3 Modelling issues

The tubes without a coil weld are simulated with a rectangular finite element mesh. For comparison purposes, a "spiral weld" mesh is also considered for a limited number of cases, mainly to account for weld overmatching. The four spiral-welded tubes that contain a coil welded connection are modelled with a "spiral mesh", using an appropriate spiral partition on the tube in order to enable the simulation of the coil connection weld. Particularly, for the cases that contain both girth and coil welds, the tube is divided in three parts with separate geometric and material properties.

The actual material properties for each tube have been considered in the numerical models, as obtained from the corresponding tensile material tests. For each tube, an average stress-strain curve has been considered. In cases of girth-welded and coil-welded tubes, different material properties per tube part have been assigned, as indicated by the corresponding material tests.

4.4.1.4 Moment-curvature diagrams

The moment-curvature ($M-k$) diagrams for some representative tests are depicted in Figures 90. The comparison between numerical and experimental results for all tests is presented in the last four columns of Table 12.

The bending curvature reported in the numerical results is calculated as the ratio of sum of the two support rotations, over the initial constant moment length of the tube, which is equal to 8,100 mm. The moment values are normalized by the plastic moment M_{pl}, which can be approximated by the equation $M_{pl} = D_m^2 t \sigma_y$ (D_m is the mean diameter of the tube, $D_m = D - t$), whereas the bending curvature is normalized by the curvature-like quantity $k_I = t/D_m^2$.

The results from Figures 90 and Table 12 show a very good comparison between the numerical results and the experimental data, and indicate that the models under consideration are capable of quite accurately predicting the bending behaviour of spirally welded tubes in terms of both ultimate

moment capacity and deformation capacity. The latter is expressed with the "critical curvature", which is defined as the curvature corresponding to the maximum bending moment.

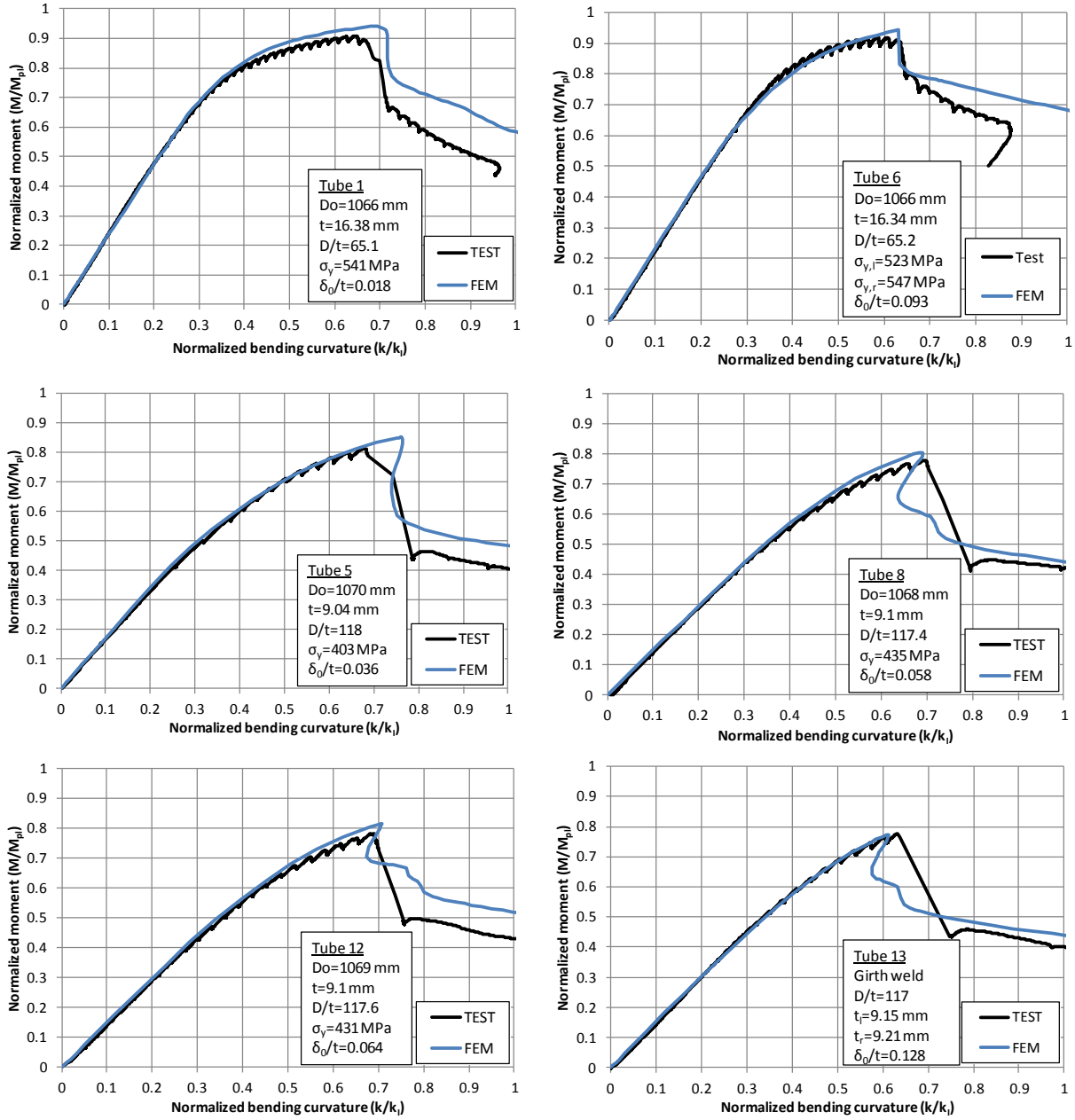

Figures 90 - Moment-curvature curves for tube specimens; comparison between numerical and experimental results.

4.4.2 Simulation of experiments carried out in Karlsruhe

These experiments were simulated by the Karlsruhe Institute of Technology (KIT).

For the bending tests performed within task 3.2 in Karlsruhe, numerical simulations with the finite element analysis software ANSYS 14.5 were conducted. The model was meshed with 4-node shell elements (shell181) with an edge length of about 50 mm or smaller. The nonlinear analysis was done with the arc-length method and automatic time-stepping. The step size was limited between 1 and 10000 sub steps per simulation. At the load path around the maximum force the smallest increments were achieved (e.g. dF ≈ 1 kN within the simulation of K2, see Figure 92.

In a first study the test rig and the support conditions have been modelled to see whether symmetry axis or simplified boundary conditions could be used. In a second step each of the performed tests K1 to K8 has been simulated with different levels of detail concerning mechanical properties and geometric imperfections to identify their influence on the bearing behaviour. Material imperfections such as residual stresses are assumed to be of minor importance and are not included in the simulation, since their distributions were irregular and difficult to generalize (report KIT task 2.4 [1]).

4.4.2.1 Influence of the test rig

Comparative pre-calculations showed that

- The self-weight of the structure can be neglected.
- A quarter of the system can represent the bearing behaviour of the complete test frame if other unsymmetrical conditions such as spiral welds are not considered.
- The support at the corners can be assumed as free to rotate.
- The test rig cannot be simplified with beam elements. This neglecting of the angle construction deformation leads to much stiffer results, although the buckling load is the same. Therefore partly modelled brackets have been used (see Figure 91).

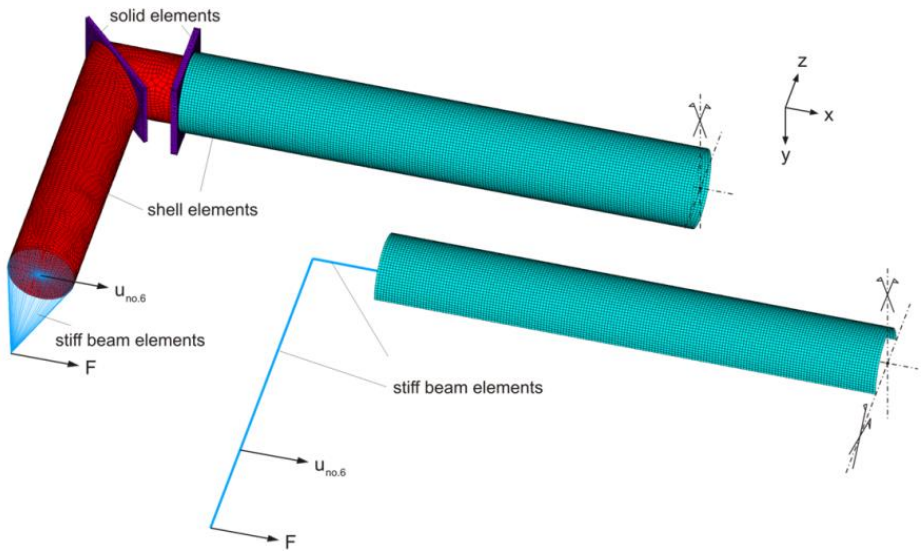

Figure 91 - Half system with partly modelled angle construction and quarter system with stiff beam elements

4.4.2.2 Influence of specimen properties

Table 13 shows a summary of the simulations that led to the most sufficient agreements with the test results. In some cases the consideration of the material properties without geometrical imperfection already led to a satisfying agreement with the test results (K2, K3 and K5). In other cases further geometric characteristics such as weld depressions (K4, K6 and K7) or a local indentation (K8) were needed.

The second column shows the used material properties. Different material laws have been used based on the results of tensile tests explained in Task 2.3. Comparisons between multilinear and bilinear material law without hardening showed that the bearing behaviour in the pre-buckling range and the buckling load can be estimated quite well by a simple bilinear material law without hardening using the yield stresses at 0.2 % plastic strain ($R_{p0.2}$).

Due to neglected hardening the failure in the simulations with the bilinear material law occurred already at significantly smaller displacements without significant plastic plateau. This did not happen with the multilinear material law which was defined to follow the measured stress-strain curves from the tensile tests.

The comparison of different tensile test results showed a strong dependency on the load level where yield starts. The development beyond this point was less important for the simulations. It can be assumed that the material coupons that were tested are possibly not the worst ones which can be the reason for overestimating load-deformation behaviour and buckling of e.g. K1 although simulation results are in good agreement qualitatively. For some specimens (K2, K3, K5) it was even necessary to define for one part of the tube different material properties to reproduce the buckling load and load pattern due to their variation (see Figure 92).

In the third column of Table 13 geometric imperfection features that were considered in the simulation are specified. Firstly a weld depression along the spiral weld was investigated with different deviations Δw from the perfect geometry. Less slender tubes (e.g. K1) did not show sensitivity towards this variation. In some cases a spiral weld depression did not fit the test results and a circular weld depression in the centre of the tube has been applied as a substitute imperfection (K4, K7 and K8). These simulations showed close agreements with the test results (K4, K7) or at least a safe reproduction of the test curve (K8).

Table 13 - Summary of the numerical simulations of the bending tests

	Material	**Geometric features**	**$(F_{FE} - F_{test}) / F_{test}$**	**Remarks**
K1	K1_C	perfect cwd*	+ 11,4 % + 4,3 %	Not sensitive to spiral weld depression. Material samples taken from specimen may not represent the worst material properties (K1_L).
K2	K2_A, K2_C	perfect cwd	+ 5,0 % + 2,1 %	Use of two materials causes failure at the transition between materials which corresponds to the test result.
K3	K3_A, K3_C	perfect	+ 1,1 %	See K2.
K4	K4_A	swd* cwd	+ 10,7 % + 1,7 %	Buckling mode caused by spiral weld imperfection (failure in the quarter points) does not correspond to failure in the centre at test.
K5	K5_A, K5_C	perfect	- 0,6 %	Consideration of the two materials causes failure at the transition between the materials which is different to the location where the failure occurred in the test.
K6	K6_C	swd	+ 2,0 %	Materials didn't show much variation. Buckling mode out of the centre caused by the spiral weld depression corresponds to the test result. Simulation fits better to test than K4.
K7	K7_A	swd cwd	+ 10,7 % + 1,5 %	See K4.
K8	K8_A	indentation (Δw = 15,5 mm)	+14,8 %	Despite consideration of a deep local indentation as pre-deformation the simulation still overestimates the test result.
* spiral weld depression (swd) and circular weld depression (cwd) both with Δw = 1,6 mm				

The relative error $(F_{FE}-F_{test})/F_{test}$ expressed as percentage of deviation of the simulated maximum force to the maximum force applied in the test illustrates that the circular weld depression approach always leads to a reduction because the buckling failure located in the centre of the tube is assumed to be the buckling mode which corresponds to the lowest buckling strength. In those cases where the

simulations with existent imperfections provided already a close agreement between simulation and test result (K3, K5, K6) the further reduction due to the buckling pattern at centre did not occur in the tests.

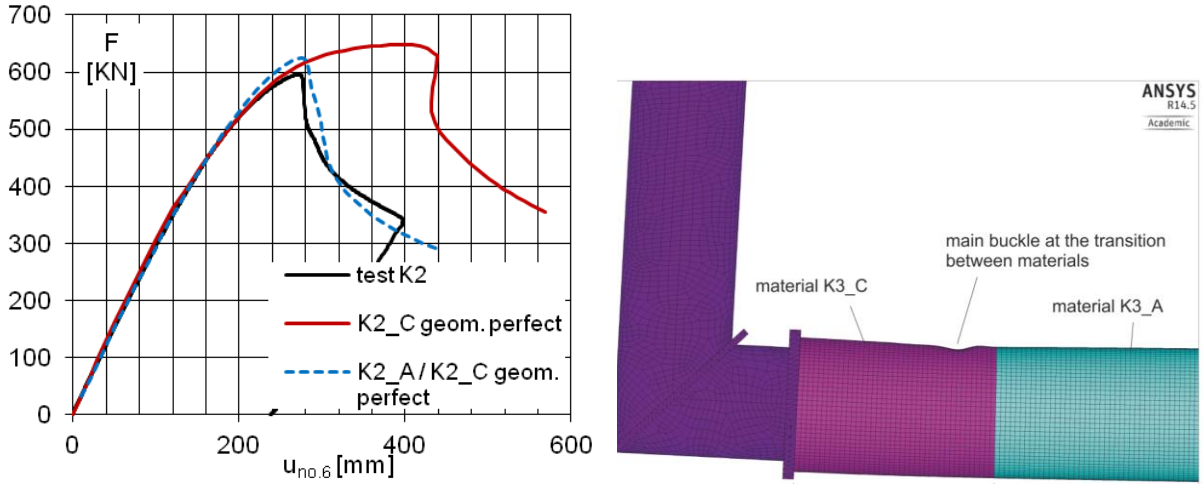

Figure 92 - Left: K2, load-displacement curves with variation of materials. Right: K3, main buckle at the transition of materials K3_A and K3_C

The simulation without any assumptions for imperfections reproduced the pattern of buckles that were observed in the test very well qualitatively (see Figure 93). The experiments showed that 6 of 8 specimens exhibited this particular buckling pattern with large centre buckle and two secondary buckles that were positioned above and below the central buckle.

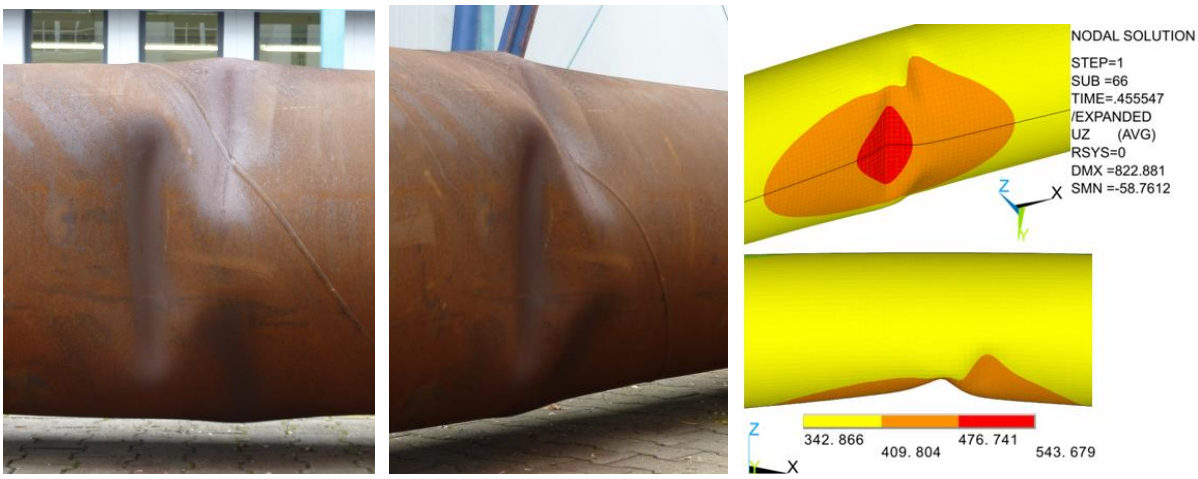

Figure 93 - K1 comparison with buckling mode simulation K1_C, geom. perfect, xz-symmetry only

4.4.2.3 Conclusion

The results of the imperfection simulations together with the bending tests revealed the decisive influences on the bearing behaviour which means that the most appropriate simulations reproduce the maximum load applied in the tests with a maximum deviation of 5.0 % only. An exception is test K8 with higher deviation which could not be associated to any specific influence.

4.4.2.4 References

[1] Ummenhofer, T; Reinke, T.: WP2 Task 2.4 Measurement of imperfections and residual stresses. Background document Combitube, KIT, 2013-11-29.

5 WP5: Numerical parametric analyses

The objectives of WP5 are the following:

- Development of a database of numerical results where the influence of all appropriate factors on the deformation capacity (curvature at which local buckling occurs) can be determined.
- Quantification of the effect of the critical parameters on the bending strength and deformation capacity (local buckling curvature) for each load case and construction detail.
- Formulation of the database in a manner that can effectively support the development of design rules of adequate simplicity for practical use and adequate complexity to produce the most economic designs.

5.1 Task 5.1: Pure bending (U-Thessaly)

Following the successful comparison of the numerical results with the experimental data, the numerical models are employed for conducting a parametric study for the effect of some key geometric and material parameters on the bending response of spiral-welded tubes. First, the effects of imperfection amplitude are examined, followed by a thorough investigation of material parameters, namely the residual stresses, the material grade and hardening, and the anisotropy of the steel material. Finally, the effects of coil and girth welds on the bending response are examined.

5.1.1 Wrinkling imperfection sensitivity

Numerical results for the imperfection sensitivity of bending response are presented for two 42-inch-diameter tubes. The first tube has thickness equal to 15.9 mm (D/t=67) and X70 steel material, and the second tube has thickness equal to 9 mm (D/t=119) with X60 steel material. A yield plateau equal to 1.5 % is assumed for both materials, while residual stresses are not considered. Loading is applied in a manner similar to the one considered in the experiments, as described in the previous sections.

The results in Figures 94 show that the response is quite sensitive to the presence of initial wrinkles in the tube wall, in terms of both the maximum moment and the critical curvature. In particular, the first tube (D/t=67) exhibits a bending response associated with substantial inelastic deformation, as a limit point is clearly observed well into the inelastic range. Following this limit point, the moment-curvature diagram “snaps-through”, characterized by a drop of moment in the post-buckling region.

The second tube is thin-walled with D/t=119 and exhibits a different bending response. In particular, for wrinkling imperfection amplitude (δ_0/t) values up to 30%, the moment-curvature diagram is quasi-linear up to the maximum moment, followed by an abrupt drop of bending moment in the post-buckling region in the form of a “snap-back”. This “snap-back” on the moment-curvature diagram is alleviated with increasing values of the wrinkling amplitude; for δ_0/t values greater than 30%, the response is smoother, characterized by a limit point on the moment-curvature diagram.

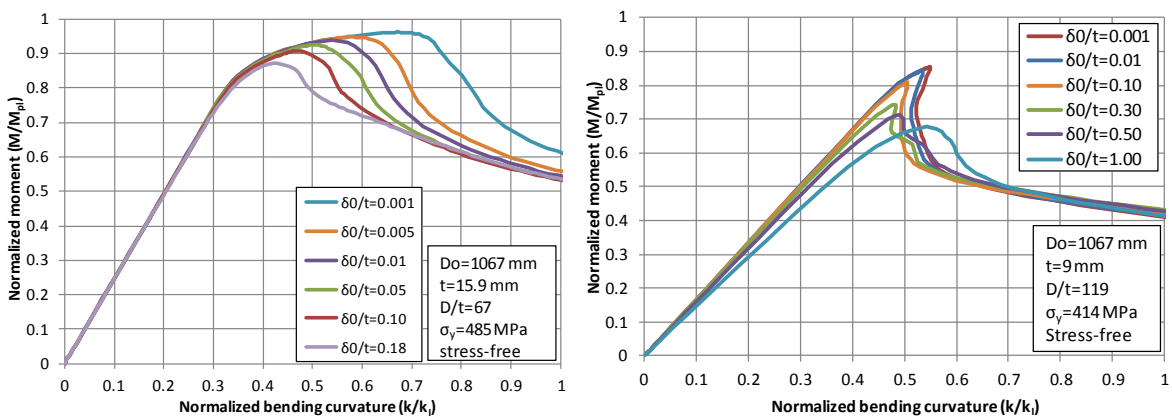

Figures 94 - Imperfection sensitivity of tubes with a) D/t=67, and b) D/t=119, subjected to bending.

5.1.2 *Effect of residual stresses*

In this subsection, the comparison between tubes with stress-free state and tubes with residual stresses is presented. Figures 95 depict the variation of normalized critical curvature k_{cr}/k_I in terms of imperfection amplitude (δ_0/t) for the two tubes considered previously, with D/t equal to 67 and 119 respectively. In Figures 96, a comparison is performed for the two tubes under consideration with and without residual stresses, in terms of the moment-curvature diagram. The numerical results demonstrate a substantial increase of deformation capacity when the analysis considers residual stresses, although the curves deviate earlier from the elastic region. This is likely attributed to the fact that the residual tension stresses at the outer fibres of the tube wall cause later yielding and as a result later loss of bending stiffness of the tube wall.

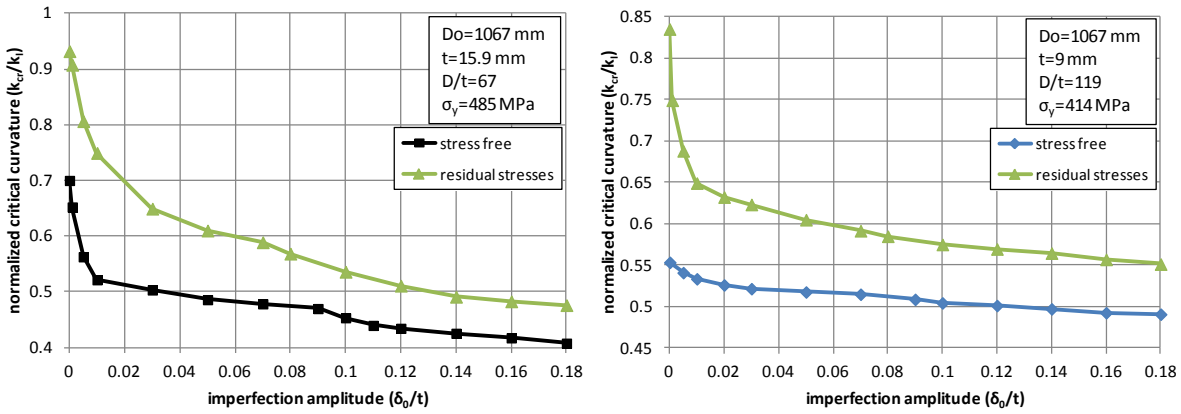

Figures 95 - Normalized critical curvature k_{cr}/k_I in terms of imperfection amplitude δ_0/t for a) X70 tubes with D/t=67, b) X60 tubes with D/t=119; effect of residual stresses.

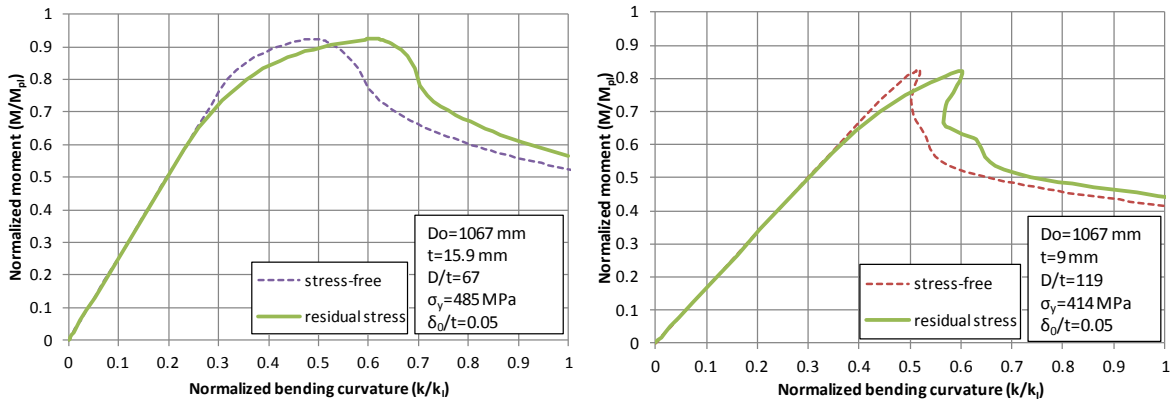

Figures 96 - Moment-curvature diagrams for a) X70 tubes with D/t=67, b) X60 tubes with D/t=119; effect of residual stresses.

5.1.3 *Effect of material properties*

Mechanical properties of steel material may have an influence on the bending deformation capacity of steel tubes. In the present section, the effect of these properties is investigated, considering variations on the material strain hardening, the yield stress, and the material anisotropy in the axial and hoop direction. The investigation is conducted for tubes with D/t ratio equal to 67 (thickness equal to 15.9 mm), imperfection amplitude equal to 4% of the tube thickness (δ_0/t =0.04), and residual stresses computed from the simulation of the manufacturing process.

The investigation into the effect of material properties was limited to one D/t ratio. It can be assumed that the results would be similar for other D/t ratios and in case of the thin walled tubes with D/t = 109 it could be expected that the effect would be minimal anyhow because of their low critical strain fir local buckling.

5.1.3.1 Material hardening

Numerical analyses are performed for a bi-linear steel material, with yield stress equal to 485 MPa, considering different values of the strain hardening modulus E'. The numerical results are shown in Figure 97a, and indicate that an increase on the strain hardening modulus has beneficial effects on the value of maximum moment and the corresponding critical curvature.

To investigate the effect of Lüder's (yield) plateau, the stress-strain curve of the steel material is considered with no hardening, immediately after yielding, up to a certain strain, denoted as ε_P. Five different values are considered for the length of the yield plateau up to ε_P=3%. The yield plateau size is expressed through the dimensionless parameter $n = \varepsilon_P / \varepsilon_y - 1$. Following the yield plateau, for strains greater than ε_P, material strain hardening is assumed, with $h = E'/E$ equal to 1/80. The variation of normalized maximum moment in terms of the value of n is depicted in Figure 97b. The decrease of bending moment capacity with the increase of yield plateau size is attributed to the fact that the yield plateau is associated with no strain hardening, reducing tube resistance and leading to earlier buckling. An extension of the yield plateau beyond 2% strain does not affect the bending response of the tube.

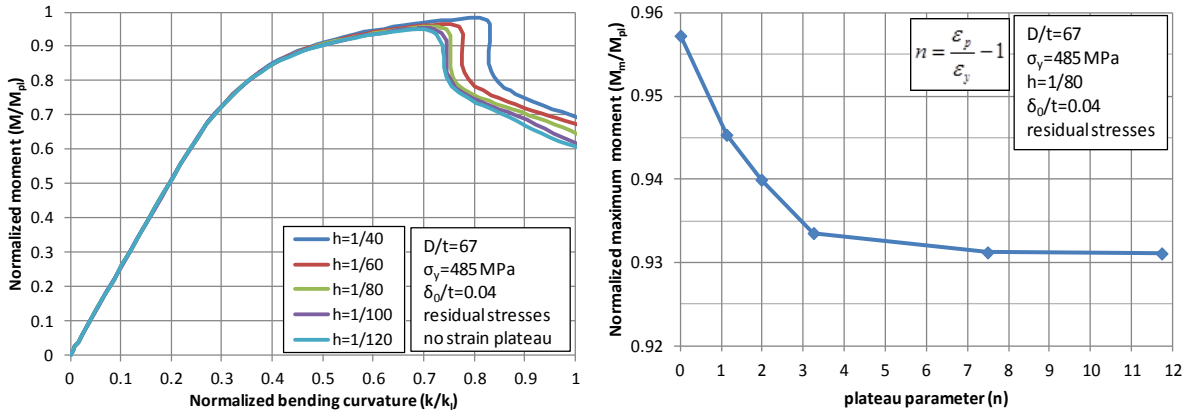

Figure 97 - a) Normalized m-k diagrams for different values of strain hardening modulus, b) Variation of maximum moment in terms of the dimensionless plateau parameter n.

5.1.3.2 Yield stress

Four values of yield stress σ_y are considered, corresponding to the nominal values of steel grades X52, X60, X70 and X80 respectively. In all analyses, a bilinear stress-strain curve is considered, without yield plateau, where the hardening modulus E' is equal to 1/80 of the elastic modulus E. To demonstrate the effect of yield stress on the deformation capacity, the value of bending moment is normalized by the moment-like quantity $M_e = Ert^2 / \sqrt{1-\nu^2}$, where r is the mean radius of the tube $r = D_m/2$, and the corresponding normalized moment is referred to as "elastically normalized moment". The normalized moment-curvature diagrams for the steel grades considered are depicted in Figures 98, showing that the value of yield stress has a considerable effect on the bending response of the tube. Increase of the value of yield stress increases the maximum moment capacity, but reduces slightly the corresponding deformation capacity.

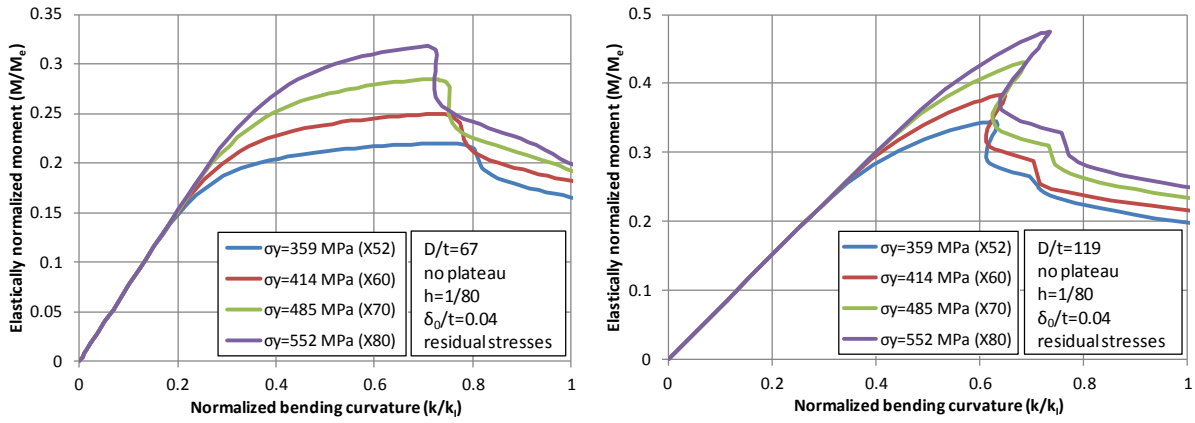

Figures 98 - Normalized m-k diagrams for different material grades; (a) $D/t = 67$; (b) $D/t = 119$.

5.1.3.3 Yield stress anisotropy

The tensile testing on coupons extracted from the tube specimens indicated that the yield stress in axial direction is higher than the one in hoop direction up to on average 7%. The effect of such a material anisotropy on the bending response is investigated, considering different values of material anisotropy. The tubes considered have D/t ratio equal to 67, initial wrinkling imperfection amplitude equal to 4% of tube thickness, and residual stresses are introduced to the numerical model.

The material anisotropy is introduced in the model through the Hill's potential function, considering different yield stresses in the axial and the hoop direction. The basic stress-strain curve of the tube material is bilinear with yield stress equal to 485 MPa, hardening modulus E' equal to 1/80 of the elastic modulus E, without a yield plateau.

The influence of an increased yield stress in the axial direction with respect to the yield stress in the circumferential direction (assumed equal to 485 MPa) is presented in Figure 99a. The ratio of yield stresses between axial (ax) and hoop (ho) direction is expressed as a percentage. The results show that the increase of yield stress in the axial direction increases the moment capacity but reduces the corresponding critical curvature.

Figure 99b presents the effect of increasing the yield stress in the hoop direction, while the yield stress in the axial direction is kept constant. The numerical results indicate that the critical curvature is somewhat influenced, but the value of ultimate bending moment is not affected.

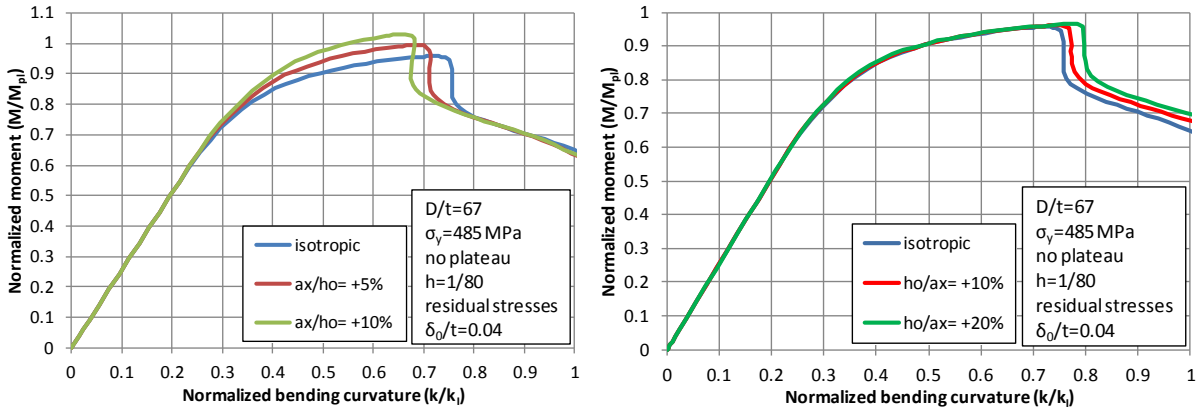

Figure 99 - Normalized moment-curvature diagrams for different values of material anisotropy; influence of increased yield stress a) in the axial direction and b) in the hoop direction.

5.1.4 *Effect of girth welds and coil connecting welds*

Girth welds are possible buckling locations of tubes subjected to bending. At this welded connection, different material behaviour of the two adjacent tubes may lead to stress and strain concentrations due to discontinuity, facilitating the formation of local buckling at the vicinity of the girth weld. The effect of the strength mismatch between left and right part of a girth-welded tube on the bending response is investigated. A dedicated numerical model was developed where the girth weld is located in the middle of the tube. The yield stress of the left part of the tube is assumed equal to 485 MPa (X70), while the yield stress of the right part varies appropriately. The strength difference between right and left part of the tube is expressed as a percentage. No yield plateau is considered, while the hardening modulus E' is equal to 1/80 of Young's modulus. No initial wrinkling imperfection is assumed, whereas residual stresses are considered from the cold-bending simulation. Furthermore, based on measurements of the tube specimens, a 2-mm girth weld cap is taken into account, while the yield stress of the girth weld material is considered equal to 552 MPa (overmatched conditions with respect to the tube material).

The numerical results in Figure 100a indicate that significant differences in yield stress between the two connecting tube parts may result in a decrease of the critical bending curvature. This is attributed to the fact that the material strength discontinuity plays the role of an imperfection that causes localization of stresses and deformation and, eventually, premature buckle formation. In addition, the numerical results indicate that buckling occurs always in the weakest part of the tube.

Another particular feature of spiral-welded tubes is the presence of a coil-connection weld (CCW) within the tube, where the ends of two different coils are welded to ensure the production continuity. It is noted that such a weld is not present in hydrocarbon pipeline applications, but is quite often the case in spiral-welded tubes used in piling applications. In such a case, there is a possibility that the material properties of the two welded coils are different in terms of their yield stress. The effect of such a mismatch on the bending response of spiral-welded tubes is investigated by a numerical model where the CCW is located in the middle of the tube.

The normalized moment-curvature curves of the aforementioned analyses are presented in Figure 100b. Five cases are presented, where the values of yield stress for the one part of the tube correspond to the material strength difference with respect to the other part of the tube. Those cases are compared with the case of equal properties. Furthermore, for the normalization of the numerical results, the properties of the weaker coil are employed. The numerical results in Figure 100b indicate that the increase of yield stress at the one part of a coil-welded tube, results in a significant reduction of the corresponding critical curvature. This discontinuity in material properties acts as an initial imperfection, causing early buckle formation. Furthermore, buckling occurs at the vicinity of the weld, at the weakest part of the tube.

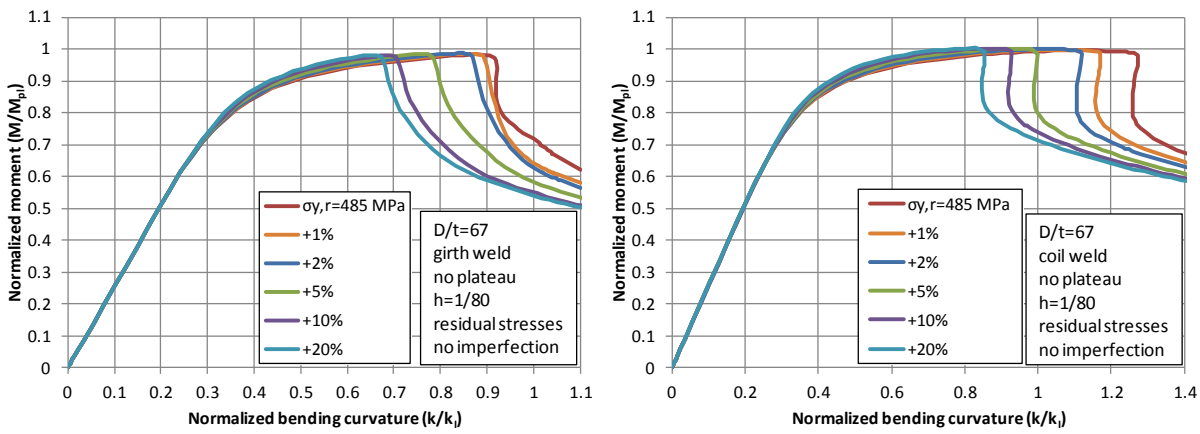

Figure 100 - Normalized moment-curvature diagrams of a 42-inch-diameter X70 tube with D/t =67 with a) a girth weld, b) a coil weld, for different yield stress values of connected tube parts.

5.1.5 Effect of spiral weld cap and overmatching

The effect of the spiral weld cap was examined for a 42-inch-diameter tube with tube thickness of 15.9 mm (D/t=67) and yield stress equal to 541 MPa, where a 2-mm-cap is considered in the spiral weld (12% higher than the tube thickness). Furthermore, material weld material overmatching was considered, assuming yield stress of weld material equal to 570 MPa, corresponding to 5 % overmatch. The numerical results indicated a minor effect of both spiral weld cap and overmatching on the tube bending response.

5.2 Task 5.2: Bending with radial loads

The Edinburgh team performed a set of detailed parametric studies to investigate the structural effect of the application of a local load to a Combitube or similar tube.

Two conditions exist. In the first, a radial load may be applied at a location where the Combitube is internally strengthened by a concrete block. This leads to a very rigid connection, but the radial load induces a shear in the tube which is most significant at the end of the concrete block. At this critical location, the bending moment may be high, but a significant shear leads to a rapidly falling moment. This situation was the first to be studied by the Edinburgh team. The findings were presented to the partners (Sadowski and Rotter, 2013h) and documented full in a written research report (Sadowski and Rotter, 2013j). All the calculations showed that the shear was in no way detrimental to the buckling resistance, but that the moment capacity rose as the shear increased. The cause was the progressive confinement of the buckle into a zone of varying moment, so that the limiting moment at the face of the concrete block junction became steadily higher. The enhanced moment capacity was relatively small except in the case of severely high shears, so the final recommendation was that this effect can be safely ignored in design (Rotter and Sadowski, 2015).

The second situation studied was that of a local transverse load applied to a tubular member at a location where no additional strengthening measures have been put in place. This was modelled as a radial local load applied at the mid-span of a tube. The study began by exploring the resistance of a tube to a pure radial load, without bending, to determine an appropriate plastic limit to the resistance, which could be used to quantify the magnitudes of lesser transverse loads. This plastic resistance was thoroughly verified. The effect of small proportions of this plastic transverse load was then applied to tubes in bending and the loss of bending resistance documented. The findings were presented to the partners (Sadowski and Rotter, 2013i) and documented full in a written research report (Sadowski and Rotter, 2013k). The effect was characterised by a set of simple algebraic equations (Rotter and Sadowski, 2015). The rules proposed in that report are suitable for direct inclusion as an amendment to EN 1993-1-6.

5.3 Task 5.3: Bending and normal force with load introduction at the top

The majority of the Combitube project focussed on the resistance of helically wound tubular members under pure bending. But in many practical applications, minor axial loads are also required to be carried, with a maximum of about 30% of the fully yielded axial resistance of the cross-section. The effect of such an axial force on the bending resistance was extensively explored by the Edinburgh team using the same computational models as had been used for the case of pure bending.

The effect of an axial force on the bending resistance was evaluated in detail in a comprehensive series of nonlinear parametric FE runs, presented to the partners (Sadowski and Rotter, 2014b) and published as a research report (Sadowski and Rotter, 2013l) and a conference paper (Rotter and Sadowski, 2014). The effect on the complete bending resistance against slenderness relationship of an axial load was quantified for several different axial load levels up to 30% of the squash load. A convenient algebraic characterisation of the reduced buckling resistance is documented in the Edinburgh team's final report on the design recommendations (Rotter and Sadowski, 2015). The rules proposed in that report are sent in for direct inclusion as an amendment to EN 1993-1-6.

5.4 Task 5.4: Bending with large ovalisation

5.4.1 Introduction

In this section, the bending strength and local buckling behaviour of tubes with large ovalisation is examined. Such loading conditions can be developed due to transverse loads from connected sheet piles and earth loads on infill sheeting, as shown schematically of Figures 94. The results of this investigation are analysed to quantify the effect of these critical parameters on the bending strength and deformation capacity (local buckling curvature).

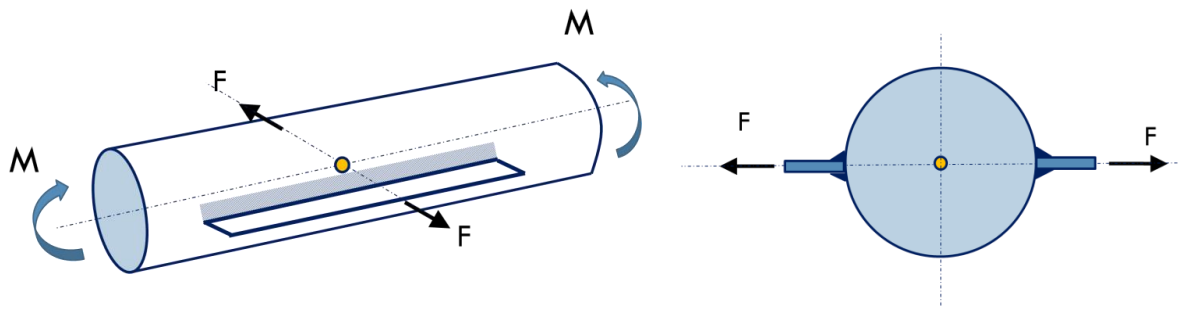

Figure 101 - Schematic representation of the numerical model.

5.4.2 Numerical modelling

An appropriate finite element model for the investigation of the effect of large ovalisation was developed in ABAQUS. Initially, in order to simulate the loads from connected sheet piles, lateral tensile load is applied at two reference nodes. These nodes are coupled with two corresponding nodes' sets at the right and left side of the tube respectively, as shown in Figure 102. Subsequently, keeping the lateral load constant, bending is applied until buckling. The lateral load is applied at a line of nodes of length equal to four times of the tube diameter, as accordingly advised by construction and engineering consulting companies. The diameter-to-thickness ratios (D/t) of the tubes analysed are equal to 67 and 119, while the diameter is equal to 1067 mm. The material properties employed refer to the actual material properties of the tube T9, tested experimentally at the Delft laboratory. In particular, the yield stress σ_y is equal to 570 MPa. A wrinkling imperfection amplitude of 5% of the tube wall thickness is considered, while residual stresses have been employed in the numerical model.

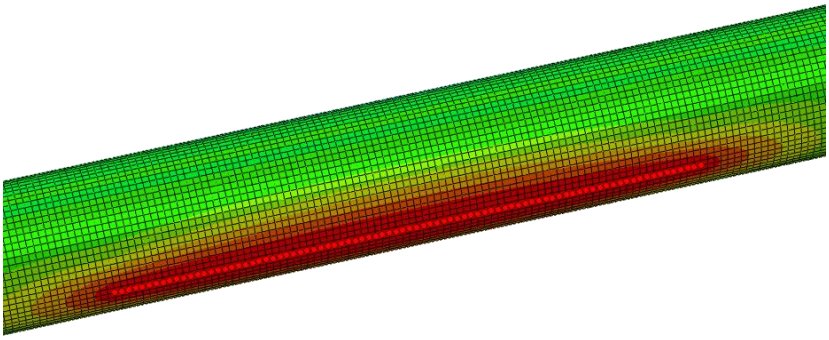

Figure 102: Lateral tensile load applied at the side nodes of tube.

5.4.3 Numerical results

The moment-curvature (m-k) curves for the tubes with the two different D/t ratios examined (i.e. D/t=67 and 119) are depicted in Figures 103. Moreover, the variation of critical curvature and maximum moment in terms of the normalized pulling force is presented in Figures 104. Several values for the lateral tensile load have been examined. In particular, the applied pulling force (F) is

normalized by the limit force F_p that causes full plastification of the tube wall (e.g. Gresnigt et al., 2007, [1]) and is given by the following equation.

$$F_p = \frac{\sigma_y t^2}{R}$$

The numerical results in Figures 103 show that for the relatively thick tubes (D/t=67, left figure), a gradual loss of bending strength in the post-buckling region is observed, indicating a clear limit point. However, for higher lateral tensile forces (i.e. values of F close to F_p) it is observed that the decrease of bending strength is smoother. On the other hand, for the thinner tubes (D/t=119), the bending response is somewhat different, indicating that the connected sheet piles have a more significant effect in this case. In particular, it is shown an abrupt drop of bending moment in the post-buckling region in the form of a "snap-back". However, it is observed that after this sudden drop, the tube does not lose further its bending strength. On the contrary, the bending stability of the tube is maintained at least until a quite large bending curvature.

The numerical results in Figures 104 indicate that both the critical curvature and maximum moment decrease with increasing lateral force. This is attributed to the larger ovalisation that is imposed to the tube as well as to the higher initial stresses and strains that result in a sooner yielding. This sooner yielding is also demonstrated by the earlier deviation from the linear elasticity of those M-k curves (Figures 103) which correspond to high values of lateral force F.

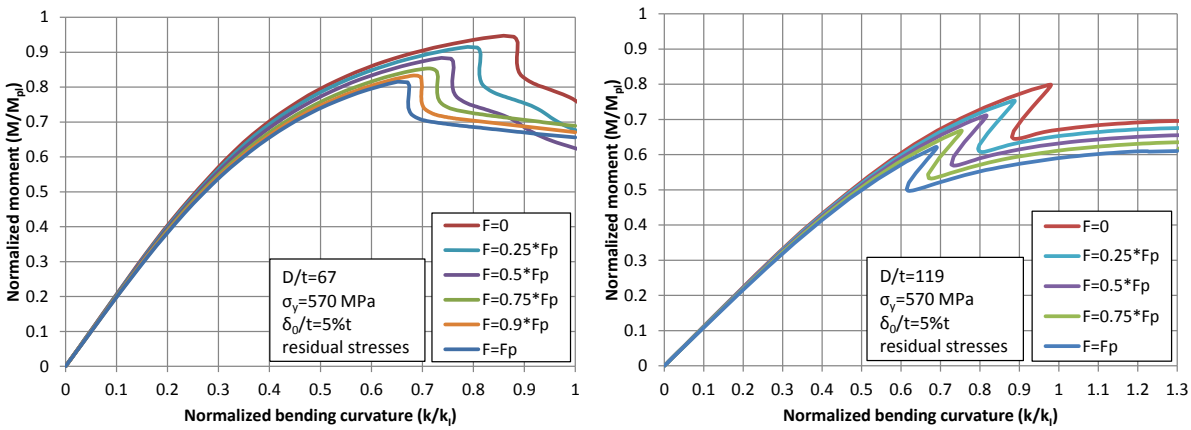

Figures 103 - Moment-curvature (m-k) curves for tubes with a) D/t =67 and b) D/t=119; effect of loads from connected sheet piles.

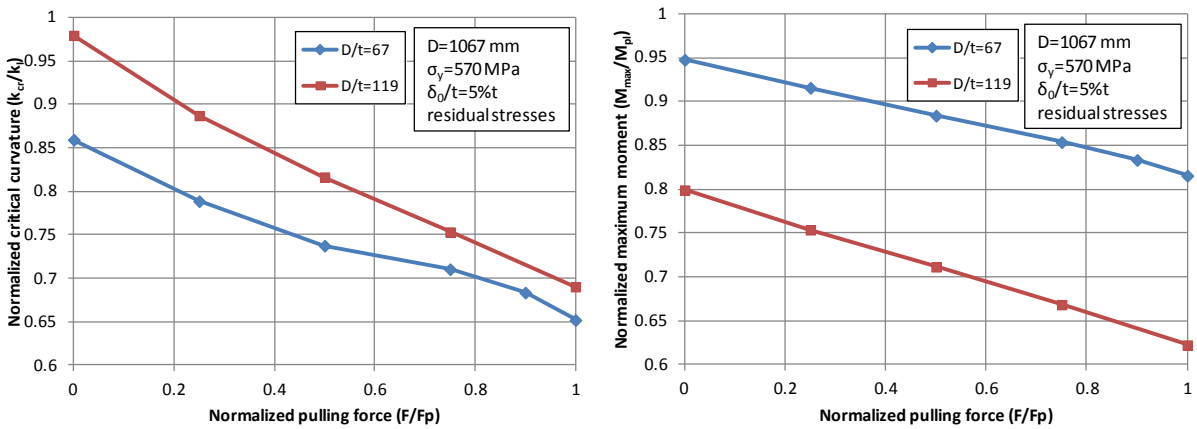

Figures 104 - Variation of a) normalized critical curvature and b) normalized maximum moment in terms of the normalized pulling force for tubes with connected sheet piles.

5.4.4 Discussion of the numerical results

The results of Figures 103 indicate that the bending response of tubes with connected sheet piles is influenced by the D/t ratio of the tube. In particular, it was observed that the post-buckling

behaviour of thin tubes (D/t=119) is different than the behaviour of relatively thick tubes. The observation of the buckling shapes of the corresponding tubes, depicted in

Figures 105 can assist in the interpretation of these different behaviours. It is shown that for the relatively thick tubes (D/t=67, left figure), buckling occurs at the end of the connected sheets, allowing the formation of the full buckling mode as well as the drop of the bending strength. On the other hand, for thinner tubes (D/t=119), buckling occurs in a region restrained by the connected sheets, and as a result the catastrophic consequence of buckling cannot further progress.

Actually, the connected sheets may induce an initial ovalisation which is detrimental to the buckling strength (see Figures 104). However, due to this restriction, the tube ovalisation in the mentioned area is not further significantly evolved. Therefore, the connected sheets may also contribute to the maintenance of the post-buckling bending strength in the case that buckling will occur inside this restrained region.

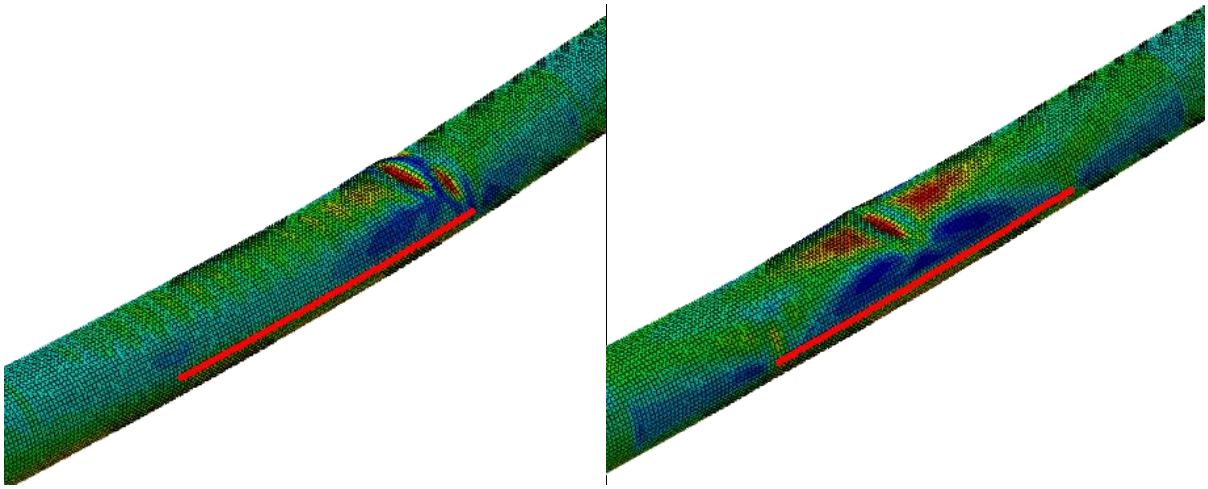

Figures 105 - Buckling shapes for tubes with connected sheet piles; a) D/t =67 and b) D/t=119.

5.4.5 References

[1] Gresnigt, A.M., Karamanos, S.A., and Andreadakis, K., (2007). “Lateral Loading of Internally Pressurized Steel Tubes”, Journal of Pressure Vessel Technology, ASME, Vol. 129, pp. 630-638.

6 WP6: Development of design guidelines

The objectives of WP6 are the following:

- Development of design guidelines.
- Preparation of background documents.
- Development of design examples.

6.1 Task 6.1: Safety evaluation for development of design rules

CombiWalls with tubular primary elements have been used in the Netherlands since the 1980's. Generally, elastic design criteria were adopted. The D/t ratios were in the range between 70 and 100. The yield strength of the piles was between 355-415 N/mm² (S355, X52, X56, X60).

With the large scale application of CombiWalls for the railway tunnel under the river Maas (Willemsspoortunnel) in Rotterdam (1987-1992), the first steps were made in methodically addressing the influence of the infill sheeting on the primary elements. The tensile forces that act on the interlocks, either caused by hydrostatic loads on the infill sheeting or by vertical misalignment of the piles, will tend to ovalise the tube.

The research for the application of the combined walls at the Willemsspoortunnel were laid down in a report by the Dutch railways (1988), which was later on the start document for the part on combined walls in ENV1993-5 Piling.

Over all these years no failures are known that had to be attributed to unsafe design rules for the tubes as in the ENV 1993-5 Piling.

Another important safety feature is the long term and extensive research on pipelines, onshore as well as offshore. Numerous bending tests have been performed all over the world. The design rules for local buckling as presented in the guidelines have proven to be adequate in pipeline design such as the Dutch pipeline standard NEN 3650, EN 1993-4-3 on pipelines, EN 1954 for gas transmission pipelines, the Canadian pipeline standard CSA-Z662-11 (2011) and in several other applications including ENV 1993-5 on Piling.

As is explained before, there are two basic approaches for the design; one can be called "strain based" and the other "stress based". In ENV 1993-5 strain based design is applied and in EN 1993-1-6 stress based design.

The Combitube research has confirmed the design rules for local buckling for spirally welded tubes. In addition several influences on the local buckling strain have been quantified and adequate design rules have been developed.

The Combitube research also has as an important result improved design rules for EN 1993-1-6, validated with numerous finite element parameter studies.

6.2 Task 6.2: Design guidelines

In the project team intensive discussions were held on the set up of the design guidelines. It was recognized that especially the design rules for local buckling in the present EN 1993-1-6 need modification for the tubes as applied in combined walls because the present design rules do not sufficiently take into account plasticity of the cross section of the relative small values of the Diameter/ Wall thickness ratio in tubes for CombiWalls.

From the comparison of design rules as reported in WP1 it may follow that also the design rules in EN1993-1-1 should be modified; in particular the slenderness limits for the different classes. In the Combitube project this has not been investigated further.

Also EN 1993-5 Piling needs modification, because it insufficiently takes into account all special features in the design of tubes in combined walls, such as soil loads, loads from infill sheeting and support from sand fill. There is a close interaction between these special features and the bending moment capacity and local buckling behaviour and especially also the safety aspects related to the post buckling behaviour. Therefore a dedicated set of design guidelines has been developed for tubes as primary elements, to be included in EN 1993-5 Piling.

Such dedicated set of design guidelines is helpful and is urgently requested by designers because the designer of CombiWalls than needs only one dedicated document. It will avoid confusion and possible errors due to the more complicated set-up of EN 1993-1-6, with a much broader scope than needed for tubes in CombiWalls. Such dedicated design rules are not unique. They are also in the design rules for pipelines in EN 1993-4-3 [8].

In the project team both needs were discussed at length. Finally it was decided to report two sets of design guidelines:

(1) A set of dedicated guidelines for the design of combined walls valid for Diameter / Wall thickness ratios from 50 to 140, fulfilling the needs of EN 1993-5 Piling.

and

(2) A set of general guidelines valid for Diameter / Wall thickness ratios from 50 to 6000 that are focussing on determination of the bending moment capacity, fitting the needs of EN 1993-1-6 Shell Structures.

6.2.1 Design guidelines for EN 1993-5 Piling

The design guidelines provide guidance and design rules for the design of steel tubes as primary elements in combined walls. They enable safe determination of the bending moment –curvature diagram up to local buckling, taking into account all relevant influences.

The guidelines are valid for steel tubes where:

- The diameter to wall thickness ratio is between 60 and 140.
- The steel strength is up to grade S700 (specified minimum value – same definition as for other parts in EC3).
- The fabrication is executed according to the rules in EN 1090-2.
- There is no pressure difference between the inside and outside of the tube.
- The tube may or may not be filled with sand of sufficient quality to improve the mechanical properties of the tubes, in particular the bending moment capacity and the critical curvature.

The moment curvature relationship of a tube in a combined wall in bending is influenced by several factors. The most important are the diameter, the wall thickness, the imperfections and the stress-strain relationship (in particular yield stress and strain hardening properties).

There are several more factors that have an influence on the bending moment and especially also on the curvature at which local buckling occurs.

In Figure 106 the bending moment curvature relationship is given for a tube loaded in pure bending up to local buckling. Due to other influences, the maximum moment is decreased and also the curvature at which local buckling occurs is smaller.

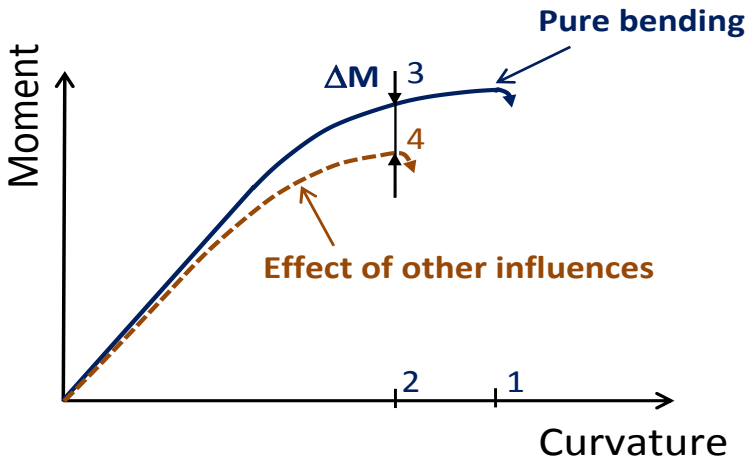

The numbers 1 and 2 are critical curvatures (local buckling) in pure bending and in case of other influences.

The numbers 3 and 4 are bending moment capacities in pure bending and with other influences at the critical curvature.

Figure 106 - Moment curvature relationship to illustrate the effect of other influences on the bending moment curvature diagram.

Examples of other influences

- Compressive normal force and shear force in the tube reduce the bending moment capacity.
- Sand fill may have a positive effect on the critical strain and the post buckling behaviour.
- Infill sheeting will cause forces on the tube wall and will have an effect on the bending moment capacity and the ovalisation.
- Ovalisation due to forces from infill sheeting, forces from anchors and waling beams, attachments etc. have an influence on the bending moment capacity and on the critical curvature.
- Geometrical imperfections (wavy patterns) in the tube wall, in particular in longitudinal direction) have an influence on the critical curvature.
- Other geometrical Imperfections such as offset at girth welds (high lows), dimples, etc. also have an influence on the critical curvature.
- Residual stresses have an effect on the bending moment and on the critical curvature.
- Strain hardening may have an effect on the bending moment and on the critical curvature.

Verification procedure

- First the bending moment curvature diagram is constructed without the effect of other influences, not yet taking into account local buckling. These are a set of rather simple equations.
- Then the bending moment curvature diagram is constructed with the effect of other influences, not yet taking into account local buckling. In this calculation also the ovalisation is determined.
- Then the critical curvature is determined (number 2 in Figure 106).
- With the critical curvature and the bending moment curvature diagram known, the bending moment capacity of the tube can be determined (number 4 in Figure 106).

Bending moment-curvature diagram **without** other influences

The elastic part of the moment-curvature diagram may be constructed with the following expressions.

$$M = C \cdot EI \tag{5}$$

Where:

$$EI = E\pi r^3 t \tag{6}$$

$$C = \frac{\varepsilon}{r} \quad \text{with} \quad \varepsilon \le \varepsilon_y = \frac{\sigma_y}{E} \quad \text{and} \quad r = (D-t)/2 \tag{7}$$

The elastic-plastic part of the moment-curvature (*M-C*) diagram may be constructed with the following expressions.

$$M = M_{\mathrm{p}}\ 0{,}5\left(\frac{\theta}{\sin\theta} + \cos\theta\right) \tag{8}$$

Where:

$$M_p = 4r^2 t\sigma_y \tag{9}$$

$$\theta = \arcsin(\varepsilon_y / \varepsilon) \quad \text{with} \quad \varepsilon \ge \varepsilon_y \tag{10}$$

$$C = \frac{\varepsilon}{r} \tag{11}$$

$$\varepsilon = \frac{\varepsilon_y}{\sin\theta} \quad \text{with} \quad \varepsilon \ge \varepsilon_y \tag{12}$$

<u>Bending moment-curvature diagram **with** other influences</u>

Below a summary of the main equations is given. For the full set of equations and background see the references {….}

The maximum plastic bending moment with other influences (M_m) is.

$$M_{\mathrm{m}} = g \cdot h \cdot v \cdot n \cdot M_{\mathrm{p}} \tag{13}$$

Where:

The factor *g* takes into account the effect of bending moments and normal forces in circumferential direction in the tube wall due to e.g. ovalisation due to the bending moment, soil loads and forces from the infill sheeting.

$$g = \frac{c_1}{6} + \frac{c_2}{3} \tag{14}$$

Where:

$$c_1 = \sqrt{4 - 3\left(\frac{n_{\mathrm{y}}}{n_{\mathrm{p}}}\right)^2 - 2\sqrt{3}\frac{|m_{\mathrm{y}}|}{m_{\mathrm{p}}}} \tag{15}$$

$$c_2 = \sqrt{4 - 3\left(\frac{n_{\mathrm{y}}}{n_{\mathrm{p}}}\right)^2} \tag{16}$$

$$n_y \le n_p = t\,\sigma_y \tag{17}$$

$$m_y \le m_p = 0{,}25\ t^2\sigma_y \tag{18}$$

n_y and m_y are normal force and bending moment in the tube wall per unit of length due to bending moment, soil loads, loads from infill-sheeting, etc..

The factor *h* takes into account the effect of ovalisation due to e.g. bending moment, soil loads and forces from the infill sheeting.

$$h = 1 - \frac{2}{3}\frac{a}{r} \tag{19}$$

This implies an iterative calculation process. A first estimate for the ovalisation due to bending moment can be taken from

$$a_{pl,ini} = C_{pl,ini} \cdot C_e \cdot \frac{r^5}{t^2} \tag{20}$$

With

$$C_{pl,ini} = 0,5\frac{t}{r^2} \tag{21}$$

$$C_e = \frac{f_y}{E \cdot r} = \frac{\varepsilon_y}{r} \tag{22}$$

It gives

$$a_{pl,ini} = 0,5\,\varepsilon_y \frac{r^2}{t} \tag{23}$$

The estimate for $C_{pl,ini}$ is about 2 times the critical curvature for local buckling.

For the total ovalisation *a,* the contributions of the soil load and other loads can be taken from the equations as given in the references [1] [2] [3] [8].

The factor *v* takes into account the effect of shear force in the tube:

$$v = \sqrt{1 - \left(\frac{V}{V_{\mathrm{p}}}\right)^2} \tag{24}$$

The factor *n* takes into account the effect of normal force in the tube:

$$n = 1 - \left(\frac{N}{N_{\mathrm{p}}}\right)^{1,7} \tag{25}$$

In these equations V_p and N_p are the plastic shear force capacity and plastic normal force capacity.

For constructing the bending moment-curvature diagram **with** other influences a similar set of equations is developed as for the bending moment-curvature diagram **without** other influences [1] [2].

<u>The critical compressive strain and curvature</u>

For the critical strain the following equations are used

$$\varepsilon_{cr} = 0,25\frac{t}{r_o} - 0,0025 \qquad \text{for} \quad \frac{r_o}{t} \le 60 \tag{26}$$

$$\varepsilon_{cr} = 0,10\frac{t}{r_o} \qquad \text{for} \quad \frac{r_o}{t} \ge 60 \tag{27}$$

Where ε_{cr} is the critical compressive strain and r_o is the local radius in the compressed part of the cross section as indicted in Figure 107.

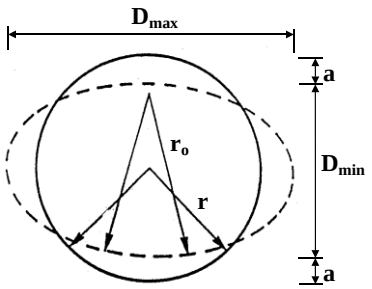

$$r_o = \frac{r}{1 - \frac{3a}{r}} \qquad (28)$$

Figure 107 - Definition of ovalisation and radius r_o in an ovalised cross section.

The ovalisations depend on the diameter and the wall thickness, the stress strain diagram, bending moment and curvature and external loads like earth loads and loads from the infill sheeting.

For pure bending the effect of ovalisation can be neglected. The reason is that the validation of these equations is done on pure bending tests, where ovalisation due to pure bending was included, so that in this case: $r_0 = r$.

The critical curvature follows from:

$$C_{cr} = \frac{\varepsilon_{cr}}{r_o} \qquad (29)$$

Then the effects of "other influences" on the critical compressive strain are calculated to determine the critical compressive strain with other influences (ε_{cr}^{*}).

$$\varepsilon_{cr}^{*} = \varepsilon_{cr} \cdot \alpha_{geo} \cdot \alpha_{sh} \cdot \alpha_{sand} \qquad (30)$$

The critical curvature with other influences follows from:

$$C_{cr}^{*} = \frac{\varepsilon_{cr}^{*}}{r} \qquad (31)$$

Where

ε_{cr} is the critical compressive strain in pure bending

α_{geo} is the largest of the following geometrical imperfections:

- α_{un} is the effect of tube surface undulations
- $\alpha_{high-low}$ is the effect of misalignment (high low) at welds
- α_{dple} is the effect of dimples or dents
- $\alpha_{local-load}$ is the effect of a local deformations due to local loads, e.g. waling beams

α_{sh} is the effect of strain hardening

α_{sand} is the effect of sand fill

A complete set of equations to determine the various factors is given in the references [1] [2].

6.2.1.1 Application

Figure 108 and Figure 109 show the application of the model for two of the tested tubes. A summary of the results is given Table 14.

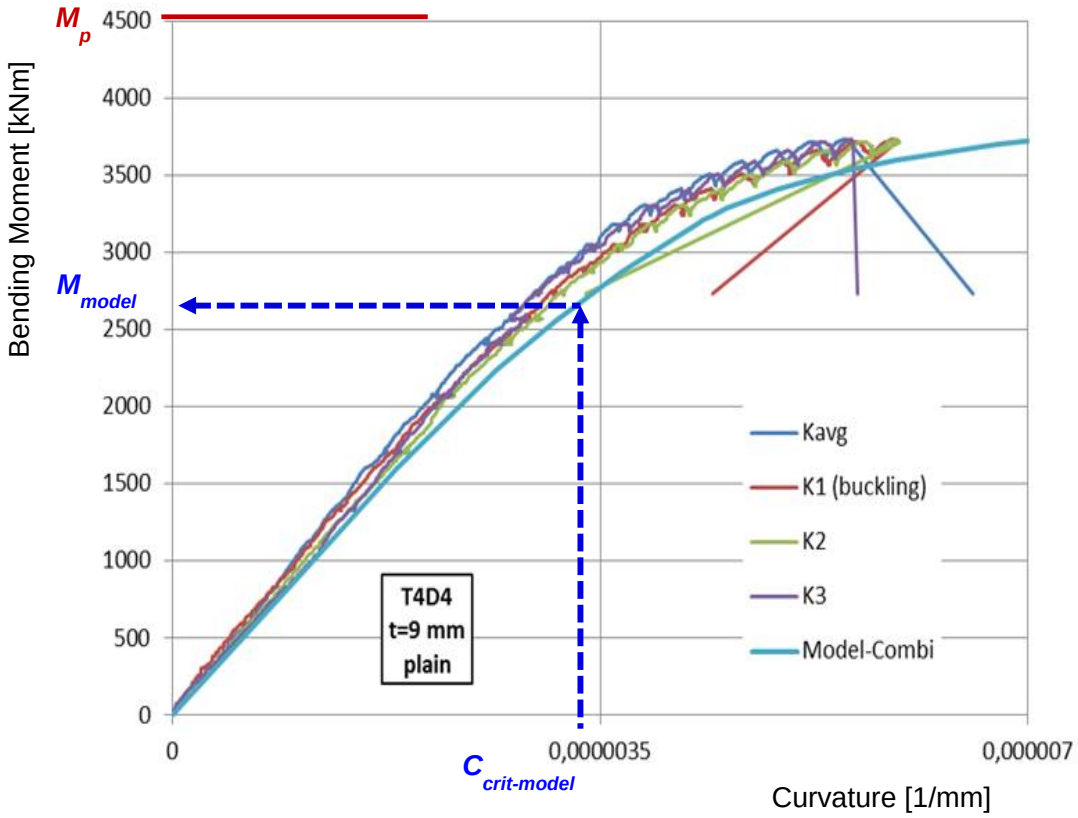

Figure 108 - Test results for test T4D4, compared with the result of the Model-Combi calculation.

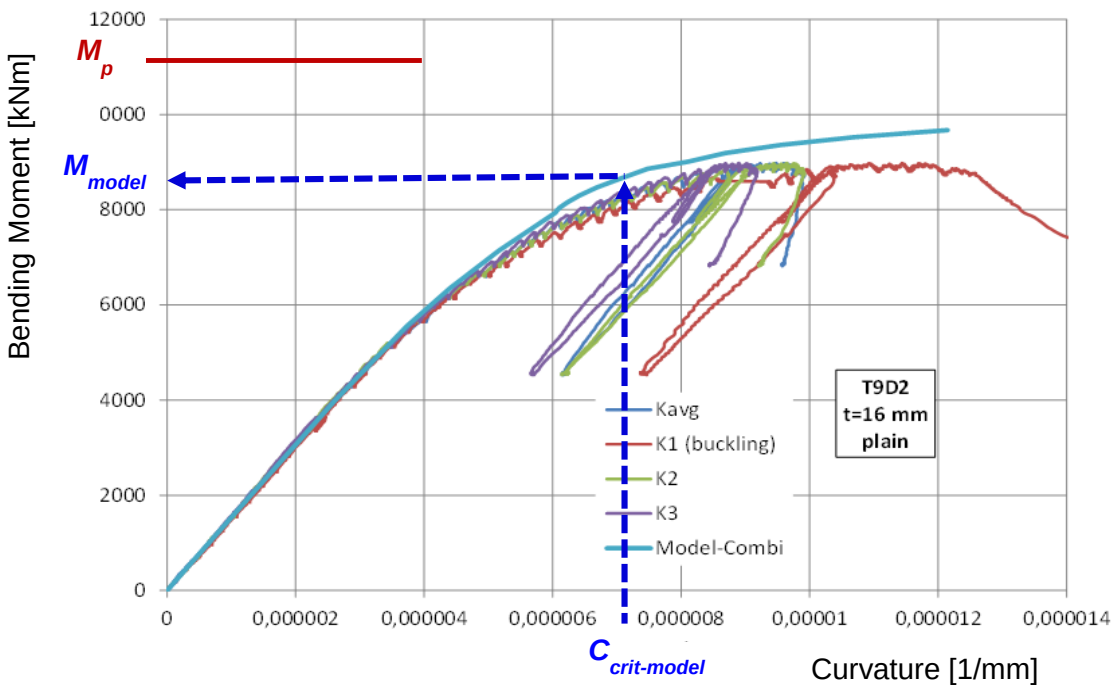

Figure 109 - Test results for test T9D2, compared with the result of the Model-Combi calculation.

The blue dashed lines in Figure 108 indicate: $C_{crit\text{-}model}$ = 3.33E-06 mm^{-1} M_{model} =2656 kNm $M_p = (D\text{-}t)\, t\sigma_{yield}$ =4503 kNm. Values are also given in Table 14.

Figure 109 is similar to Figure 108 with $C_{crit\text{-}model}$ =7.14E-06 mm^{-1} M_{model} =8640 kNm $M_p = (D\text{-}t)\, t\sigma_{yield}$ = 11135 kNm.

Table 14 - Results of design rule calculations.

Tube	**T4D4**	T7D1	**T9D2**	T10D6	T15D16
Type	plain	GW/CCW	plain	GW/CCW	plain
Diameter D_u [mm]	1065	1068	1069	1070	1068
Wall thickness t [mm]	9.16	16.34	16.34	12.8	9.82
D_u / t	116.2	65.4	65.4	83.0	72.3
Imperfection δ_{un} [mm]	0.60	1.8	2.53	3.6	0.9
Yield strength f_y [MPa]	441	614	615	333	507
Mp [kNm]	4503	11070	11135	4764	5575
G [-]	0.938	0.938	0.938	0.938	0.938
a [-]	32.7	25.4	25.4	17.7	35.251
h [-]	0.959	0.968	0.968	0.978	0.956
M_m [kNm]	4050	10050	10110	4369	4998
f_{yr} [MPa]	397	557	558	305	455
M_e* [kNm]	3181	78938	7940	3432	3925
C_e* [1/mm]	3.66E-06	5.17E-06	5.17E-06	2.82E-06	4.19E-06
a_{un} [-]	0.994	0.865	0.810	0.785	0.938
a_{strain} [-]	1.110	0.778	0.944	1.205	1.023
$a_{high\text{-}low}$ [-]	1.0	1.0	1.0	0.98	1.0
C_{crit} model [1/mm]	3.327E-06	6.335E-06	7.143E-06	0.00158*	3.572E-06
M at C_{crit} (model) [kNm]	2656	7854	8640	0.84*	3042
C_{crit} test [1/mm]	5.50E-06	8.50E-06	11.00E-06	0.0016*	5.20E-06
M at C_{crit} test [kNm]	3550	7800	8800	0.85*	4240
C_{crit} model / C_{crit} (test) [-]	**0.60**	**0.75**	**0.65**	**0.99**	**0.69**
M model / M test [-]	**0.75**	**1.01**	**0.98**	**0.99**	**0.72**
* For this test the values of C_{crit} and M at C_{crit} are normalized by D/t^2 and M_p respectively.					

In Table 14 it can be seen that the Combi-model gives safe results for the critical curvature, except for tube T10D6.

In tube T10D6 with a coil connection weld and a girth weld, rather big variations of the material properties (yield strength) were present on both sides of the coil weld and girth weld. In such cases

the curvature tends to concentrate in a narrow zone on one side of the weld. With a larger measuring length it results in a smaller (average) curvature and consequently critical curvature.

From Figure 108 and Figure 109 it appears that the safety for the critical curvature in both tubes is about the same.

The difference is in the bending moment capacity. For the relatively thick walled tube T9D2 with D/t = 65.4, the reduction in strength is small (factor 0,98), while for the thinner walled tube T4D4 with D/t = 116,2, the reduction in strength is much larger (factor 0,75).

6.2.1.2 Conclusions

1. The proposed guidelines are basically a refinement of the long existing design method in ENV 1993-5 Piling which, as mentioned before, enabled economic and apparently safe quay walls designs (no failures are known as a result of not correct design rules). Influences that were not taken into account in the ENV version are now addressed and equations are presented to quantify the effect on the critical curvature and bending moment capacity.
2. In developing these guidelines, the input of the CUR research program as mentioned before was highly valued to include the effect of sand fill. Sand fill has a positive effect on the critical curvature and the bending moment capacity, in particular also on the post buckling behaviour. With sand fill the post buckling behaviour is much smoother (less steep drop) and therefore enables better redistribution of loads in a quay wall.
3. Comparisons with test results in the Combitube project have demonstrated good agreement for (1) stiffness (which is affected by ovalisation and residual stresses), (2) critical curvature and (3) bending moment capacity.
4. The effect of imperfections, ovalisation, residual stresses, steel grade with different strain hardening properties, soil loads, bending moments in the tube wall, normal force and shear force on the bending moment capacity is much larger for thinner walled tubes than for thicker walled tubes. Therefore safety factors should depend on the D/t ratio.
5. The most important failure mode with largest scatter in critical curvature is local buckling which is highly dependent on the D/t ratio.
6. The design guidelines offer the possibility to quantify the critical curvature and to take care of adequate safety factors on the critical curvature to achieve the desired safety level. The necessary reduction in bending moment capacity is much less for thicker walled tubes than for thinner walled tubes.

6.2.1.3 References

[1] Gresnigt Arnold M, Van Es, Sjors H.J., Vasilikis, Daniel, Karamanos, Spyros A. (2016). “Strain-based design procedures for spiral-welded steel tubes in combined walls.” International colloquium on stability and ductility of steel structures – SDSS 2016, Timisoara, Romania, 30 May - 1 June 2016.

[2] Van Es, Sjors H.J., Gresnigt Arnold M. (2016). Guidelines for the design of tubes in CombiWalls, TU-Delft.

[3] Gresnigt, A.M. (1986). “Plastic design of buried steel pipes in settlement areas”, *HERON 1986-4*. Delft University of Technology.

[4] CUR (2013). “Handbook Quay Walls 2nd Edition.” Publication N. C211E, Centre for Civil Engineering Research and Codes (CUR), Gouda, The Netherlands.

[5] Hübner, A., (2007). “Tubular piles – buckling design in a complex situation.” *Dissertation Karlsruhe University,* Germany.

[6] Hübner, A. et al. (2007). “Enhanced economy of tubular piles by improved buckling design (ETIB).” *Eur report 23851, European Commission. Research Fund for Coal and Steel,* Brussels.

[7] Nader Yoosef-Ghodsi, Istemi Ozkan, Qishi Chen (2014). "Comparison of compressive strain limit equations." *Paper IPC2014-33182 10th International Pipeline Conference IPC2014*, Calgary, Canada.

[8] EN 1993-4-3 (2007). "Eurocode 3 – Design of Steel Structures – Part 3-4: Pipelines." CEN, Brussels.

[9] EN 1594 (2000). European Committee for Standardization. 2000. European Pipeline Standard – Gas Supply Systems: Pipelines – Maximum Operating Pressure over 16 bar. CEN, Brussels.

[10] DNV-RP-C202 (2010). "Recommended Practice – Buckling strength of shells." Det Norske Veritas, Høvik, Norway.

[11] DNV-OS-F101 (2012). Submarine Pipeline Systems. DNV Offshore Standard DNV-OS-F101, Det Norske Veritas Classification A/S, Høvik, Norway.

[12] CSA Z662-11 (2011). Oil and Gas Pipeline Systems. Canadian Standards Association, Mississauga, Ontario, Canada.

[13] Zimmermann, S., Karbasian, H., Knoop, F.M. (2013) "Helical Submerged Arc Welded Line Pipe Engineered For Strain Based Design" *Proceedings of the International Offshore and Polar Engineering Conference (ISOPE),* Anchorage, Alaska, U.S.A.

6.2.2 Design guidelines for EN 1993-1-6 Shell Structures

The Edinburgh team has produced a comprehensive set of design guidelines in a final report (Rotter and Sadowski, 2015, [1]). It has about 80 pages with numerous graphs with results of FEA parameter studies. And it contains a proposal for amendment of EN 1993-1-6 Shell Structures.

This research report reviews all the critical questions addressed by the Combitube project, identifying which could be regarded as of secondary importance and which were primary factor. The report then produced a synthesis of all the numerical and experimental data available to the Edinburgh team and produced carefully crafted design guidelines founded on a rigorous scientific assessment of this data. Not only are the recommendations produced in terms of the bending resistance to buckling and yielding, but recommendations that are compatible with these are deduced for those wishing to use strain based design.

In the report the progress towards better design rules is mentioned: The new 'Reference Resistance Design' shell buckling design method, devised at Edinburgh and already incorporated as an approved amendment to EN 1993-1-6 (Rotter, 2013a,b,c,d, [2] [3] [4] [5]), fully addresses the critical original aims of the Combitube project by reconciling the predictions of this standard with those of EN 1993-1-1 for tubes in the intermediate *D*/*t* range.

In next section a comparison is made with test results (not in the final report of Rotter and Sadowski, 2015, [1]). For more information on the design guidelines reference is made to the report [1] and the proposed amendment E to EN 1993-1-6.

Note: As indicated before, after intensive discussions in the project team, it was decided to develop two sets of guidelines.

6.2.2.1 Comparisons with test results

Comparisons of bending moment capacity according the design guideline [1] [5] with test results in the Combitube project are given in Figure 110, Figure 111 and Figure 112.

The bending moment slenderness relations as given [1] are for various levels of normal force. The parameter S in the Figures is $N/N_{plastic}$. The lines go up to 30% of $N_{plastic}$. All TU-Delft tests are S=0 (no normal force). The tests in Karlsruhe vary between 5% and 7% normal force. The lines for S=0 and S=0.1 are very close to each other, indicating that small normal forces do not really have an effect on the bending moment capacity.

All test results are plotted in all three Figures for different quality classes. It is known that some test specimens had better quality than other. These are of course on the lower end of the comparisons.

There are no comparisons for the critical curvature, because the guidelines do not give guidance on critical curvature.

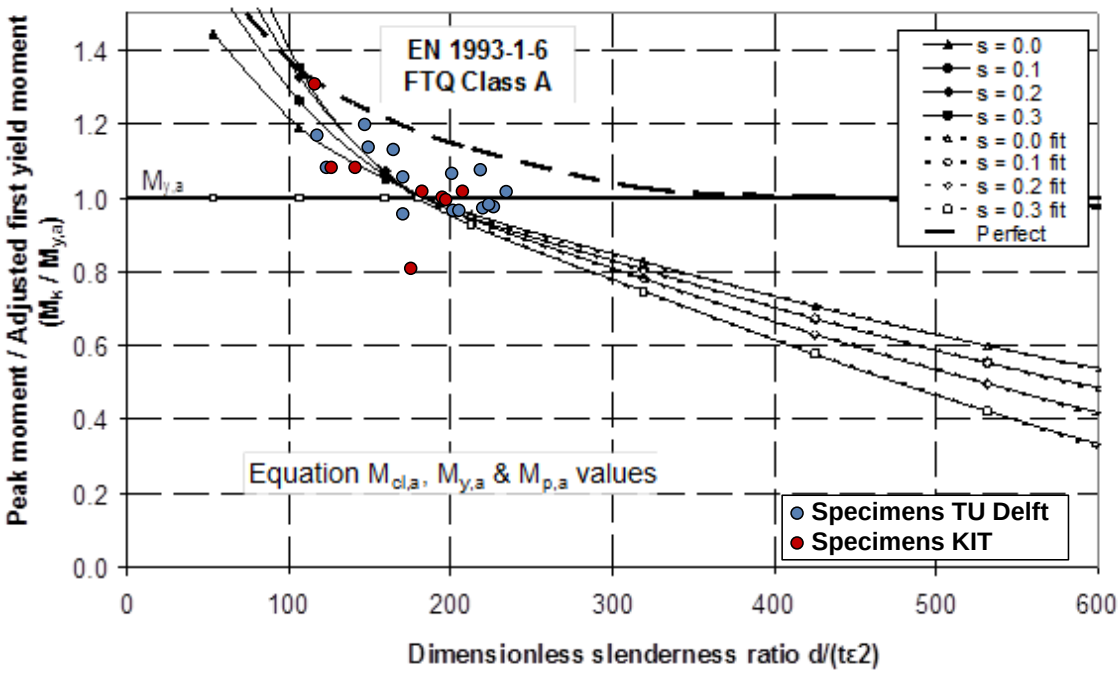

Figure 110 – Comparison of bending moment according to UEDIN design guideline with test results for class A quality tubes; $S=N/N_{pl}$.

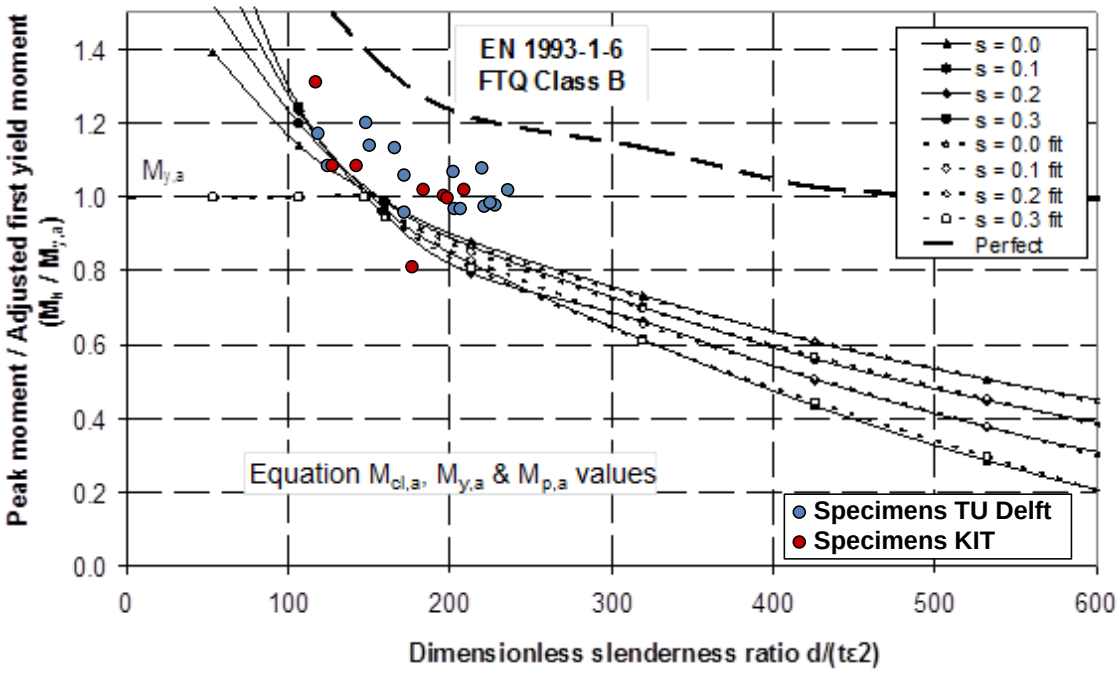

Figure 111 – Comparison of bending moment according to UEDIN design guideline with test results for class B quality tubes; $S=N/N_{pl}$.

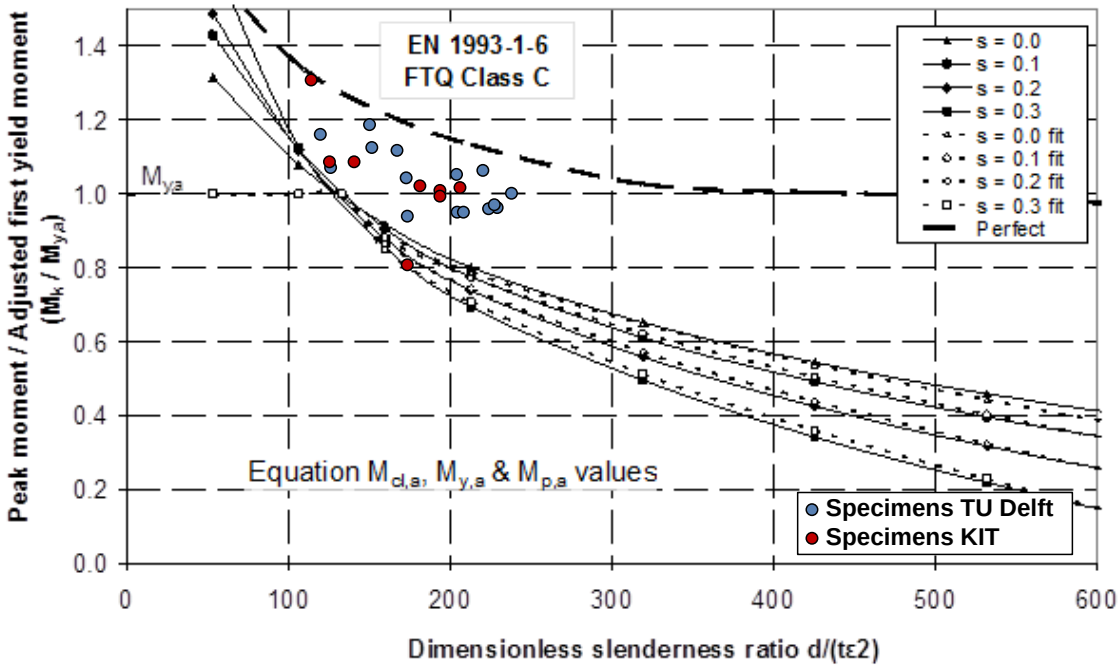

Figure 112 – Comparison of bending moment according to UEDIN design guideline with test results for class C quality tubes; $S=N/N_{pl}$.

6.2.2.2 Conclusions

The conclusions in the final report (Rotter and Sadowski, 2015, [1]) are as follows.

During the course of this study of the bending resistance of large tubular members, a very significant advance has been made in resolving the conflicts and mismatches that formerly existed in this field. A new method of shell structure design, termed Reference Resistance Design has been devised. It has been implemented and adopted into EN 1993-1-6 as an approved amendment. A new Annex E.1 to EN 1993-1-6 (2007) has been drafted to define the resistance of tubular members and cylindrical shells subject to global bending. This annex was submitted and approved as an amendment, so that there is a new regulatory framework in place already before the closure of the project to address the specific needs of Combitubes.

This extensive report has documented the many factors that can affect the buckling resistance of tubular members for CombiWalls, and the discussion has identified which factors are critically important and which can be ignored as having only a secondary influence on resistance. These aspects have all been considered in the development of appropriate design rules.

A full set of design rules has been developed. Since the Eurocode on piles is required to refer to the standards EN 1993-1-1 (2005) for steel structural members in the cross-section classes 1, 2 and 3, and to EN 1993-1-6 (2007) for steel shells for those that fall into Class 4, the proposals developed here have been made compatible with both standards. The complete description given here has already been approved as an amendment to EN 1993-1-6 (2007) and the outcomes for less slender tubes are almost ready for implementation as an amendment to EN 1993-1-1 (2005). This comprehensive study permits tubular members and thin shell structures to be designed to a consistent and seamless set of rules that should be of considerable benefit to the structural engineering community.

There are several issues which could not be resolved within this project; most notable amongst these are the lack of standardised control of yield plateau and strain hardening characteristics of the steels from which these tubes are made. Since these properties have a strong influence on the resistance in the critically important range of design for Combitubes, this lack of standardisation is unfortunate.

The second aspect that requires further study is the question of appropriate measures of geometric imperfections in these tubulars. Although extensive measurements were made of the specimens that were tested in the course of this study, it is not clear that these test specimens are securely representative of all similar tubes. Furthermore there is scope for minor modifications to the standard EN 1993-1-6 (2007) to improve its tolerance requirements and its definitions of assumed imperfection to bring them into line with evidence from structures in service, when that becomes available.

6.2.2.3 References

[1] Rotter, J.M., Sadowski, A.J. (2015) "Final Report for Combitube WP6 Task 6.2: Design Guidelines for Tubes in CombiWalls." Research Report RR 15-01 Institute for Infrastructure and Environment, The University of Edinburgh, Edinburgh, UK / Research Report Department of Civil and Environmental Engineering Imperial College London, UK

[2] Rotter J.M. (2013a). "New segment in EN 1993-1-6 to cover design using reference resistances." Amendment AM-1-6-2013-05 to EN 1993-1-6, approved by CEN TC250 SC3, November 2013, Zurich, Switzerland.

[3] Rotter J.M. (2013b). "New segment in Annex E of EN 1993-1-6 to cover cylindrical shells under uniform bending." Amendment AM-1-6-2013-13 to EN 1993-1-6, approved by CEN TC250 SC3, November 2013, Zurich, Switzerland.

[4] Rotter, J.M. (2013c) "Revision of buckling parameters for axial compression in Annex D", Amendment AM-1-6-2013-12 to EN 1993-1-6. Approved by CEN TC250 SC3, November 2013, Zurich, Switzerland.

[5] Rotter, J.M. (2013d) "Separation of elastic buckling strength reduction factor for α, into geometric and imperfection components and clarification of the terminology for χ", Amendment AM-1-6-2013-11 to EN 1993-1-6, Approved by CEN TC250 SC3, November 2013, Zurich, Switzerland.

6.3 Task 6.3: Background documents

In this final report many relevant references are given at the various work packages and tasks. Also reference is made to the many publications already from the Combitube project as mentioned in the list in chapter 8 with publications from the Combitube project.

Many more are in preparation and will be published in conferences and peer reviewed journals.

6.3.1 Ongoing research – PhD thesis

Finally it is noted that research on the behaviour and spirally welded tubes for quay walls is ongoing.

In Delft Sjors van Es is preparing his PhD thesis on this subject, to be finalized in 2016. It will certainly lead to more refinement and closer agreement with test results.

At the same time simplified design models are developed that can more easily be applied, see e.g. ref [1] in paragraph 6.2.2.3.

6.4 Task 6.4: Design examples

6.4.1 According to the design guidelines for EN 1993-5 Piling

The design guidelines have been applied to several tested tubes in Delft, see the above section on design guidelines.

6.4.2 According to the design guidelines for EN 1993-1-6 Shell Structures

A nice design example has been prepared by ArcelorMittal [1] including the effect of the infill sheeting and earth and water pressure, see Figure 113.

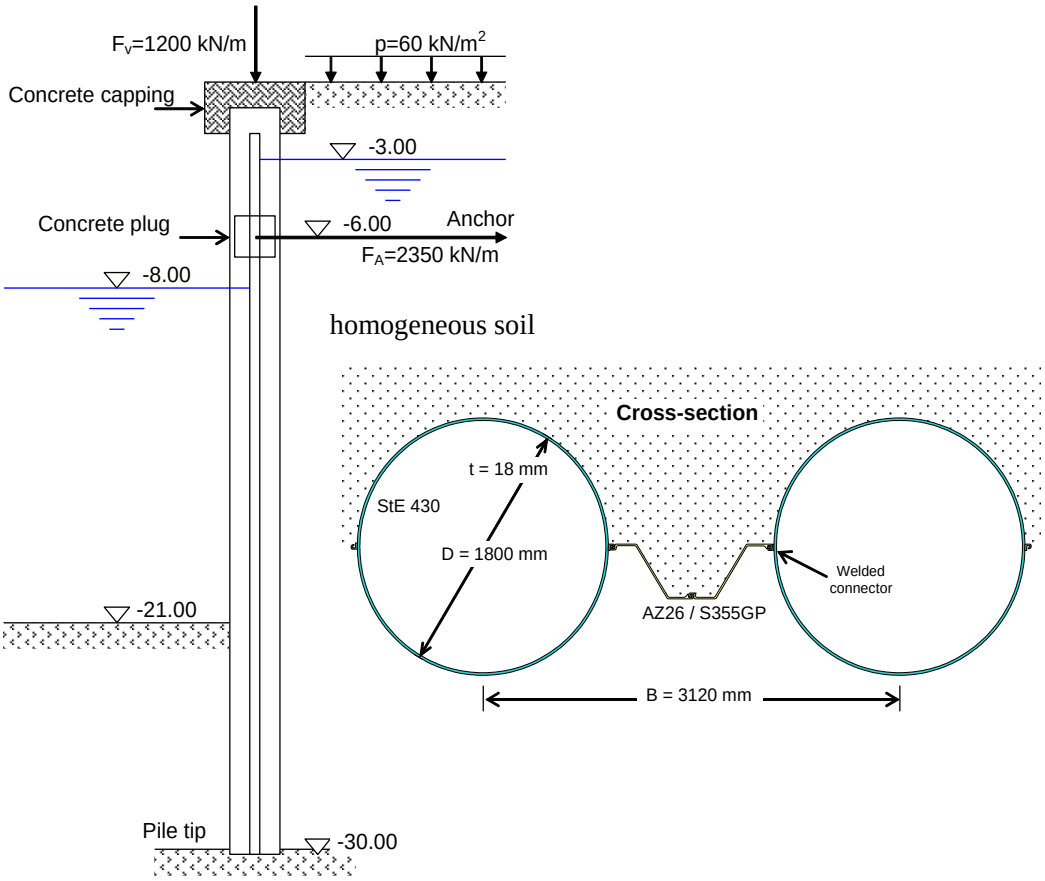

Figure 113 - Design example.

The verification of this design has been performed relative to the rules in EN 1993-5 Annex D, EN 1993-1-1 and EN 1993-1-6: 2010 and the proposed new set of equations for EN 1993-1-6 Annex E.

For the design a tube in X70 with $f_y = 483MPa$ and D/t = 104 was selected.

A summary of the outcome is given in Table 15.

Since the tube relative slenderness is rather high, the section is far into the Class 4 range.

The safety check against the published EN 1993-1-6 showed that the design was safe with a 14% margin.

The safety check against the Amendment to EN 1993-1-6 using Reference Resistance Design showed that the design was safe with a 39% margin.

Table 15 – Summary of design example calculations.

Source of the rules	**Outcome**
Ovalisation to EN 1993-5 Annex D	$\frac{e}{r} = 0{,}013 < 0{,}1$
Classification according to EN 1993-1-1	$\frac{D}{t} = 104 > 90\left(\sqrt{\frac{235}{483}}\right)^2 = 44$ ➔ Class 4 so EN 1993-1-6 applies
Verification according to EN 1993-1-6: 2010	Design safety check $0{,}86 \leq 1{,}0$
Verification according to Amendment to EN 1993-1-6 using Reference Resistance Design 2015	Design safety check $0{,}61 \leq 1{,}0$

The rules of EN 1993-1-6 are relatively complicated, but they can be coded into a spreadsheet and they permit slender designs of this type to be verified.

6.4.2.1 References

[1] ArcelorMittal Luxemburg (2014). Theoretical example for the shell buckling verification of tubular piles.

7 WP7: Project coordination

The objectives of WP7 were the following:

- Draft minutes of meetings between partners, indicating project progress and future actions.
- Coordinate and prepare intermediate and final reports of the project, including needs for future work and proposal to Eurocode 3 for design guidance in Eurocode 3 part 5 Piling and part 1-6 Strength and Stability of Shell Structures.

7.1 Task 7.1: Establish an efficient management process

The coordinator thanks the partner s for their input and fine cooperation. In total 8 project meetings were held. The input from universities as well as from the industry is highly valued.

Also the cooperation with TGS8 and officials in Brussels was highly valuated and helpful.

7.2 Task 7.2: Monitoring of project activities and evaluation of progress

Every now and then there were heavy discussions in the project team, in particular on the choices for test specimens and the conditions for the testing. But at the end always a solution was found that could be accepted by everybody.

7.3 Task 7.3: Progress and final reports

Progress and final reports were prepared and delivered. Comments and questions from the evaluators in TGS 8 were helpful. Many thanks for that.

8 Publications from the Combitube project

1. Van Es, S.H.J., Gresnigt, A.M., Kolstein, M.H. and Bijlaard F.S.K. (2013). Local Buckling of Spirally Welded Tubes-Analysis of imperfections and Physical Testing. ISOPE 2013.
2. Sadowski A.J. and Rotter J.M. (2013). Solid or shell finite elements to model thick cylindrical tubes and shells under global bending. International Journal of Mechanical Sciences, 2013.
3. Sadowski A.J. and Rotter J.M. (2013). On the relationship between mesh and stress field orientations in linear stability analyses of thin plates and shells. Finite Elements in Analysis and Design, 2013.
4. Gresnigt, A.M. and Van Es S.H.J. (2013). Stability of Spiral Welded Tubes in Quay Walls, PSSC 2013.
5. Sadowski A.J. and Rotter J.M. (2014). Modelling and behaviour of cylindrical shell structures with helical features. Computers and Structures.
6. Sadowski A.J. and Rotter J.M. (2014). Thin Tubular Members Design for Bending - Uniform Bending with Small Axial Loads. Eurosteel 2014.
7. Van Es, S.H.J., Gresnigt, A.M., Kolstein, M.H. and Bijlaard, F.S.K. (2014). "Strain based design of spirally welded pipes, local buckling in 4-point bending." *Proceedings of the Twenty-fourth (2014) International Ocean and Polar Engineering Conference,* Busan, Korea, June 15-20, 2014.
8. Sadowski A.J. and Rotter J.M. (2013). "Solid or shell finite elements to model thick cylindrical tubes and shells under global bending." International Journal of Mechanical Sciences, 74, 143-153.
9. Sadowski A.J. and Rotter J.M. (2014). "Modelling and behaviour of cylindrical shells structures with helical features." *Computers and Structures*, 133, 90-102.
10. Sadowski A.J., Rotter J.M., Reinke T. and Ummenhofer T. (2015a). "Statistical analysis of the material properties of selected structural carbon steels." *Structural Safety*, 53, 26-35.
11. Sadowski A.J., Rotter J.M., Reinke T. and Ummenhofer T. (2015b). "Analysis of variance of tensile tests from spiral welded carbon steel tubes." *Construction and Building Materials*, 75, 208-212.
12. Sadowski A.J., van Es S.H.J., Reinke T., Rotter J.M., Gresnigt A.M. and Ummenhofer T. (2015c). "Harmonic analysis of measured initial geometric imperfections in large spiral welded carbon steel tubes." *Engineering Structures*, 85, 234-248.
13. Ummenhofer, T. and Knödel, P. (1996) "Typical imperfections of steel silo shells in Civil Engineering", Proc. Intl Workshop on Imperfections in Metal Silos: Measurement, Characterisation and Strength Analysis, CA-Silo, Lyon, France, 19 April, pp 103-118.
14. Ummenhofer, T., Peil, U. and Schulz, U. (1997) "A rigorous model for assessing the buckling strength of silos", Proc., Int. Conf. on Carrying Capacity of Steel Shell Structures, Brno, 1-3 October 1997, pp 91-97.
15. Ummenhofer, T. and Reinke, T. (2014) "Bending resistance of steel tubes in CombiWalls – Test results", Combitube – WP3 Task 3.2, Karlsruhe Institute of Technology,
16. Vasilikis D., van Es S.H.J., Karamanos S. A. and Gresnigt A.M. (2014). "Bending deformation capacity of large-diameter spiral-welded tubes." *Proc. 10th Int. Pipeline Conf. IPC 2014*, Calgary, Alberta, Canada, Sep 29 – Oct 03.
17. Reinke, T., Sadowski, A. J., Ummenhofer, T., Rotter, M. J. (2014). "Large scale bending tests of spiral welded steel tubes." Eurosteel 2014, 7th European conference on Steel and Composite Structures, Naples, Italy, 10-12 September 2014.
18. Peters D.J. (Dirk Jan), Broos E.J. (Erik), Gresnigt A.M. (Nol) and Van Es S.H.J. (Sjors), (2015). "Local Buckling Resistance of Sand-filled Spirally Welded Tubes". *Proceedings of the Twenty-fifth (2015) International Ocean and Polar Engineering Conference, Hawaii, USA, June 21-26, 2015.*
19. Van Es S.H.J., Vasilikis D., Gresnigt A.M. and Karamanos S.A. (2016). "Ultimate bending capacity of Spiral-Welded Steel Tubes – Part I: Experiments." To be published in *International journal Thin-Walled Structure.*
20. Vasilikis D., Karamanos S.A., Van Es S.H.J. and Gresnigt A.M. (2016). "Ultimate bending capacity of Spiral-Welded Steel Tubes – Part II: Predictions." To be published in *International journal Thin-Walled Structures.*

21. Sjors H. J. van Es, Arnold M. Gresnigt, Daniel Vasilikis, Spyros A. Karamanos (2016). "Experimental and numerical investigation of the bending capacity of spiral-welded steel tubes." *International colloquium on stability and ductility of steel structures – SDSS 2016,* Timisoara, Romania, 30 May - 1 June 2016.
22. Arnold M. Gresnigt, Sjors H. J. van Es, Daniel Vasilikis, Spyros A. Karamanos (2016). "Strain-based design procedures for spiral-welded steel tubes in combined walls." *International colloquium on stability and ductility of steel structures – SDSS 2016,* Timisoara, Romania, 30 May - 1 June 2016

List of Figures

Figure 1 - Typical harbour wall or quay wall construction. 5
Figure 2 - Schematic and photo of a CombiWall (combined wall of tubes and infill sheeting connected with welded slots to the tube). 5
Figure 3 - Left: Welding of the slots for the tube-sheeting connection; Right: installation of tubular piles in the soil. 6
Figure 4 - Left: Installation of infill sheeting; Right: CombiWall with waling for the new central railway and metro station in Rotterdam (2008). 6
Figure 5 - Effect of other influences such as imperfections, soil loads, residual stresses, ovalisation of the cross section, etc. on the bending moment-curvature behaviour for a thick walled tube and for a thinner walled tube. 8
Figure 6 - Critical strains for tubes in steel S480; Heron is according to reference [4]. 20
Figure 7 - New quay wall in harbour extension Rotterdam into the North Sea. 22
Figure 8 - Wilhelmina quay wall Groningen, The Netherlands. 22
Figure 9 - A4 Motorway underpass (highway between The Hague and Amsterdam). 22
Figure 10 - A4 Ringvaart Aquaduct (highway between The Hague and Amsterdam; the Ringvaart is the canal around the Haarlemmermeer polder, where the airport Schiphol is situated) 23
Figure 11 - An example of a CombiWall with loads. 23
Figure 12 - Scatter in test results in pure bending as collected in the Combitube project, compared with equation (26). The red line is the equation (26). Note that the scales in this figure are logarithmic. 25
Figure 13 - Simulation of buckling formation, in a bending test of a 24-inch-diameter tube (D/t=72); from Dama et al. (2007). 27
Figure 14 – Design of test set-up in Delft in 4-point bending. 33
Figure 15 – Test rig in Delft in 4-point bending. 34
Figure 16 - K1: Coil weld at the end, K2: Coil weld in the centre. 35
Figure 17 - Test setup, pulling device, support scheme and position of displacement transducers. ... 35
Figure 18 – Overview of test rig in Karlsruhe with buckled test K1. 36
Figure 19 - Location of material specimens on four point bending test specimens. 37
Figure 20 - Overview of material tensile testing specimens dimensions. 37
Figure 21 - Overview of tensile test setup (two figures left) and compressive setup by TU-Delft. 38
Figure 22 - Overview of restraining tool for compressive tests. 38
Figure 23 - Tensile test results of specimen T1D9. 39
Figure 24 - Tensile test results of specimen T3D13. 39
Figure 25 - Tensile test results of specimen T7D1. 39
Figure 26 - Tensile test results of specimen T10D6. 39
Figure 27 - Comparison of yield strength of tubes ($f_{0.2\%}$), normalized by the average value in that direction (longitudinal or circumferential) for that specimen or specimen part. 39
Figure 28 - Comparison of tensile strength of tubes (f_t), normalized by the average value in that direction (longitudinal or circumferential) for that specimen or specimen part. 40
Figure 29 - Results of tensile test of specimen part T6D10 Left including a spiral weld specimen. 40
Figure 30 - Results of tensile test of specimen T8D5 including a spiral weld specimen. 40

Figure 31 - Comparison of tensile test and compression test with similar orientation and location: D1D9 longitudinal outside. 40
Figure 32 - Comparison of tensile test and compression test with similar orientation and location: T2D11 longitudinal outside. 40
Figure 33 - Locations of material samples. 42
Figure 34 - Stress-strain curves of the most different materials (A: left end, C: right end) 43
Figure 35 - Overview of measurement grid. 45
Figure 36 - Laboratory test setup to measure initial geometrical imperfections. 45
Figure 37 - Measured tube diameters and the spread of the measured data. 46
Figure 38 - Measured tube thicknesses and the spread of the measured data. 46
Figure 39 - Laser scan of initial imperfection in Tube T2, compression zone. 47
Figure 40 - Laser scan of initial imperfections with overlay of visible roller marks in tube T1, compression zone. 47
Figure 41 - Overview of ring before (left) and after cutting (right) with measurement of opening at four points (d_2-d_1), skewness (S_1 and S_2) and increase in radius (ΔR). 48
Figure 42 - Photos of cut rings Ring 481 (left) and D10R (right); since D10R appeared to close, more plate material was removed to let the ring freely deform. 49
Figure 43 - Overview of the old motorway and new motorway under construction (image source www.beeldbank.rws.nl). 49
Figure 44 - Inside of building pit during construction with accessible combined walls. 49
Figure 45 - Measuring of imperfections in building pit. 51
Figure 46 - Coil connection welds in specimens K1 and K2. 52
Figure 47 - Specimen K1: longitudinal section top / bottom. 52
Figure 48 - Specimen K1: longitudinal section front / back. 53
Figure 49 - Specimen D9: Fitted 2D spline surface to net 'cleaned' imperfections in the global cylindrical coordinate system. 55
Figure 50 - Specimen D11: Fitted 2D spline surface to net 'cleaned' imperfections in the global cylindrical coordinate system. 55
Figure 51 - Specimen D13: Fitted 2D spline surface to net 'cleaned' imperfections in the global cylindrical coordinate system. Note the occurrence of a girth weld in the middle of the specimen, leading to a sudden change in the measured surface. 55
Figure 52 - Specimen K1: Fitted 2D spline surface to net 'cleaned' imperfections in the global cylindrical coordinate system. 56
Figure 53 - Drilling mill and strain gage in the hole-drilling-method. 59
Figure 54 – Measurement locations. 59
Figure 55 - Residual stresses in specimen D9, x-y stresses. 60
Figure 56 – Left: Overview of test setup. Right: Overview of middle support and floor anchorage. Note the fill in with triplex at the internal load application to prevent the strap from loading only the spiral weld. 62
Figure 57 - Overview of TU-Delft test setup. 63
Figure 58 – Left: Overview of ovalisation measurements locations. Right: Schematics of ovalisation bracket with flexible strip and strain gauges. 64
Figure 59 – Layout of curvature measurements during TU-Delft testing. 64
Figure 60 – Laser measurements of the tube during testing. 64
Figure 61 – Moment curvature results of test T1D9 and T6D10. Local curvature measurement in which the local buckle formed is marked as such. 66
Figure 62 – Moment curvature results of test T4D4 and T15D16 (note, the latter is a longitudinally welded tube). Local curvature measurements in which the local buckle formed is marked as such. 66
Figure 63 – Measured ovalisations during test T2D11. 67
Figure 64 – Measured ovalisations during test T3D13. 67
Figure 65 – Comparison of initial imperfections and measured tube wall profile at the onset of buckling for test T10DD6. The local buckle forms at the girth weld, where a misalignment of about 3 mm is present. 68

Figure 66 – Comparison of initial imperfections and measured tube wall profile at the onset of buckling for test T4D4. The local buckle formed at a regular, fabrication related, imperfection. The initial imperfection has increased 5 times in size. 68
Figure 67 - Comparison of measured ovalisations with laser cart and ovalisations brackets at two different curvatures: before buckling (b.b.) and after buckling (a.b.) 68
Figure 68 - 3D image of a specimen that buckled at the girth weld. Close inspection shows that both the girth weld and the spiral weld to the lower right of the girth weld are visible. 69
Figure 69 – Critical strains of all test specimens. Strains based on average curvatures. 69
Figure 70 –Ratio between maximum measured local curvature and average curvature for all specimens. 70
Figure 71 - Maximum resisted bending normalized moment for all specimens. 70
Figure 72 – Ratio between curvature at maximum bending moment and load drop-off. Left: average curvatures. Right: local curvatures at buckling location. 71
Figure 73 - Photo of the only observed buckle close to a spiral weld. 72
Figure 74 – Force-displacement diagram for K1 and K7. 75
Figure 75 – Failure mechanism of specimens with D/t ≈ 73. 75
Figure 76 – Failure mechanism of specimens with D/t ≈ 105. 76
Figure 77 - Failure mechanisms of specimens K3 and K8. 76
Figure 78 - Experimental values of critical stress for different values of D/t and comparison with the predictions from the 2 constitutive models. 78
Figure 79 - Experimental values of critical strain for different values of D/t and comparison with the predictions from the 2 constitutive models. 78
Figure 80 - Schematic representation of the manufacturing process of spirally welded tubes. 79
Figure 81 - (a) Finite element numerical model of spiral cold bending simulation; (b) Longitudinal motion of the plate through the rollers results in the formation of the spirally welded tube. 80
Figure 82 - Basic geometric characteristics of the numerical model for spiral-weld forming. 80
Figure 83 - Distribution of axial, hoop and shear normalized residual stresses across tube thickness. 81
Figure 84: Evolution of normalized residual stresses during the forming process. 82
Figure 85 - Distribution of residual stresses over thickness for different values of D/t ratio; (a) axial stresses and (b) hoop stresses. 82
Figure 86 - (a) Rectangular finite element mesh; (b) Wrinkled pattern in the compression side - shape of the first eigenmode imperfection. 83
Figure 87 - a) Partitioning of tube which contains girth weld; b) Spiral mesh for the analysis of tubes containing coil weld. 84
Figure 88 - Distribution of axial, hoop and shear normalized residual stresses over tube thickness. .. 84
Figure 89 - Numerical model of four-point bending in ABAQUS. 85
Figures 90 - Moment-curvature curves for tube specimens; comparison between numerical and experimental results. 87
Figure 91 - Half system with partly modelled angle construction and quarter system with stiff beam elements 88
Figure 92 - Left: K2, load-displacement curves with variation of materials. Right: K3, main buckle at the transition of materials K3_A and K3_C 90
Figure 93 - K1 comparison with buckling mode simulation K1_C, geom. perfect, xz-symmetry only .. 90
Figures 94 - Imperfection sensitivity of tubes with a) D/t=67, and b) D/t=119, subjected to bending. 91
Figures 95 - Normalized critical curvature k_{cr}/k_I in terms of imperfection amplitude δ_0/t for a) X70 tubes with D/t=67, b) X60 tubes with D/t=119; effect of residual stresses. 92
Figures 96 - Moment-curvature diagrams for a) X70 tubes with D/t=67, b) X60 tubes with D/t=119; effect of residual stresses. 92
Figure 97 - a) Normalized m-k diagrams for different values of strain hardening modulus, b) Variation of maximum moment in terms of the dimensionless plateau parameter n 93
Figures 98 - Normalized m-k diagrams for different material grades; (a) $D/t = 67$; (b) $D/t = 119$..... 94
Figure 99 - Normalized moment-curvature diagrams for different values of material anisotropy; influence of increased yield stress a) in the axial direction and b) in the hoop direction. 94

Figure 100 - Normalized moment-curvature diagrams of a 42-inch-diameter X70 tube with D/t =67 with a) a girth weld, b) a coil weld, for different yield stress values of connected tube parts. 95
Figure 101 - Schematic representation of the numerical model. 97
Figure 102: Lateral tensile load applied at the side nodes of tube. 97
Figures 103 - Moment-curvature (m-k) curves for tubes with a) D/t =67 and b) D/t=119; effect of loads from connected sheet piles. 98
Figures 104 - Variation of a) normalized critical curvature and b) normalized maximum moment in terms of the normalized pulling force for tubes with connected sheet piles. 98
Figures 105 - Buckling shapes for tubes with connected sheet piles; a) D/t =67 and b) D/t=119. 99
Figure 106 - Moment curvature relationship to illustrate the effect of other influences on the bending moment curvature diagram. 103
Figure 107 - Definition of ovalisation and radius r_o in an ovalised cross section. 106
Figure 108 - Test results for test T4D4, compared with the result of the Model-Combi calculation. 107
Figure 109 - Test results for test T9D2, compared with the result of the Model-Combi calculation. 107
Figure 110 – Comparison of bending moment according to UEDIN design guideline with test results for class A quality tubes; $S=N/N_{pl}$. 112
Figure 111 – Comparison of bending moment according to UEDIN design guideline with test results for class B quality tubes; $S=N/N_{pl}$. 112
Figure 112 – Comparison of bending moment according to UEDIN design guideline with test results for class C quality tubes; $S=N/N_{pl}$. 113
Figure 113 - Design example. 115

List of Tables

Table 1 - Overview of testing program in Delft. 32
Table 2 - Summary of specimens. 34
Table 3 - K1 – K4: Comparison of yield strength $R_{p0,2}$ for different test directions. 42
Table 4 - Material properties. 43
Table 5 - Overview of results of ring cutting tests. 48
Table 6 - Overview of field measurement programme. 50
Table 7 - Selected tubes for measurements. 52
Table 8 - Overview of test program performed at TU Delft. 61
Table 9 - Overview of test results of tests performed at TU Delft. 71
Table 10 - Specimen specifications. 73
Table 11 - Test results. 74
Table 12 - Summary of bending tests; comparison between numerical and experimental results. 86
Table 13 - Summary of the numerical simulations of the bending tests 89
Table 14 - Results of design rule calculations. 108
Table 15 – Summary of design example calculations. 116

HOW TO OBTAIN EU PUBLICATIONS

Free publications:

- one copy:
  via EU Bookshop (http://bookshop.europa.eu);
- more than one copy or posters/maps:
  from the European Union's representations (http://ec.europa.eu/represent_en.htm);
  from the delegations in non-EU countries (http://eeas.europa.eu/delegations/index_en.htm);
  by contacting the Europe Direct service (http://europa.eu/europedirect/index_en.htm) or
  calling 00 800 6 7 8 9 10 11 (freephone number from anywhere in the EU) (*).

(*) The information given is free, as are most calls (though some operators, phone boxes or hotels may charge you).

Priced publications:

- via EU Bookshop (http://bookshop.europa.eu).

KI-NA-278-29-EN-N

CombiTube provides economic and safe design guidance for tubes in combined walls (CombiWalls), in particular for spirally welded tubes. Because local buckling is the leading failure mechanism, the focus was on quantifying the effect of key parameters that influence local buckling: the diameter to wall thickness ratio (D/t), material properties, residual stresses and geometrical imperfections including weld misalignment and dimples. Extensive theoretical and experimental research has been performed leading to proposals for better design guidelines for EN1993-1-6 on Strength and Stability of Shell Structures and for EN1993-5 on Piling. There was a good cooperation with the Dutch SBRCURnet on the effect of sand-fill. Results of their research are used in CombiTube.

The following intermediate targets have been achieved:

- Critical evaluation of design procedures and available test data for tubular members has shown that there are many test results on seamless and longitudinally welded tubes, but few on spirally welded tubes. The Dutch design procedures result in most economical applications (WP1).
- In Delft 13 tests were performed on spirally welded tubes and 2 on longitudinal welded tubes (diameter 1067mm, wall thicknesses 9-16mm, steel grade X52 to X70). In Karlsruhe 8 tests were performed (diameter 820-863mm, wall thicknesses 8-11mm, steel grade X52). Advanced methods were used to measure imperfections and residual stresses, followed by innovative modelling and characterisation (WP2, WP3).
- Numerical models for local buckling calculations in the plastic range were examined and validated with experimental test results (WP4).
- A database of numerical results with the effect of relevant factors that influence the bending moment and critical curvature has been established and evaluated (WP5).
- Two sets of guidelines have been developed. One general set for EN1993-1-6 and the other for applications as in EN1993-5 Piling (WP6).

Publications Office

ISBN 978-92-79-57673-7
10.2777/961346